

SMALL DIAMETER PARTICLE DISPERSION IN A COMMERCIAL AIRCRAFT CABIN

by

JEREMY MICHAEL BENEKE

B.S., Kansas State University, 2010

A THESIS

submitted in partial fulfillment of the requirements for the degree

MASTER OF SCIENCE

Department of Mechanical and Nuclear Engineering
College of Engineering

KANSAS STATE UNIVERSITY
Manhattan, Kansas

2010

Approved by:

Co-Major Professor
Dr. Mohammad H. Hosni

Approved by:

Co-Major Professor
Dr. Byron W. Jones

Abstract

Airline cabins represent an indoor environment in which the spread of particles or contaminants is of interest due to the large number of passengers and distances they travel. In fact, hundreds of millions of passengers travel each year spending extended periods in close proximity to one another. This close proximity causes concern about the spread of disease and contaminants amongst passengers. These passengers move from region to region of the world increasing the potential for worldwide epidemics. In an effort to understand the aircraft cabin environment and the dispersion of fine particles, an experimental study was conducted. The cabin used for the experiments is a simulated Boeing 767-300 with eleven rows, each comprised of seven seats. The particles release occurred in a short burst in all the seats across the second row simultaneously. This design focused on the longitudinal dispersion of particles throughout the cabin. The particles from this release had corrected aerodynamic diameters between 0.87 and 1.70 micrometers. The collection and analysis of data took place based on five criteria. The first analysis focused on the total particle counts at 27 locations throughout the cabin. The second analysis made use of a reference location for each of the tests and presents the exposure in each of those locations as a fraction of the reference during the same test. The third analysis centers its attention on the transient behavior as the particles were counted at various locations. The fourth and fifth types of data analysis focus on the time required for each tested location to reach either 100 total particle counts or ten percent of the total seen at that location during that test. The tests show the regions close to the source experience higher levels of exposure, less time to reach the time limits, and higher levels of variation from test to test. The locations farther from the source show lower exposure levels, longer times to reach the limits, and less variation from test to test. This indicates the variations close to the source stem from the chaotic nature of the airflow rather than from irregularities of the dispersion system. The data agree well with previous work and suggest further studies would improve the understanding of the aircraft cabin environment and the spread of airborne particles and contaminants.

Table of Contents

List of Figures	vi
List of Tables	ix
Acknowledgements	x
CHAPTER 1 - Introduction and Literature Review	1
CHAPTER 2 - Experimental Setup	5
2.1 Test Chamber	5
2.1.1 Spaces	5
2.1.2 Elements	6
2.1.2.1 Chamber duct work	6
2.1.2.2 Seats	7
2.1.2.3 Mannequins	7
2.2. Air Supply System	8
2.2.1. Air Handling	8
2.2.1.1 Duct	8
2.2.1.2 Fan	9
2.2.2. Air Conditioning	9
2.2.2.1. Water-Glycol System	9
2.2.2.1.1. Primary Loop	9
2.2.2.1.2. Cooling Loop	10
2.2.2.1.3 Heating Loop	10
2.2.2.2. Electric Heater	11
2.2.3. Filters	11
2.2.3.1. Inlet Filter	11
2.2.3.2. HEPA	11
2.2.4. Control Systems	12
2.2.4.1. Flow Measurement and Control	12
2.2.4.2. Temperature Measurement	12
2.2.4.3. Temperature Control	13

2.2.4.3.1. Primary Loop Temperature Control	13
2.2.4.3.2. Duct Heater Temperature Control	13
2.3. Particle Systems	13
2.3.1. Particle Measurement	14
2.3.2. Particle Dispersion	14
CHAPTER 3 - Experimental Procedure	28
3.1 Equipment Setup	28
3.2 Testing Locations	28
3.2.1 Reference Tests	29
3.2.2 Exchange Tests	29
3.3. Test Preparation	30
3.4 Data Collection	30
CHAPTER 4 - Results	32
4.1. Exposure Tests	32
4.1.1. Total Exposure	32
4.1.2. Exposure as a Fraction of the Reference Location	33
4.2. Time Series Data	33
4.2.1. Centerline Time Series	34
4.2.2. Row 4 Time Series	34
4.2.3. Row 7 Time Series	34
4.2.4 Threshold Time Data	35
CHAPTER 5 - Data Analysis	57
5.1. Normalization	57
5.2. Settling Losses	58
5.2.1 Aerodynamic Diameter Correction	58
5.2.2. Settling Rate	59
5.3. Averaging Methods	60
5.4. Uncertainty Analysis	61
5.4.1. Particle System Uncertainties	61
5.4.1.1. Cabin Supply Air	61
5.4.1.2. Particle Dispersion System	61

5.4.1.3 Particle Counting	63
5.4.2. Result Uncertainties	63
5.4.2.1. Exposure Test	64
5.4.2.2. Time Series	65
5.5 Exposure Analysis	65
5.5.1 Total Exposure	66
5.5.2 Exposure as a Fraction of the Reference Location	66
5.6 Time Series Analysis	67
5.6.1. Dynamic Particle Counts	67
5.6.2. Cumulative Exposure	68
5.6.3. Exposure Threshold Times	69
5.7 Verifications	70
5.7.1 Particle Measurement	70
5.7.2 Dispersion System	70
5.7.3 Normalization	71
CHAPTER 6 - Conclusions and Recommendations	79
6.1. Exposure	79
6.2. Transient Behavior	80
6.3. Recommendations	81
References	82
Appendix A - LabView Programs	84
A.1. Cannon Control Program	84
A.2. DAQ Analog Out Program	88

List of Figures

Figure 2.1: Chamber Exterior, Inlets, and Exhaust Fans	16
Figure 2.2: Chamber Hallways and Crawl Space	16
Figure 2.3: Cabin Interior	17
Figure 2.4: Chamber Floor Joist and Decking	17
Figure 2.5: Cabin Supporting Ribs	18
Figure 2.6: Chamber View from North End	18
Figure 2.7: Cabin Air Exits	19
Figure 2.8: Cabin Air Distribution Duct	19
Figure 2.9: Cabin Diffuser Outlets	20
Figure 2.10: Cabin Cross-section	20
Figure 2.11: Cabin Overhead Seat Arrangement	21
Figure 2.12: Mannequin Seated in Cabin	21
Figure 2.13: Supply Air Handling System	22
Figure 2.14: Supply Fan and VFD Controllers	22
Figure 2.15: Primary and Cooling Loops of Air Conditioning System	23
Figure 2.16: Heating Loop Water Heater	23
Figure 2.17: Water-Glycol System Schematic	24
Figure 2.18: Inlet Filter Housing	24
Figure 2.19: Supply Air Louvered Inlet	25
Figure 2.20: Inlet Filters	25
Figure 2.21: APS' in Testing Positions	26
Figure 2.22: Particle Dispersion Cap and Air Nozzle	26
Figure 2.23: Particle Dispersion System in Row 2	27
Figure 2.24: Charging Tank for Particle Dispersion System	27
Figure 3.1: Measurement Plate and Tray for Pre-Test Cap Loading	31
Figure 4.1: Centerline Total Exposure	37
Figure 4.2: Centerline Total Exposure, Rows 6 through 11	37
Figure 4.3: Row 4 Total Exposure	38

Figure 4.4: Row 7 Total Exposure	38
Figure 4.5: All Rows Total Exposure	39
Figure 4.6: Overview of Cabin Total Exposure	39
Figure 4.7: Centerline Fractional Exposure	40
Figure 4.8: Centerline Fractional Exposure, Rows 6 through 11	40
Figure 4.9: Row 4 Fractional Exposure	41
Figure 4.10: Row 7 Fractional Exposure	41
Figure 4.11: Rows 4 and 7 Fractional Exposure	42
Figure 4.12: Overview of Cabin Fractional Exposure	42
Figure 4.13: Centerline Particle Count Time Series	43
Figure 4.14: Centerline Particle Count Time Series, Reduced Count Scale	43
Figure 4.15: Centerline Cumulative Exposure	44
Figure 4.16: Centerline Cumulative Fraction of Total Exposure	44
Figure 4.17: Centerline Particle Count Threshold Times	45
Figure 4.18: Centerline Particle Count Threshold Times, Rows 1 through 5	45
Figure 4.19: Centerline Fraction of Total Exposure Threshold Times	46
Figure 4.20: Centerline Fraction of Total Exposure Threshold Times, Rows 1 through 5	46
Figure 4.21: Row 4 Particle Count Time Series	47
Figure 4.22: Row 4 Seat 4A Particle Count Time Series	47
Figure 4.23: Row 4 Seat 4B Particle Count Time Series	48
Figure 4.24: Row 4 Seat 4C Particle Count Time Series	48
Figure 4.25: Row 4 Seat 4D Particle Count Time Series	49
Figure 4.26: Row 4 Seat 4E Particle Count Time Series	49
Figure 4.27: Row 4 Seat 4F Particle Count Time Series	50
Figure 4.28: Row 4 Seat 4G Particle Count Time Series	50
Figure 4.29: Row 4 Cumulative Particle Counts	51
Figure 4.30: Row 4 Cumulative Fraction of Total Exposure	51
Figure 4.31: Row 4 Particle Count Threshold Times	52
Figure 4.32: Row 4 Fraction of Total Exposure Threshold Times	52
Figure 4.33: Row 7 Particle Count Time Series	53
Figure 4.34: Row 7 Cumulative Particle Counts	53

Figure 4.35: Row 7 Cumulative Fraction of Total Exposure	54
Figure 4.36: Row 7 Particle Count Threshold Times	54
Figure 4.37: Row 7 Fraction of Total Exposure Threshold Times	55
Figure 4.38: Overview of Cabin Particle Count Threshold Times	55
Figure 4.39: Overview of Cabin Fraction of Total Exposure Threshold Times	56
Figure 5.1: Rows 4 and 7 Total Exposure with Row Averages	74
Figure 5.2: Rows 4 and 7 Fraction of Reference Exposure with Row Averages	74
Figure 5.3: Centerline Particle Count Threshold Times with Linear Trend	75
Figure 5.4: Centerline Fraction of Total Exposure Threshold Times with Linear Trend	75
Figure 5.5: APS Comparison of Total Counts by Particle Size	76
Figure 5.6: APS Comparison Time Series, 60 Second Averaging	76
Figure 5.7: APS Comparison Time Series, 10 Minute Averaging	77
Figure 5.8: Normalization Effect Time Series	77
Figure 5.9: Particle Dispersion Visual Verification at 0.1 Second Intervals	78
Figure A.1: Cannon Control Program Front Panel	84
Figure A.2: First Level of the Wiring Diagram with Frame 1 in the Sequence	85
Figure A.3: Wiring Diagram, Frame 0 in the Sequence	85
Figure A.4: Wiring Diagram, Frame 2 in the Sequence	86
Figure A.5: Wiring Diagram, Frame 3 in the Sequence	86
Figure A.6: Full Cannon Control Program Hierarchy	87
Figure A.7: Front Panel of the DAQ Analog Out Program	88
Figure A.8: DAQ Analog Out Terminals	88
Figure A.9: DAQ Analog Out Wiring Diagram with sequence 0	89
Figure A.10: DAQ Analog Out sequence 1	89

List of Tables

Table 4.1: Total Exposure Particle Counts	35
Table 4.2: Fraction of Reference Exposure	36
Table 4.3: Particle Count Threshold Times	36
Table 4.4: Fraction of Total Exposure Threshold Times	36
Table 5.1: Example Data for Total Exposure Tests	72
Table 5.2: Pooled Deviations for Threshold Tests	72
Table 5.3: Normalization Effects on Centerline Tests	72
Table 5.4: Dispersion System Consistency Summary with Outlier Effects	72
Table 5.5: Dispersion System Consistency Data from Row 1 and 3 Exchange Tests	73

Acknowledgements

I would like to thank my friends and family for supporting me throughout the completion of this thesis. I would also like to mention I truly appreciate their continued encouragement and sacrifices made through all of my educational endeavors. I would like to thank the FAA and the ACER program in cooperation with Boeing for funding this project and making it all possible. I'm grateful for Dr. Fenton taking the time to be on my committee and agreeing to be part of this whole thing. I also wish to express my gratitude to Dr. Jones and Dr. Hosni for the guidance and patience I received during the last few years to see this project to its completion.

In addition to funding from the U.S. Federal Aviation Administration, the facilities used in this research were developed, in part, through funding from the Boeing Company and the Kansas State University Targeted Excellence Program.

The results presented in this thesis are from research funded by the U.S. Federal Aviation Administration (FAA) Office of Aerospace Medicine through the National Air Transportation Center of Excellence for Research in the Intermodal Transport Environment under Cooperative Agreement 07-C-RITE-KSU. Although the FAA has sponsored this project, it neither endorses nor rejects the findings of this research. The presentation of this information is in the interest of invoking technical community comment on the results and conclusions of the research.

CHAPTER 1 - Introduction and Literature Review

In recent years the world has been shifting toward a more connected and integrated society in which information and people can travel quickly across the globe. A key player in the transport of large numbers of people from one region to another is the continually growing airline industry. The development of the airline infrastructure continues through projects such as the Next Generation Air Transportation System. This development also means an increased risk of spreading diseases and contaminants more quickly, and over greater distances (ACER-CEO 2009). Whether this spread is accidental or of a malicious intent remains irrelevant, and a better understanding of contaminant spread in aircraft cabins is needed to help prevent epidemics.

To address this need in the commercial airline industry, the Federal Aviation Administration (FAA) acting through a cooperative agreement entitled, the National Air Transportation Center of Excellence for Research in the Intermodal Transport Environment, formed the Aircraft Cabin Environmental Research (ACER) Center. The experiments in this thesis are part of the “comprehensive and integrated program of research and development” in the aircraft cabin (ACER-COE 2009). Support for this type of research stems from the more than 710 million revenue passenger enplanements, which traveled more than 780 billion revenue passenger miles between February 2009 and January 2010 (BTS 2010). These numbers represent the international and domestic flights for the United States alone. Due to the large number of individuals spending time in commercial aircraft each year, concern has risen about the spread of diseases such as Severe Acute Respiratory Syndrome (SARS), Tuberculosis, Avian Influenza (H5N1), and Swine Influenza (H1N1). This concern along with others involving the health of both passengers and crew, have driven the various projects now in existence as part of ACER.

The topics of interest in the ACER program encompass 8 universities and 29 collaborators. This project, as part of the ACER program, focuses in the area of contaminant transport in an aircraft cabin. For the research of contaminant transport two approaches are being utilized, the first is computational fluid dynamics or CFD simulation and the second is the experimental collection of data in simulated aircraft cabins. While this project is separate from the previous works of (Lebbin 2006) and (Padilla 2008) at Kansas State University, they share similarities and it provides a reference for the creation of CFD models. All of the results

collected and presented in this thesis have come from the experimental collection of data within a simulated Boeing 767-300 aircraft cabin. The test cabin itself is part of Kansas State University's involvement in ACER and is an 11 row representation of the aircraft. Other previous projects in Kansas State University's ACER aircraft cabin include velocity measurements and tracer gas studies that are part of (FAA 2008). Results from previous tests in this simulated cabin are compiled and presented in (Jones 2009).

The conditions within the cabin are determined by the supply air provided and the heat generated by the mannequins in the cabin. The cabin air supply's temperature is 60 degrees Fahrenheit, as it is when it leaves the air conditioning packs on an actual aircraft (Hunt 2005). The flow rate of the supply air is 1400 cubic feet per minute (cfm) providing about 18 cfm for each of the 77 seats in the cabin, which is appropriate for this aircraft (Hunt 2005). The humidity of the air supplied is not a controllable element of this simulated cabin and meeting the 15 to 20 percent relative humidity observed on commercial aircraft, is not a possible at this time (ASHRAE 2007). The supply air is 100 percent outside air, and is passed through HEPA filters before entering the cabin. The airflow within the cabin is responsible for the distribution of the particles. For this thesis the tests focus on the longitudinal spread of fine particles released across an entire row

Fine particles as defined by the Environmental Protection Agency (EPA) are particles that have a diameter of less than 2.5 micrometers (μm). Particles of this diameter are of concern because they are believed to pose the largest health risks since they can lodge deeply into human lungs (NAAQS 2010). Bacterial and fungal spores as well as viruses when accompanied by sputum or saliva all have diameters between 1 and 2 μm (ASHRAE 2005b). Particles inhaled within the range 1 to 2 μm are most likely for deposition into the lobules in the lungs (Hatch 1961). While only 50 percent may settle in the respiratory tract at these diameters, even very low exposures can have adverse effects if the particulate matter is considered hazardous (ASHRAE 2005a). For this thesis, the particles measured have corrected aerodynamic diameters between 0.87 and 1.70 μm and categorizing them as fine particles.

As previously mentioned the release of the fine particles occurs across the width of the cabin. There are seven dispersion points, one in each of the seats in the second row. The release occurs over a short duration, initiated by a 15ms (millisecond) burst of air which causes the preliminary dispersion. The short duration of the spread occurs quickly to simulate the timing of

a sneeze or cough, which is well known to be less than one second in duration. Another affect of this quick dispersion, is that the particular air flows in the cabin at the time of the release can impact the movement of the particles. The goal of the short burst is also to release the particles in a local area quickly while maintaining the integrity of the cabin's own air flows. The tests cover both the total accumulation of fine particles from this release and the transient nature of the particles spread throughout the cabin.

The measurement of the dispersed particles occurs at 27 locations in the cabin. They are along the centerline of the cabin, across rows four and seven, and various seats in rows one, three, and five. In the first look at the spread of particles to these locations, the total counts throughout the cabin are compared. This comparison shows that particles released in row two dissipate over the cabin's full length to row 11. The counts at the farthest location are but a fraction of the highest counts occurring closest to the source. The results also show the spread across the entire width of the cabin at rows four and seven and that this spread is not necessarily even. The quantity of particles released is controlled and reasonably repeatable but the exact number remains unknown. Therefore, a reference location is used to normalize a series of tests from other locations. The normalized data show results similar to those found from the total exposure tests and in some areas amplify the trends observed.

The total counts and relative numbers from the tests utilizing a reference only reveal part of the picture available from the experimental data collected. Three different methods are chosen to present the transient behavior of the test data. The first method looks at the time series data from which quantitative results are not the goal, but rather an understanding of the way each location reaches its total count. With the time series results in mind, two different time limits or thresholds are used to quantify the rate at which the particles spread throughout the cabin.

Of the two threshold tests, the first is set by the amount of time required for each location to reach a total particle count, or total exposure, of 100 particles. The 100 particle limit is chosen since it is a value large enough not to occur from background counts and is small enough to remain applicable to all locations. The total exposure time limits show the particles released in row two traverse the length of the cabin to row 11, in less than five minutes. This time limit also shows a linear trend over most of the cabin's length, with variations across rows four and seven.

A second version of this total exposure threshold uses the total particle counts at each location as a reference. With this reference, the time limit is then established as the time

required to accumulate ten percent of the total counts observed. While this type of test does not have a direct real world application, it provides information useful for CFD modeling and comparison to other tests. The results from the percent of exposure tests are similar to those of the exposure limit tests, in which the longitudinal dispersion again shows a linear trend. The location farthest from the injection site, recorded ten percent of its total in just over three minutes on average. For this method of data evaluation, variations are again seen in the results across rows four and seven.

The results of the tests in this thesis are similar to those previously found in the same cabin and given in (FAA 2008). The dispersion throughout the entire cabin indicates the likely existence of a secondary flow, potentially in the aisles. Also the variations across rows four and seven are not unexpected, as the symmetric layout of the cabin doesn't necessarily translate into symmetric results (Hunt 1995) (Lin et al 2005a). The results suggest more tests need to be conducted to further the understanding of the complex flows within the cabin. The integration of this data and CFD models could eventually be used to predict the exposure risks in the case of an incident regardless of the intent.

CHAPTER 2 - Experimental Setup

The experimental setup for the tests summarized in this thesis consists of four general elements. These components are the testing chamber, air supply system, particle dispersion setup, and the particle measurement equipment. The testing chamber is constructed in a manner such that its interior cabin mimics the interior space of a Boeing 767 aircraft with a coach or economy class configuration. Ventilation for the chamber is provided by a blower, heater, chiller, and filter arrangement which is similar to systems commonly found in residential settings. Particle dispersion is achieved by utilizing compressed air to blow powder out of a series of small caps resulting in a puff of dust that has a sneeze-like timing. Finally the measurement of the particles is achieved by equipment specifically designed for the sizing of particles between 0.5 and 20 microns in diameter. All the elements of the experimental setup, as briefly explained above, will be discussed in greater detail in the following paragraphs.

2.1 Test Chamber

The test chamber is the largest physical element of the setup and is designed to simulate the interior geometry and conditions of a Boeing 767 aircraft cabin. As shown in Figure 2.1 the outside of the chamber appears to be a large box, and measures 32 feet long, 24 feet wide, and 16 feet in height. The chamber is comprised of 4 main spaces and 3 functional components. The spaces are divided into the crawl space, the cabin interior, and two hallways as illustrated in Figures 2.2 and 2.3. Included within these spaces are the air duct components, airliner chairs, and mannequins.

2.1.1 Spaces

The base of the chamber is a crawl space 45 ½ inches high, allowing access to the underside of the test section. The crawl space is used for distribution of electrical power and data cables. Prefabricated trusses and ¾ inch plywood decking cover the crawl space and provide a solid working surface for the rest of the chamber as shown in Figure 2.4.

A system of trusses and ribs constructed of ½ inch plywood provides the structure above the established floor. Figure 2.5 illustrates the design of the 17 plywood ribs that provide the interior cabin's shape. The centerline height is 6 feet 5 ¾ inches, the length is 31 feet 5 ¼

inches, and the width is 15 feet 6 inches at the widest point just above the arm rests of the seats. The specific details of the cabin's profile listed in (FAA 2008). The south end of the cabin is plywood and is painted on the interior surface. At the north end of the cabin there are two standard 36 inch wide exterior doors that provide access to the interior space of the cabin. The doors have weather stripping that provide a seal to preserve the integrity of the cabin air. The north end of the chamber also has a 2 inch hole for communication cables. The features of the north end of the chamber are shown in Figure 2.6. The contoured surface spanning the ribs and separating the cabin interior space from the hallways is galvanized steel sheeting. The interior surface of the metal has been painted antique white with ACE Royal Touch interior acrylic latex, flat wall paint to provide a more appropriate interior surface.

Located along either side of the interior cabin space are two hallways. They provide access to the exterior of the contoured metal surface, locations to install data acquisition systems, and play a key role in the exhaust of the air from the cabin. At both the north and south ends of each of the hallways are 36 inch wide exterior doors identical to those mentioned previously in the cabin. When the cabin doors are closed, as during an experiment, the only location air can pass from the cabin to the hallways is through a gap 5 inches high at the base of either side wall of the cabin. Figure 2.7 shows this gap along the bottom of the cabin walls. The hallways therefore play a role as part of the air duct system installed in the chamber.

2.1.2 Elements

The spaces that compose the test chamber contain and are in some cases integrated into three functional elements, the chamber duct work, seats, and mannequins. While the spaces of the test chamber provided the structure for the experiments, these next components provide the functionality.

2.1.2.1 Chamber duct work

The air duct system begins with an inlet at the south end of the chamber with a 10 inch diameter and is shown in Figure 2.1. After the duct passes through the south wall, it continues the length of the chamber and along the centerline above the cabin. The duct has 34 ports which connect it to the two diffusers via 3 inch clear smooth plastic hoses as shown Figure 2.8. Detailed dimensions, images, and diagrams of the distribution duct and diffusers are given in (FAA 2008). Both the duct and the diffusers are authentic elements from a Boeing 767 aircraft.

The duct and diffuser receive the supply air and distribute it to the two ports located 6 ½ inches on either side of the centerline of the cabin as shown Figure 2.9. Once the air enters the chamber, it exits into both hallways by means of the gaps along the floor on both sides of the cabin. These gaps shown in Figure 2.7 allow the air to exit the cabin in the same location it would on an actual aircraft. Once the air enters the hallway portion of the duct it rises and is drawn out the south end of the chamber by two fans. The fans illustrated in Figure 2.1 manage the positive pressure created on the cabin by the air supply system keeping it to a minimum. This is the last element of the chamber's air duct system and once the air leaves the chamber, it is not recirculated as 100% outside air is used for the cabin ventilation.

2.1.2.2 Seats

The interior space of the cabin contains two key elements, the seats and the heated mannequins. The seats are Boeing 767 seats and are all identical with the exception of the pattern of the fabric. An aluminum channel 1 inch by ¾ of an inch is used to adapt the seats to the floor in the cabin. The seats in the three chair configuration are 53 ¼ inches wide and 41 ½ inches wide in the two chair arrangement. Both are 42 ½ inches tall at the back and are organized into 11 rows with 7 seats in each row. All elements of the seats are dimensioned with greater detail in (FAA 2008). Each row is in a 2-3-2 configuration as seen in the cross-section of the cabin 2.10 as well as the overhead view 2.11. Further specifics of the seats individual locations are detailed in (FAA 2008).

2.1.2.3 Mannequins

All of the seats within the chamber are equipped with heated mannequins. The mannequins consist of two main elements. The inflatable mannequin and the heating element affixed to them. The inflatable mannequins are number 1724 male adult inflatable mannequins from Rubie's Costume Company. In order to best simulate human passengers the mannequins are wrapped with 82 feet of Omega TFCY-015 thermocouple wire which connects to 115 volt AC power. The wire attached to each mannequin produces 102 watts and is comparable to the total adjusted heat produced by a resting adult (ASHRAE 2005c). As shown in Figure 2.12 the wire is attached to the surface of an inflated mannequin with duct tape and then the mannequins are placed in the interior of the cabin. During this series of experiments mannequins producing a total of 6936 watts of thermal energy occupied 68 of the cabins 77 seats.

The power supply for the mannequins is from a set of custom extension cables designed purposely for the spacing of the rows. All the power circuits are protected by breakers, and in turn controlled by a two pole definite purpose contactor rated at 40 amps. The contactor is connected to a thermostat located on the rear wall of the cabin, which is wired in series with a pressure switch in the air supply system. The thermostat and pressure switch are safety measures designed to disable the mannequins when the internal temperature is too high or airflow into the chamber is too low.

2.2. Air Supply System

The air supply system represents the second major component of the overall experimental setup. It includes four pieces, the air handling, air conditioning, filter components, and the control system. The air handling system brings in outside air, passes it through the filter and air conditioning elements, and finally into the test chamber. The air conditioning system is responsible for the temperature control of the air supplied to the test chamber. Filters clean the air to suitable levels for the experiments conducted and the control system monitors and regulates aspects of the air conditioning and air handling systems.

2.2.1. Air Handling

The air handling system provides outside air to the chamber through two parts, the duct that directs the air and the fan which provides the necessary flow.

2.2.1.1 Duct

The three main sections of duct connect the various elements of the air supply system. All lengths of the ductwork are insulated and are shown in Figure 2.13. The first element brings outside air in from the intake to the fan and is 12 feet long with a diameter of 14 inches. The second section carries the air 12 ½ feet from the exit of the air conditioning system to a 90 degree bend and then another 5 feet to the HEPA filter box. This second section of duct is 16 inches in diameter. Once the air has passed through the HEPA filter enclosure it enters the third and final section of duct. A 90 degree bend and 13 feet of 16 inch duct carry the air vertically to the final 90 degree turn. There the diameter is reduced to 10 inches where the flow enters the test chamber.

2.2.1.2 Fan

To provide the air flow necessary the air supply system uses a 12 ¼ inch Dayton brand centrifugal fan. The fan is capable of providing 2020 cfm at 3.00 inches of water of static pressure. Power and regulation of the fan speed are provided from a variable frequency drive (VFD) as shown in Figure 2.14 along with the fan itself. The VFD is discussed in more detail in section outlining the control system.

2.2.2. Air Conditioning

While conditioning the air for use in the test chamber, interaction occurs with two systems. The first is a cross-flow heat exchanger, providing heat exchange between a water-glycol mixture and the air brought in from outside. When conditions require it, the bulk of the thermal exchange is done with the water to air heat exchanger. This allows the second system, an electric heater, to fine tune the supply air temperature.

2.2.2.1. Water-Glycol System

As mentioned, the water-glycol system provides the necessary energy exchange to bring the air to appropriate conditions to allow the electric heater system to function properly. To do so, the system is composed of three flow loops that all interact. The primary and cooling loops, both share the same 30 percent ethylene glycol and 70 percent water mix as the working fluid. The heating or third loop contains only water, is pressurized, and transfers energy to the primary loop through an Alfa Laval model CB27-18H compact plate heat exchanger. Figure 2.15 illustrates the first two loops and shows the interaction points between all three. The following paragraphs describe the properties of the individual components of the system. Specifications that are more extensive and the manufactures' data are found in (FAA 2008).

2.2.2.1.1. Primary Loop

The primary loop consists of the air to water cross-flow heat exchanger previously mentioned, a flow meter, a centrifugal pump, and a second heat exchanger. The first of these elements is a custom-built copper heat exchanger. It is 24 inches by 24 inches and 9 inches thick and acts as the only point in which heat energy transfers between the air and water-glycol mix.

A flow meter is located near the exit of the heat exchanger and allows visual monitoring of the flow rate. The flow meter is an Omega model FL7204. A centrifugal pump that operates

at fixed speed and drives the flow. After the water passes through the pump, it enters the second heat exchanger, the Alfa Laval compact plate heat exchanger previously mentioned. This heat exchanger transfers heat energy from the heater loop to the primary loop when required. Flow in the primary loop leaving this heat exchanger either returns directly to the air to water heat exchanger or blends with water flowing from the cooling loop. This occurs at the junction illustrated in Figure 2.15 and the shown valve controls blending of the primary and cooling loops. The valve is discussed in section about the control system. The flow from the blending junction returns to the air to water heat exchanger completing the loop. A system schematic, Figure 2.17, illustrates all of the main elements of the water-glycol system.

2.2.2.1.2. Cooling Loop

The cooling loop connects to the primary loop at the previously mentioned blending junction shown in Figure 2.15. The water that returns from this point flows directly into the Thermal Care model LQ2R1503 water chiller system. The water chiller capacity is 15.9 tons or 190,800 BTU/hr of cooling and can provide water between 30 and 65 degrees Fahrenheit. An internal pump circulates the water at a flow rate of 50 gallons per minute at up to 50 psi of pump pressure. Flow from the chiller passes through a King 7200 series flow meter allowing visual confirmation of the flow rate. The blending valve discussed in the Control Systems section, regulates the flow from the chiller into the primary loop.

2.2.2.1.3 Heating Loop

The interaction between the heating loop and the primary loop occurs at the second heat exchanger as described in the primary loop and shown in Figure 2.15. The flow exiting travels through 90 foot length of 1 inch diameter copper pipe insulated with standard foam pipe insulation along the west side of the building to the water heater. The heater is a Rheem Commercial Tankless Water Heater and has an operational output of 19500 to 199500 BTUs. The heater is equipped with Rheem Pronto model UMC-117 control panel that allows water at chosen constant temperature to be supplied to the heat exchanger. After exiting the water heater the water returns to the pump through a second section of insulated copper pipe similar to the first. The heater and its corresponding supply and return lines are shown in Figure 2.16. Upon return to the pump, the water is fed through the heat exchanger at a rate established by the speed of the pump. The centrifugal pump is controlled by a VFD operated by an attached computer

and described in the control system section. It should be noted that the heating loop is a closed loop and incorporates a pressure tank between the pump and heat exchanger to provide sufficient water pressure for correct operation of the water heater. The pump, pressure tank, and plate heat exchanger are all shown in Figure 2.15.

2.2.2.2. Electric Heater

Following the major temperature adjustment the inlet air receives from the water-glycol system, a variable but small amount of heating is required for fine temperature control. The electric heater, an AccuTherm DL6-9-3 duct heater, provides up to 9kW of thermal energy to reach the desired temperature for the air supplied to the test chamber. The heater operates on 220 volts and manufactures data is available in (FAA 2008). In addition, the control systems section describes the regulation of the electric heater's output.

2.2.3. Filters

The supply air for the cabin filtering occurs in two stages, the first stage is a coarse filter primarily for the protection of the equipment in the air supply system and the second stage is a HEPA filter for regulation of small particles in the chamber supply air.

2.2.3.1. Inlet Filter

The filters that provide the first stage of filtering are located in the plywood enclosure as shown in Figure 2.18. The enclosure itself allows outside air to be drawn into the system through a louvered entrance, then through two ACE 2025134 filters arranged in parallel providing 1000 square inches of cross-sectional area. These elements are shown in Figures 2.19 and 2.20, respectively. The outlet of the filter enclosure connects to the air handling duct described earlier.

2.2.3.2. HEPA

The second stage of filtering occurs after the air temperature is set by the air conditioning system and removes a sufficient number of particles from the supply air for these experiments. The filter housing measures 2 feet high, 6 feet long, and 4 feet wide with a 16 inch inlet and outlet. The enclosure is constructed with $19/32$ inch thick plywood, sealed at the corners with latex calking, and reinforced on the sides with 2x4 lumber. The exterior of the HEPA filter box is visible in Figure 2.1. The interior houses three HEPA filters arranged in parallel giving the

filters a total cross-sectional area of 12 square feet. This arrangement of HEPA filters is 99.97 percent effective on particles 0.3 μ m in diameter.

2.2.4. Control Systems

The regulation of the air handling and air conditioning systems are both integrated into a combined control system. The control system is essential for maintaining the proper air flow rate and temperature provided to the test chamber. Both air flow and temperature are measured and in turn controlled to meet specified set points.

2.2.4.1. Flow Measurement and Control

Measurement of the volumetric flow rate into the test chamber is achieved through the use of a straight length of duct of a known cross-sectional area and a pitot tube setup. Flow measurement occurs in the straight section of duct connecting the air conditioning system to the HEPA filters. The pitot tube is connected to an Omega, model PX653-0.1D5V, 0.1 inch differential pressure transducer. A second Omega, model PX653-05D5V, 5 inch differential pressure transducer is also used to compare the static pressure within the duct versus that of the atmosphere for density calculations. Both pressure transducers are in turn connected to the computer data acquisition (DAQ) system.

The computer program calculates the measured flow rate and compares it to the set point with a proportional-integral-derivative (PID) algorithm. Adjustment of the flow rate is achieved through the same program and DAQ system used to measure the flow. The DAQ system controls a Yaskawa GPD315/V7 VFD which powers the fan motor.

2.2.4.2. Temperature Measurement

Temperatures are measured in several different locations throughout the air conditioning system within the air flow and water-glycol loops. All temperature probes are connected to the computer software through the National Instruments Field Point DAQ system. Air temperatures are collected in three locations within the duct. The first is located in the duct between the inlet filter housing and the intake of the fan, and is referenced as the intake air temperature. The second air temperature sensor, or heater temperature, is located just downstream of the electric heater. The last air temperature reading is taken in the duct just prior to the air entering the test chamber at the cabin supply air inlet illustrated in Figure 2.1. This final, or supply temperature,

is read with an Omega 3-wire RTD model PR-10-2-100-1/4-6-E sensor, as is the intake air temperature.

Water-glycol temperatures are recorded at four locations, three in the primary loop and one in the heating loop. Within the primary loop temperature is monitored at both the supply and return sides of the custom water to air heat exchanger as well as the inlet to the plate heat exchanger. The temperature of the heating loop is monitored at a similar location just before the water in that loop enters the heat exchanger. All of the four water-glycol temperature monitoring points use the same model of Omega RTD sensors as mentioned with the air temperature measurement.

2.2.4.3. Temperature Control

The supply air temperature set point is reached by controlling two main elements, the temperature of the water-glycol in the primary loop, and the output of the electric duct heater. The goal of the primary loop is to bring the air temperature to a point suitable to allow the electric duct heater to fine tune the temperature to the set point.

2.2.4.3.1. Primary Loop Temperature Control

The primary loop, as described in the air conditioning section, receives its cooling and heating capacities from the cooling and heating loops, respectively. To provide cooling and reduce the temperature of the primary loop a Johnson Controls model VA-7152-1001 valve has a linear nature and is controlled by a PID controller. As the valve is opened it allows the water chiller to pump water into the primary loop upstream of the air to water heat exchanger.

In order to provide heat to the primary loop, the DAQ program controls a Yaskawa VS Mini VFD shown in Figure 2.14 and is connected to the pump in the heating loop. The motor speed is varied, supplying water at a set temperature at varying flow rates to the heat exchanger.

2.2.4.3.2. Duct Heater Temperature Control

The electric duct heater provides the last controlled temperature adjustment before the air enters the test chamber. The computer controls an Omega solid state relay through a pulse width modulating controller as part of the Field Point DAQ system. The desired output of the heater is calculated with a PID controller and converted to an appropriate duty cycle.

2.3. Particle Systems

This thesis concentrates on particles between one and two μm in diameter and their subsequent distribution in a passenger airliner cabin. The use of particles requires both a method for distribution and a means of measuring their displacement. Particle dispersion is achieved with the use of compressed air in a short burst to aerosolize the particulate matter. To measure the particles, instruments designed for particle sizing and counting are used.

2.3.1. Particle Measurement

To count and size the particles released in these experiments, two TSI Aerodynamic Particle Sizers are used. They are both model 3321 capable of sizing particle from 0.523 to 19.810 microns in diameter and separating the particles into 52 different categories within that range. The first modification to the APS units is the addition of an aluminum tube with an internal diameter of $\frac{3}{4}$ inch and 19 $\frac{1}{2}$ inches long on the inlet port. The tube is used to create a sampling location 46 $\frac{1}{2}$ inches above the floor when the APS' are in place. Secondly, a small piece of card stock is used to divert the outlet air from the cooling fans in the APS' toward the floor of the chamber. This redirection of the APS' outlet air is done to minimize it's effect on the cabin air motion. Also, a piece of $\frac{19}{32}$ plywood is placed under the APS' to allow for proper ventilation. The APS' are shown in Figure 2.21 in a typical test configuration. Both particle sizers are connected to a computer running TSI's Aerosol Instrument Management software setup to collect data for both instruments once a second. The software is used to communicate with the two particle sizers and the data is written to a text file for later analysis.

2.3.2. Particle Dispersion

The release of particles into the chamber is done in a controlled, repeatable manner, with a system of air nozzles and particle containers. The first element of the system is the injection setup which consists of a 17 inch long copper tube bent in a J shape with an internal diameter of $\frac{3}{16}$ inch. Compressed air is released downward into a $\frac{1}{2}$ inch PVC schedule 40 cap containing a metered amount of powder. The powder used as a testing agent in this thesis is talcum powder and is Equate brand mild baby powder manufactured by Vi-Jon. As shown in Figure 2.22, the compressed air leaves the copper tube in a downward direction and then is redirected upward by the cap, carrying the powder with it. This system was chosen for its simplicity and the easy ability to reset and run another test. Seven tube and cap assemblies are mounted across the

armrests of the seats in the row in which the dispersion occurs. Five of these injection points are shown in 2.23 installed in the cabin.

The compressed air used to propel the particles into the air is stored and released from charging tank made of 2-inch schedule 40 PVC. The tube is 19 inches long and the total internal volume of the charging tank, as shown in 2.24, is 71.4in^3 . The pressure regulator on the Craftsman model 919.167244 air compressor regulates the air provides at 60 psig to the tank through $\frac{3}{8}$ inch diameter air compressor rated hose. Both the charge and release valves mounted on opposite ends are triggered remotely through a National Instruments SCB-68 DAQ board and computer. The computer control of the particle release allows the timing between it and the data collection process to be coordinated.

A LabView program, as given in Appendix A, controls the charging and discharging of the tank. The program controls two Dayton solid state relays which control the power to the valves. They are both ASCO Red Hat valves and are normally closed. The fill valve is a model 8262G002 while the discharge valve is a model 8210G002. When the tank has been charged and a burst of air is released it exits through a distributor and a series of hoses. The distributor is a Hydroport distributor that operates with eight ports each with its own needle valve to restrict flow if necessary. Since only seven ports are needed the extra port is closed and unused for these tests. The outlets of the distributor are connected to seven equal lengths of hose, 97 inches long, one for each copper tube and cap.

In order to ensure the balanced release of particles in each of the seven locations, the charging tank, distributor, hose, tube, and cap were all tuned. The tube and cap assemblies were mounted along a black marked background. The system was loaded and discharged repeatedly with minor adjustments to the appropriate needle valves in the distributor. The resulting particles releases were filmed and replayed to ensure even rate and height and formation of the particle clouds. Once the system was calibrated to a satisfactory level it was installed in the second row of the cabin as previously mentioned and shown in Figure 2.22.



Figure 2.1: Chamber Exterior, Inlets, and Exhaust Fans



Figure 2.2: Chamber Hallways and Crawl Space



Figure 2.3: Cabin Interior

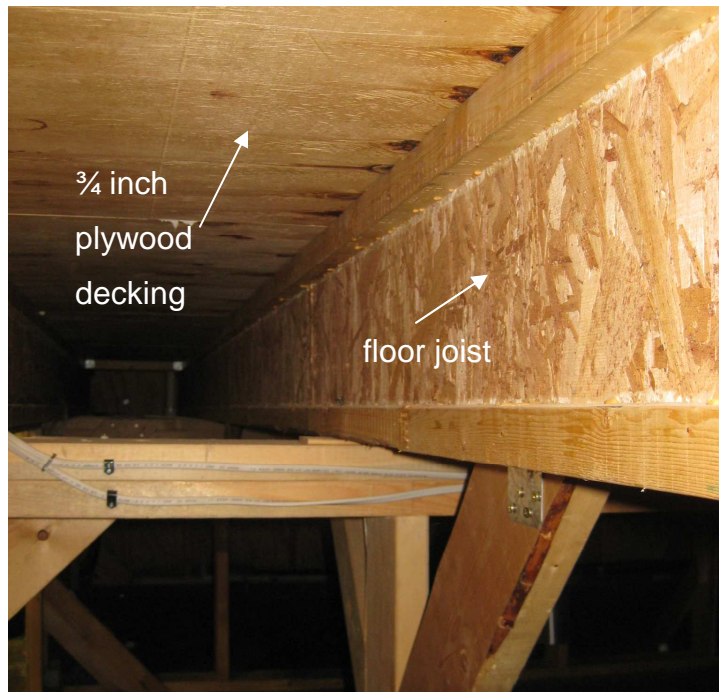


Figure 2.4: Chamber Floor Joist and Decking



Figure 2.5: Cabin Supporting Ribs

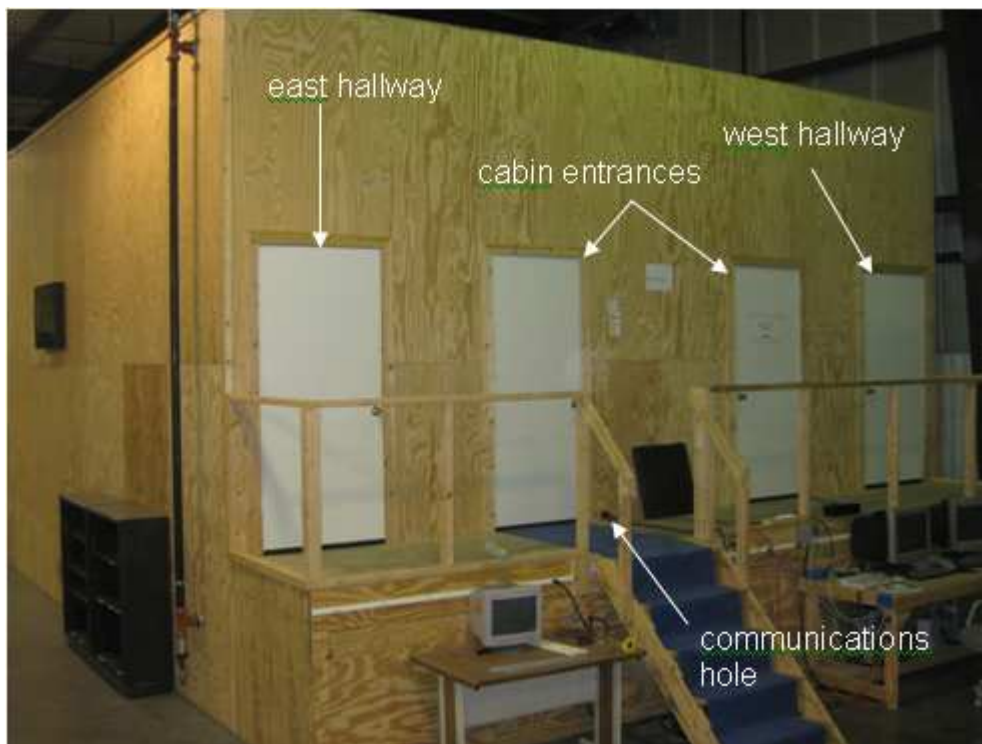


Figure 2.6: Chamber View from North End



Figure 2.7: Cabin Air Exits



Figure 2.8: Cabin Air Distribution Duct



Figure 2.9: Cabin Diffuser Outlets

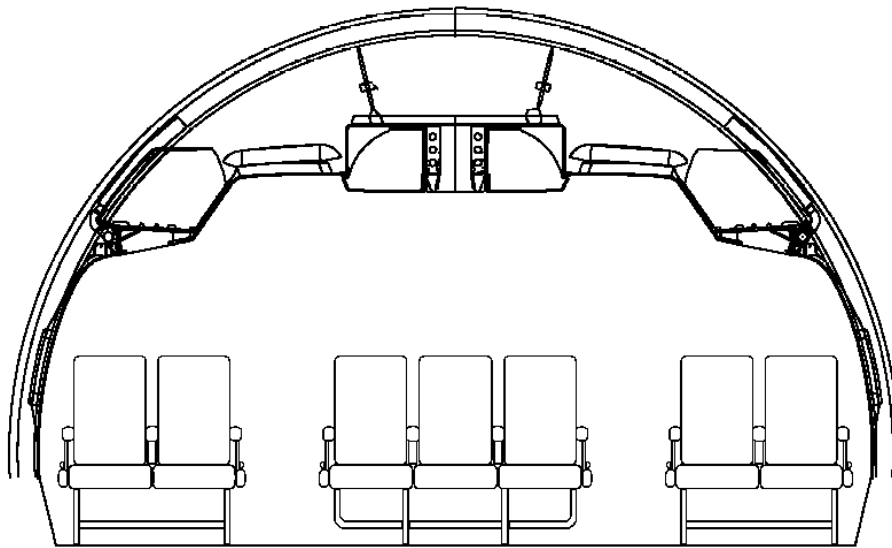


Figure 2.10: Cabin Cross-section

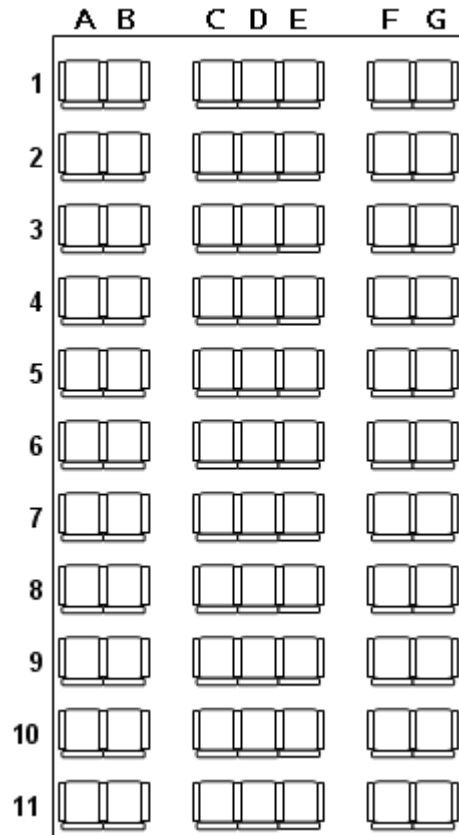


Figure 2.11: Cabin Overhead Seat Arrangement



Figure 2.12: Mannequin Seated in Cabin



Figure 2.13: Supply Air Handling System

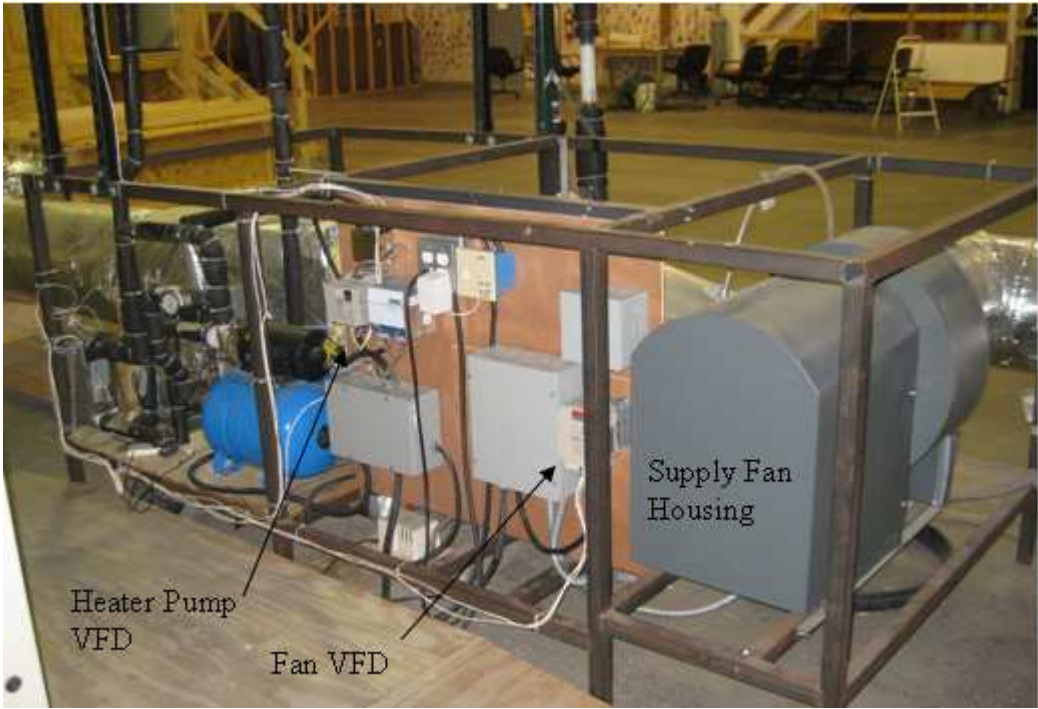


Figure 2.14: Supply Fan and VFD Controllers

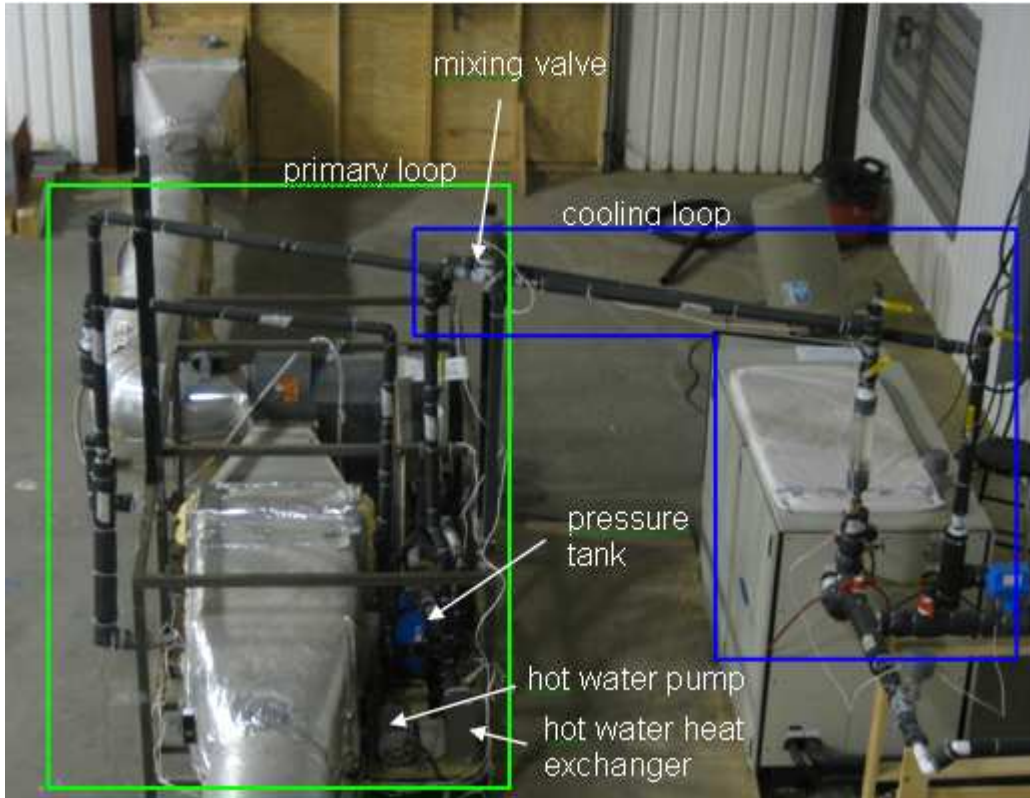


Figure 2.15: Primary and Cooling Loops of Air Conditioning System



Figure 2.16: Heating Loop Water Heater

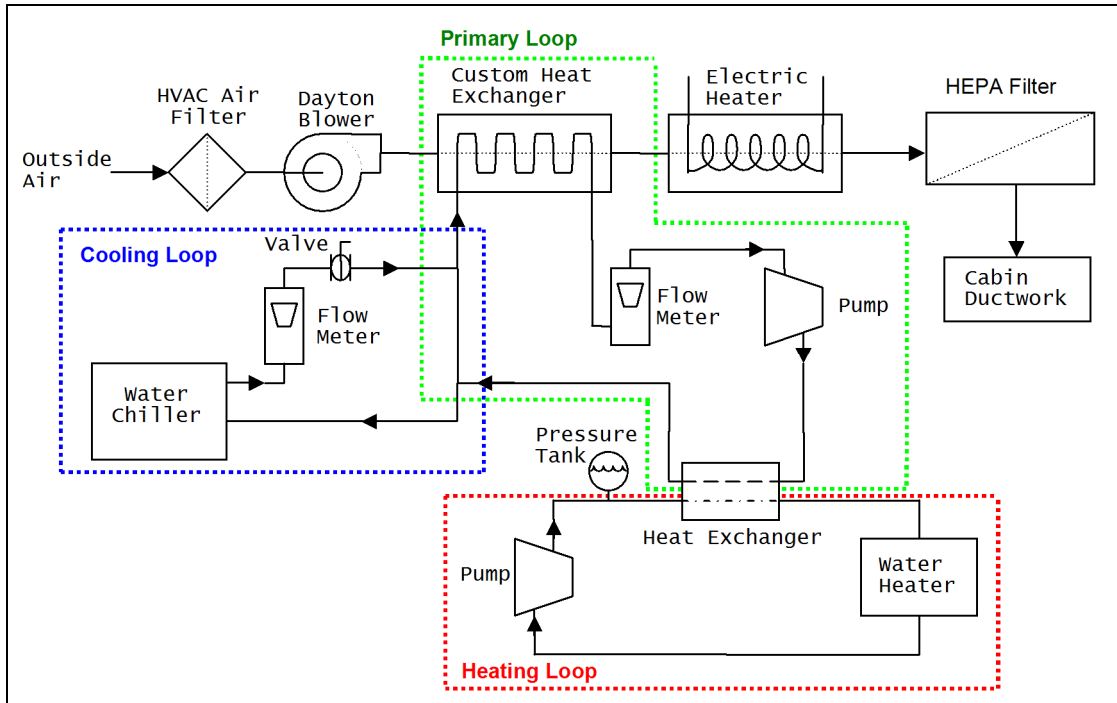


Figure 2.17: Water-Glycol System Schematic



Figure 2.18: Inlet Filter Housing



Figure 2.19: Supply Air Louvered Inlet

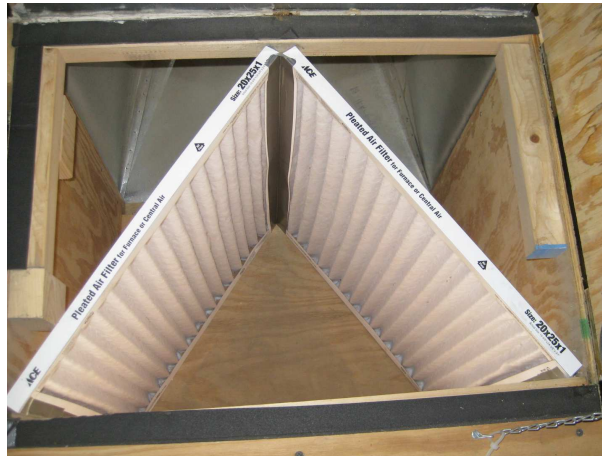


Figure 2.20: Inlet Filters



Figure 2.21: APS' in Testing Positions

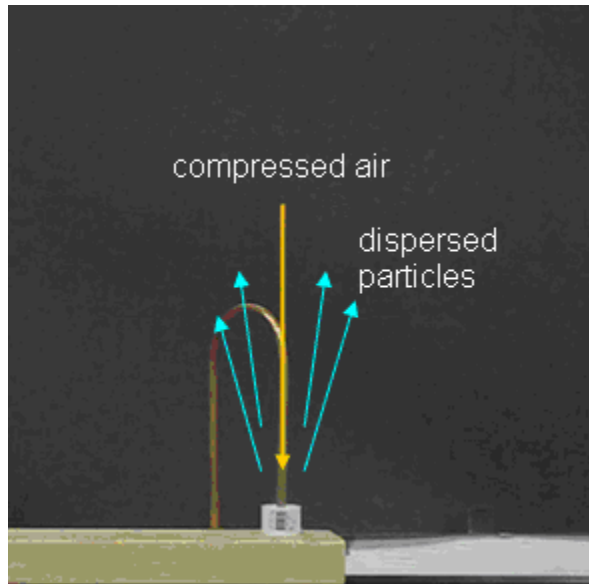


Figure 2.22: Particle Dispersion Cap and Air Nozzle



Figure 2.23: Particle Dispersion System in Row 2

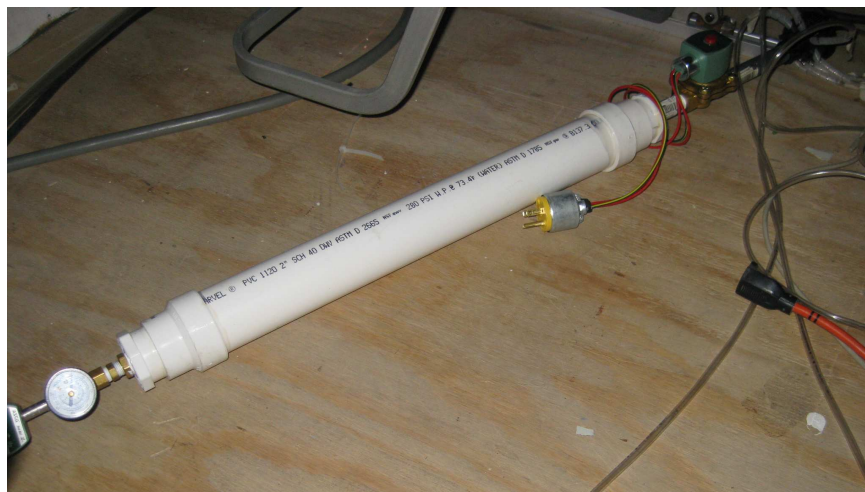


Figure 2.24: Charging Tank for Particle Dispersion System

CHAPTER 3 - Experimental Procedure

The experiments outlined in this thesis were run at operating conditions specified in the following paragraphs. The testing locations and procedures for preparation and data collection are also discussed in this section. When multiple tests are run, not all of the procedures here are repeated since the steps outlined in the preparation are for a scenario in which all the equipment is off. Once the chamber is running at steady state conditions and the equipment is performing in a satisfactory manner, only occasional monitoring of the operating conditions is necessary.

3.1 Equipment Setup

To run an experiment the test chamber conditions need to first be established and verified and then the test equipment inside the chamber needs to be prepared for a test. For all the tests run and experimental data collected for this thesis, the air supply system was set to supply air at a rate of 1400 cubic feet per minute (cfm) and a temperature of 60 degrees Fahrenheit. The flow rate of supply air and its temperature set point are based on (Hunt 1995). Before all tests, the air supply system and mannequins within the chamber are turned on and run for a minimum of 30 minutes to bring the internal surfaces to a steady state temperature. It should also be noted that all of the doors on the test chamber should remain closed while the chamber is brought to the testing conditions.

Once the test chamber temperature and air flow rate have stabilized, the test equipment needs to be prepared. The test equipment preparation consists of the particle dispersion system setup and the particle measurement placement. The specifics of the individual elements are described in the experimental setup section of the thesis. For the particle dispersion system, the pressure regulator is verified to be at a 60 psig and the charging tank is charged and the pressure is again verified at the tank. A release cycle is run and the charge tank pressure is again verified to have dropped to 45 psig. The remaining elements of the of the dispersion system are addressed after the particle measurement equipment is in place.

3.2 Testing Locations

For all the experiments conducted, particle sizing data was collected in two locations and repeated to improve the accuracy of the results. The overview of the test chamber, Figure 2.11,

labels the rows one through eleven and the columns A through G, this nomenclature will be used to describe the testing locations throughout the rest of the thesis.

Tests conducted within the cabin are separated into five different series that fall into two categories. Three series of tests were run with APS1 in seat 3D, the reference location for these tests, while APS2 was moved along three different paths. These three series of tests share a common reference location and are appropriately called, reference tests. Two additional series of tests were run with APS1 and APS2 in different seats and then they were switched and data collection repeated. The tests in which the APS units locations were swapped, are the exchange tests. At each location of an APS during a test, the mannequin that occupied that seat was removed from the chamber during the testing and then replaced for the next test. The process of mannequin removal and replacement was followed for all testing locations discussed in this thesis.

3.2.1 Reference Tests

The first series of reference tests utilized APS1 in seat 3D as previously stated, and APS2 was moved along the centerline of the chamber in seats 1D through 11D. Seats 2D and 3D since those were occupied by other equipment. Following the centerline test APS2 was positioned in the seats in row 7 for the second series. Data was collected in seats 7A through 7G and then APS2 was moved to row 4 for the final series of reference tests in seats 4A through 4G. Figure 2.11 is an overview of the chamber that illustrates the locations described above.

3.2.2 Exchange Tests

The first series of tests in which the APS units switch locations occurred in seats 5D and 5E. APS1 was placed in 5D with APS2 in seat 5E and then their locations were switched.

The final set of tests was run in seats B, D, and F, in rows one and three. For these tests the two APS instruments in the same column on opposite sides of the particle dispersion system. A test was run with APS1 in seat 1B and APS 2 in seat 3B. Then APS1 was placed in 3B and APS2 in 1B. This process was repeated for seats 1D and 3D, and 1F and 3F as well.

3.3. Test Preparation

Once the particle measurement equipment is in place for the particular test to be run the particle dispersion system setup could be completed. With the air charging and discharge elements verified the caps with particles are introduced.

Preparation of the caps starts with removal of excess powder from the measurement plate and empty caps. The plate is moved to the closed position and the talcum powder is loosely distributed across the top of the plate. A straight edge is used to remove any excess powder across the top of the plate. The excess powder removal is done such that the internal volume of the holes in the plate meter the powder. The plate is placed above the empty caps and slid to the open position then lightly tapped to release all the powder from the measurement plate. Figure 3.1 shows the measurement plate and cap loading tray.

Once loaded all seven evenly filled caps are now placed in the chamber under the appropriate nozzles. When the caps are placed under the nozzles the orientation of the nozzles should be verified to have a vertical orientation and the powder should be adjusted so it is centered in the cap. Since the chamber conditions, function of the discharge system, APS locations, and particles for dispersion have been verified, exit the chamber and ensure all doors are closed.

3.4 Data Collection

Once the cabin is prepped for a test, it is necessary to wait a minimum of ten minutes to allow any particles stirred up from activity within the cabin to be removed by the ventilation system and settling. The time was chosen after preliminary scenarios where a person would enter and exit the cabin while the APS units would monitor the particle activity. From this information, a ten minute delay is designed into the LabView program and the Aerosol Instrument Management software is set to begin collecting data at a chosen time using the computers internal clock. Once a time is chosen at least ten minutes after the chamber doors were closed, for example 1:15 pm, the LabView program's ten minute delay is started exactly at 1:05 pm. The APS software collects data for 16 minutes at a rate of 1 hertz and the data is written in a comma separated format file for later analysis. LabView is programmed to wait

another 60 seconds after the ten minute delay, before releasing a 15 millisecond burst of air to stir the particles. During these 60 seconds, the program is also set to fill the charging tank for the first 30 seconds. The 60 seconds from the test start to the release of particles allows for verification of the conditions in the chamber and establishment of a baseline. After the particles are dispersed, the 15 minutes of data collection is sufficient for the chamber to return to the baseline conditions.



Figure 3.1: Measurement Plate and Tray for Pre-Test Cap Loading

CHAPTER 4 - Results

This section presents the data collected for this thesis and was collected in two series of tests, reference tests and exchange tests as described in the Experimental Procedure. The data are categorized into exposure results and time series results. The two categories are further divided to present the data in detail to provide more insight. The averaging, normalization, and 95% confidence intervals associated with the data are explained in the data analysis section. It should be noted all confidence intervals are the 95% certainty band for the average.

4.1. Exposure Tests

The exposure tests focus on the accumulated particle counts for the entire duration of the 16 minute tests from both the reference tests and exchange tests. The results are given in two forms; the first is for the average total number of particles counted. The second is the number of particle counted at each location relative to the number accumulated in seat 3D during the same test. The normalized data are used to find the total number of particles at each location.

4.1.1. Total Exposure

The average of the total particles counted at each of the 27 different locations is given in Table 4.1. The data for the centerline of the cabin, seat D, in rows 1 and 3 through 11 are shown in Figure 4.1 and rows 6 through 11 are repeated in Figure 4.2 for clarity. For both figures the total particle count is given along the vertical axis with the rows across the bottom.

Row 4 and row 7 data are similarly represented in Figure 4.3 and Figure 4.4, respectively, with the total particle counts on the vertical axis and the seats across the bottom. Rows 1, 3, and 5 also have multiple tests taken within those rows. Seats B, D, and F in rows 1 and 3 as well as seats D and E in row 5 are represented in combination with the row 4 and 7 data in Figure 4.5.

The culmination of the average total particles counted at each location is graphically represented in Figure 4.6. The exact values for the columns shown are given in the previously mentioned Table 4.1.

4.1.2. Exposure as a Fraction of the Reference Location

The data for this section are collected only from the tests defined as reference tests in the Experimental Procedure. Table 4.2 lists the average fractional exposure for each of the 22 locations included in the reference tests. The fractional exposure from a single test is calculated with the following equation.

$$F = \frac{C_{loc}}{C_{ref}} \quad (4.1)$$

where, C_{loc} is the total counts at the location of interest
 C_{ref} is the total counts at the reference location

The graphs of the data all give the fraction of seat 3D particle counts on the vertical axis with the appropriate row or seat given across the horizontal axis. The centerline data for rows 1 and 3 through 11 is shown in Figure 4.7 with focus on rows 6 through 11 in Figure 4.8. The data point in row 3 is exactly 1 and as it is the reference point for each test.

The fractional exposure across row 4 is given in Figure 4.9 and row 7 follows in Figure 4.10. Row 4 and row 7 are combined in Figure 4.11 to show the data on the same scale. A collective view of all the reference tests is given in Figure 4.12 and represents the values from Table 4.2.

4.2. Time Series Data

The time series data looks at the transient nature of the particle counts at 22 locations in the cabin. The time scale for all tests starts at minus 60 seconds such that the release of particles occurs at time zero. The results are shown as a trailing average curve, as the integration of the total counts, and as an integration of the fraction of the total exposure. The fraction of total exposure normalizes each test against its own total by Equation 4.2.

$$f_i = \frac{c_i}{C_{loc}} \quad (4.2)$$

where, f_i is the fraction at time i
 c_i is the accumulated particle counts at time i
 C_{loc} is the total particle count at that location

4.2.1. Centerline Time Series

The time series plot for the centerline of the cabin in rows 1 and 3 through 11 is shown in Figure 4.13. The same data is shown again in Figure 4.14 with the vertical axis scale reduced from 200 to 20 average particle counted. Figure 4.15 gives the cumulative particle counts for the centerline seats and Figure 4.16 is cumulative fraction of the total particles for each location. Note the cumulative fraction grows to a value of one for all location since they are all scaled against themselves.

The average time required to reach the 100 total particles counted threshold at each location along the centerline is given in Figure 4.17. Rows 1 through 5 are shown again in Figure 4.18 with the time scale on the vertical axis reduced from 360 to 60 seconds. Figure 4.19 shows the time to reach a threshold of one-tenth (0.1) the total particles counted at each location in along the centerline and Figure 4.20 focuses on rows 1 through 5 only.

4.2.2. Row 4 Time Series

The time series of the particle counts across row 4 are shown in Figure 4.21. For each of seven seats in row 4, the curve in Figure 4.21 represents the average behavior at that location. The individual averages are shown in Figures 4.22 through 4.28 along with the separate tests and resulting average associated with seats 4A through 4G, respectively. The integration of average curve with respect to time for each location is presented in Figure 4.29 and in a similar manner the cumulative fraction of the total exposure is shown in Figure 4.30.

Utilizing the growth data shown in Figures 4.29 and 4.30, the elapsed time to reach an accumulated particle count limit of 100 particles is given in Figure 4.31. As with the centerline seats, the time for each row 4 location to reach one-tenth of its total exposure is given in Figure 4.32.

4.2.3. Row 7 Time Series

The presentation of the row 7 time series data is of the same structure as the centerline and row 4 data. Figure 4.33 shows the average time series for each of the seats across row 7. Again, the integration of particle counts in row 7 are given in Figure 4.34 and then represented as a fraction of the total exposure at each location in Figure 4.35.

The time to reach the predetermined limits of 100 total particles counted and one-tenth of the total exposure for the row 7 seats are once again obtained from the integration data just

mentioned. The times are given with the 100 particle threshold in Figure 4.36 and the one-tenth exposure threshold in Figure 4.37.

4.2.4 Threshold Time Data

The time necessary for varying locations within the chamber to reach both a given number of counts and a fraction of the total exposure is explained in the sections for the centerline, row 4, and row 7 data. A compilation of the information in Figures 4.17, 4.31, and 4.36 is given with a three dimensional perspective in Figure 4.38, illustrating the time to accumulate 100 particles counted at each of the 22 locations tested. Figure 4.39 is a compilation of the data in Figures 4.19, 4.32, and 4.37 and again shows all 22 locations, but with the time elapsed to reach one-tenth of the total exposure in each seat. It should be noted the orientation of the images are deliberately different than the representation of the total exposure in Figures 4.6 and 4.12 since the time data grows toward the rear of the cabin. The average values for each seat are used to create Figures 4.38 and 4.39 are given in Tables 4.3 and 4.4.

Table 4.1: Total Exposure Particle Counts

Average Particle Counts							
	A	B	C	D	E	F	G
1		15687		13538		17400	
2							
3		5297		10597		10471	
4	3187	3514	6168	5469	8192	7587	6951
5				5028	4576		
6				2094			
7	1442	1087	1067	2068	2529	1317	1437
8				956			
9				837			
10				736			
11				397			

Table 4.2: Fraction of Reference Exposure

Average Fraction of Reference Exposure							
	A	B	C	D	E	F	G
1					1.43		
2							
3					1.00		
4	0.36	0.29	0.50	0.49	0.90	0.55	0.46
5					0.43		
6					0.21		
7	0.15	0.12	0.14	0.20	0.22	0.15	0.14
8					0.09		
9					0.07		
10					0.07		
11					0.03		

Table 4.3: Particle Count Threshold Times

Average Time To Accumulate 100 Particles							
	A	B	C	D	E	F	G
1					6.3		
2							
3					18.4		
4	60.7	41.7	22.3	35.0	19.3	27.3	29.0
5					45.5		
6					84.3		
7	107.7	128.7	113.3	85.0	82.3	93.3	95.0
8					127.5		
9					160.0		
10					178.3		
11					235.5		

Table 4.4: Fraction of Total Exposure Threshold Times

Average Time to Accumulate 10% of Total Exposure							
	A	B	C	D	E	F	G
1					12.7		
2							
3					29.3		
4	82.0	61.7	42.0	53.8	31.7	48.0	44.3
5					64.5		
6					98.7		
7	119.0	132.7	115.7	97.7	96.7	95.3	103.0
8					126.0		
9					153.0		
10					162.7		
11					183.0		

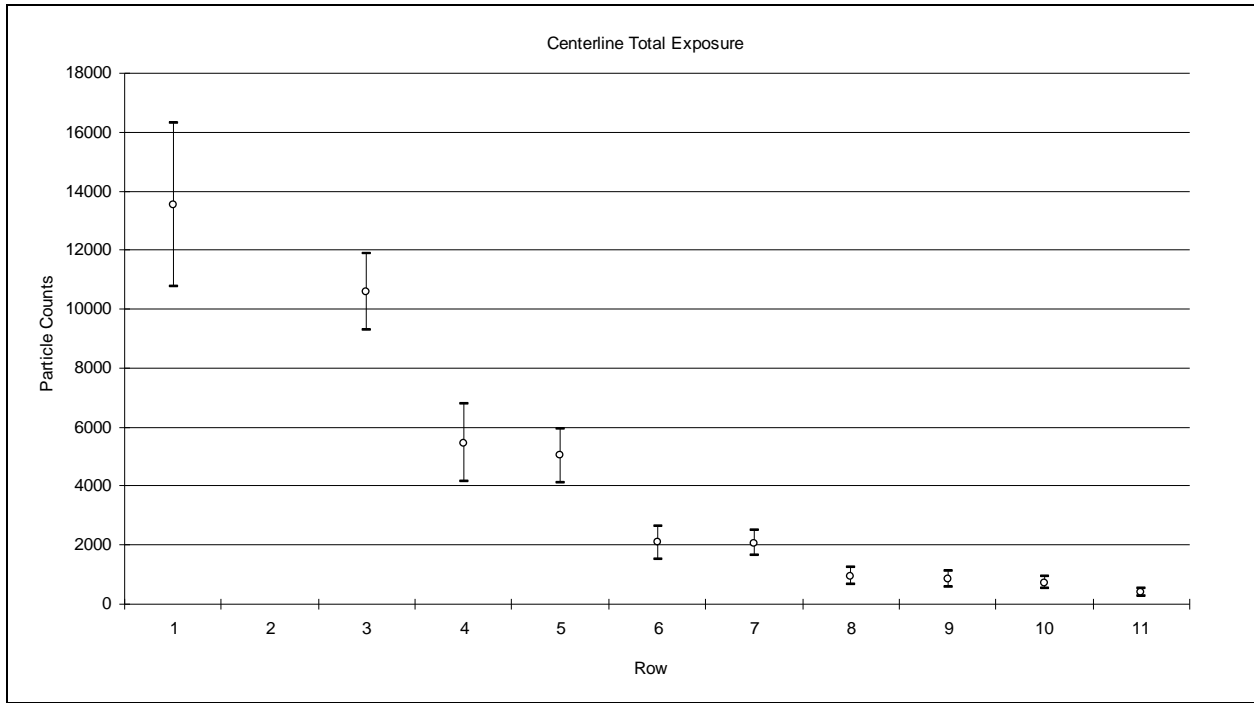


Figure 4.1: Centerline Total Exposure

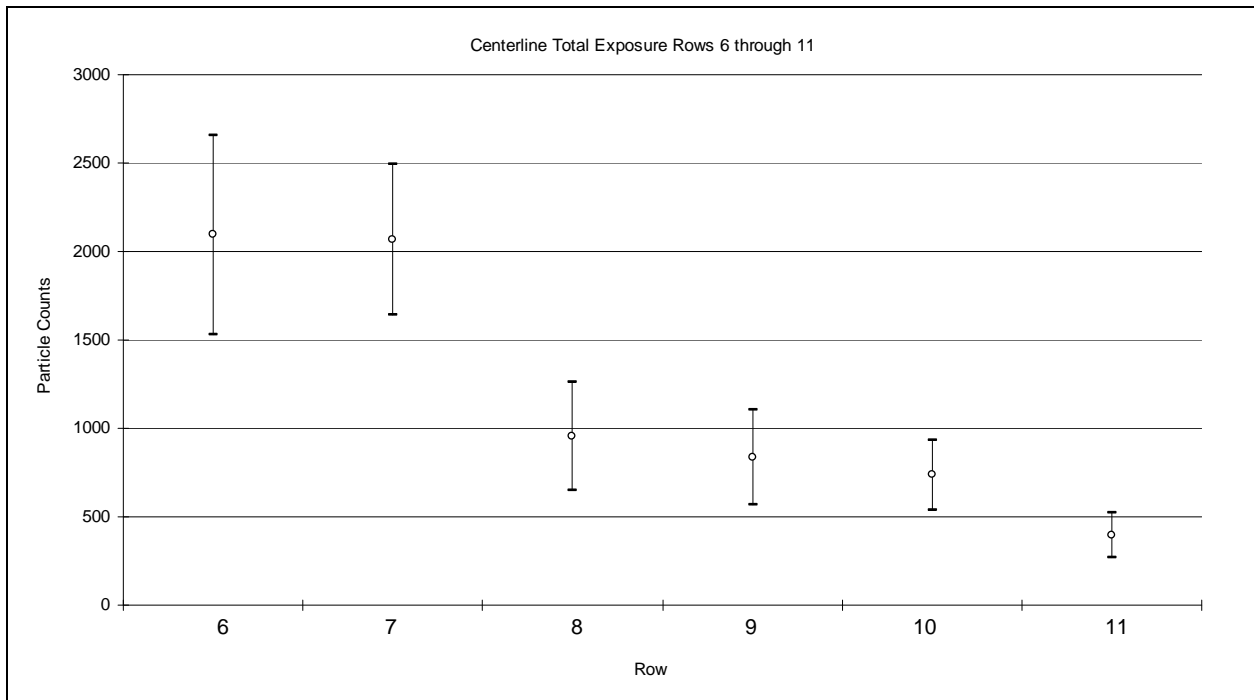


Figure 4.2: Centerline Total Exposure, Rows 6 through 11

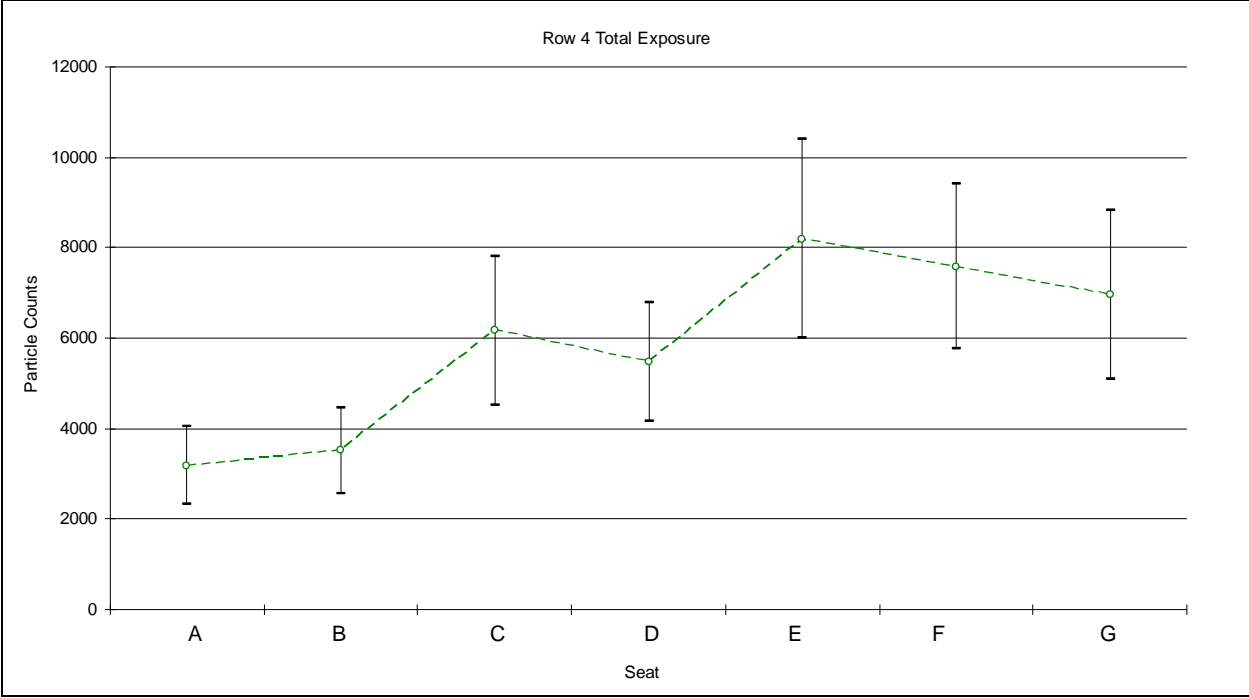


Figure 4.3: Row 4 Total Exposure

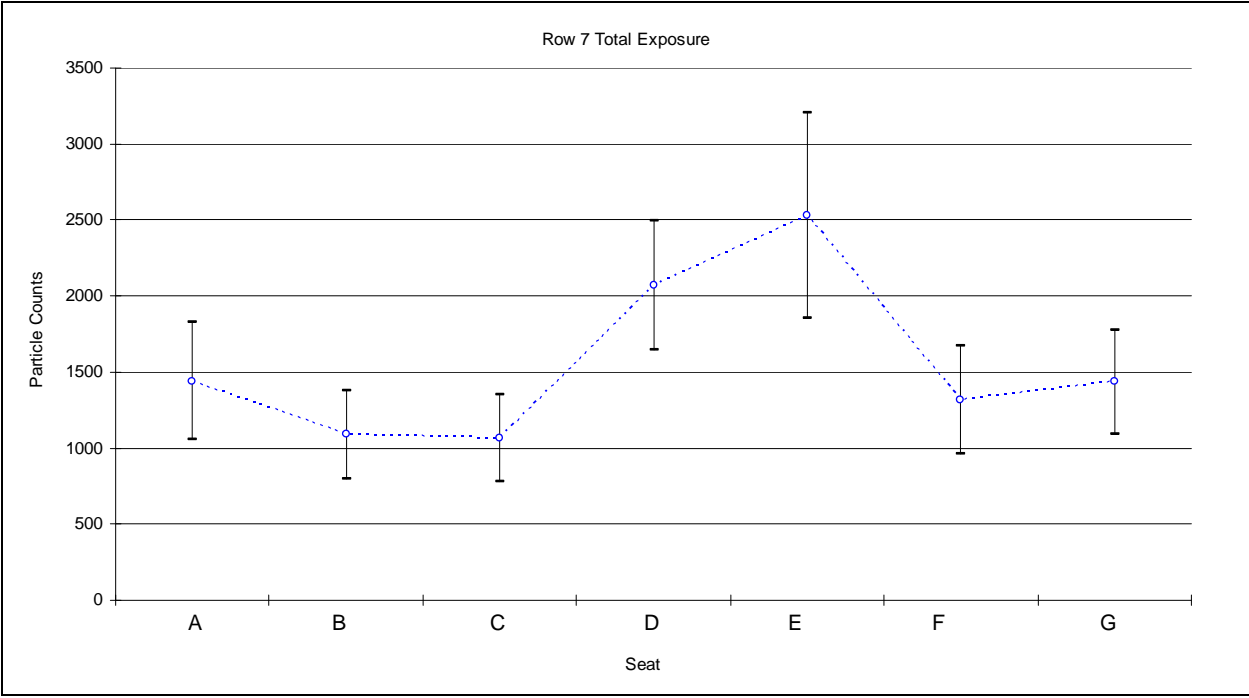


Figure 4.4: Row 7 Total Exposure

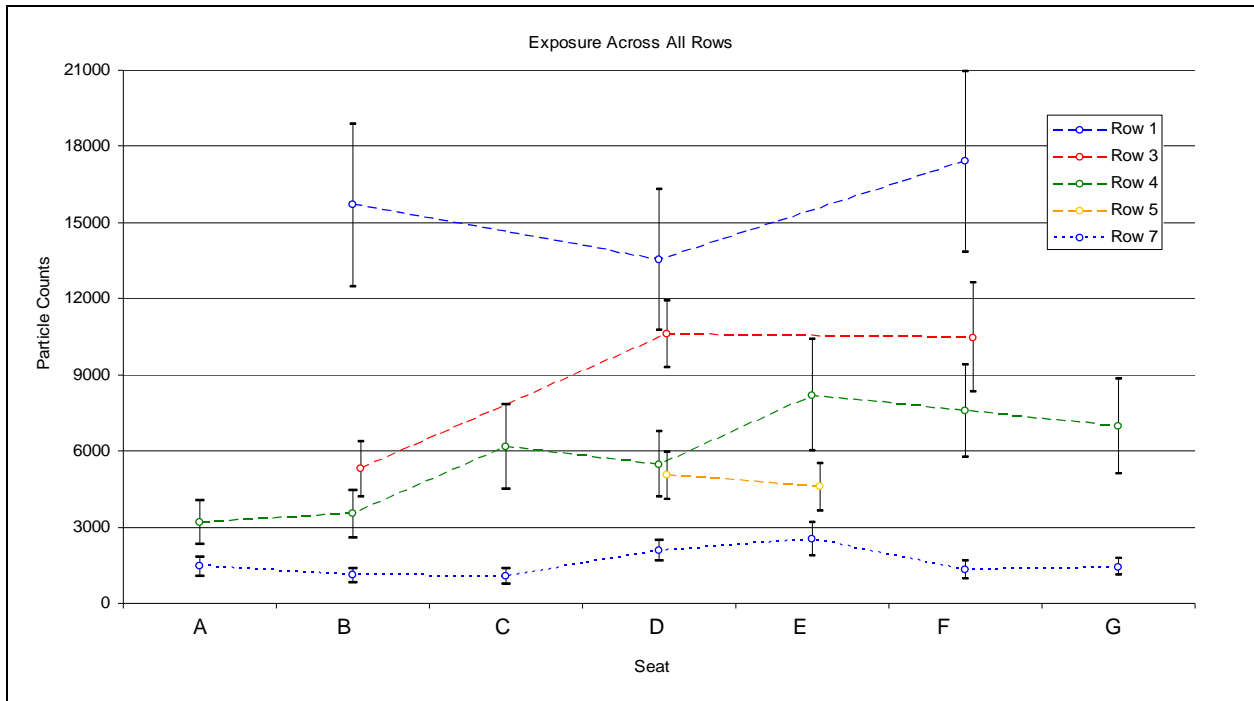


Figure 4.5: All Rows Total Exposure

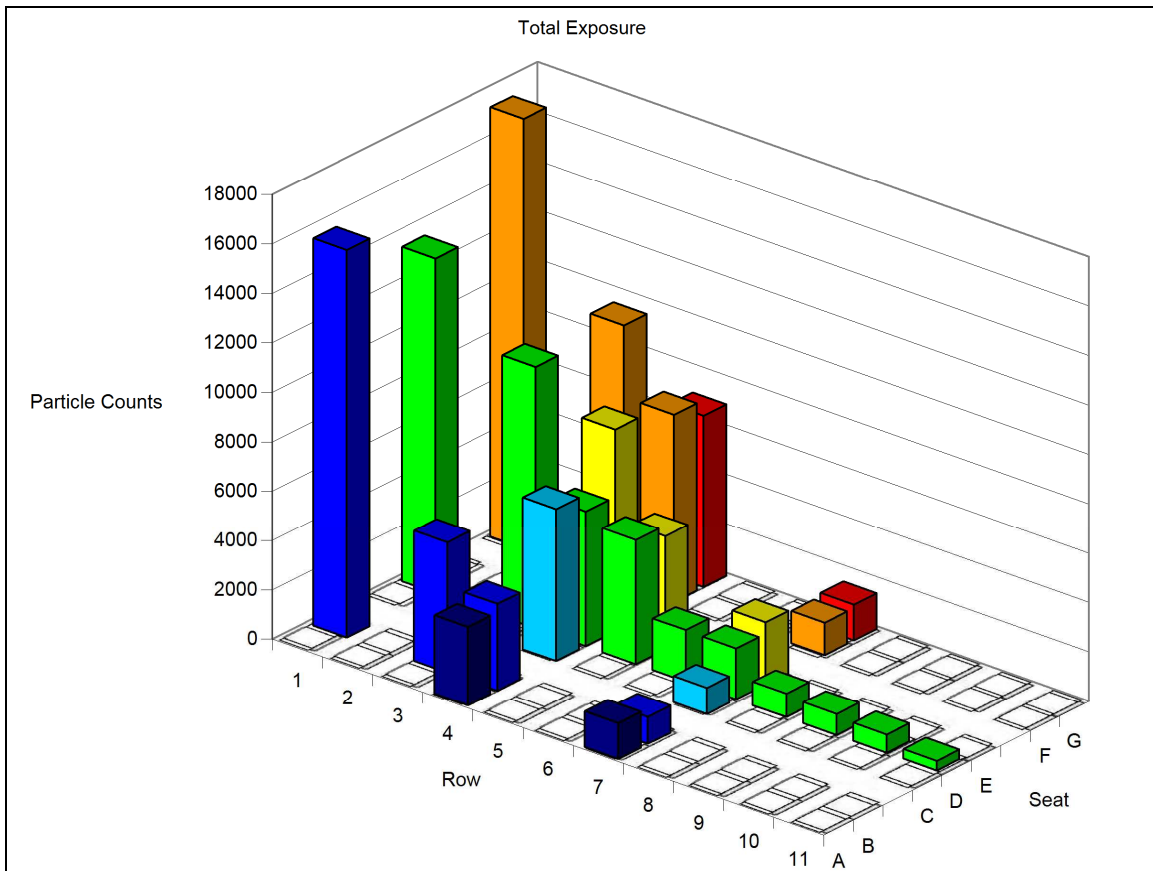


Figure 4.6: Overview of Cabin Total Exposure

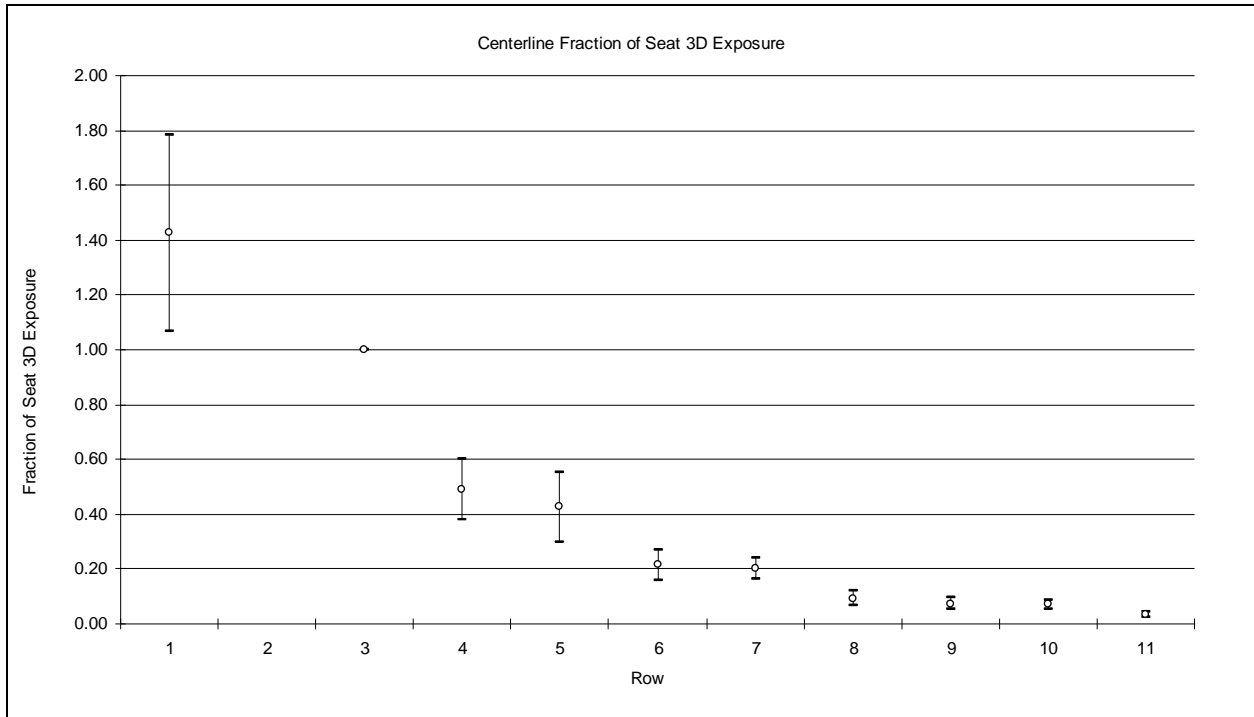


Figure 4.7: Centerline Fractional Exposure

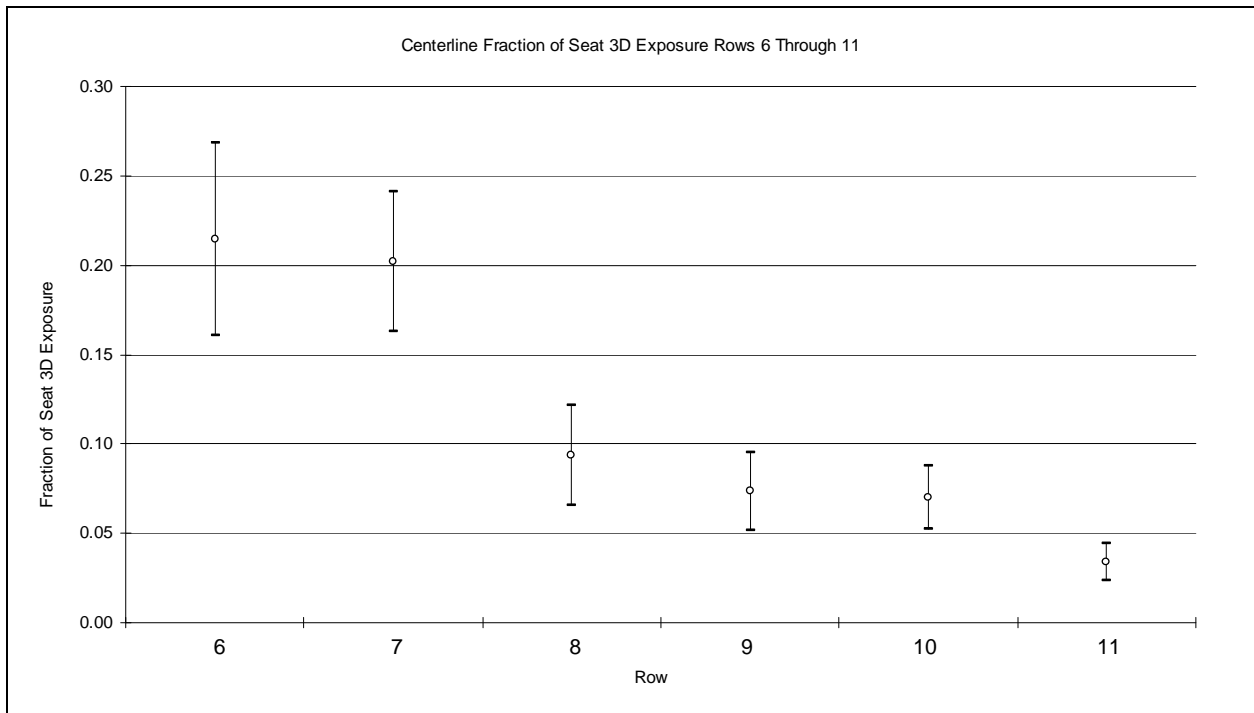


Figure 4.8: Centerline Fractional Exposure, Rows 6 through 11

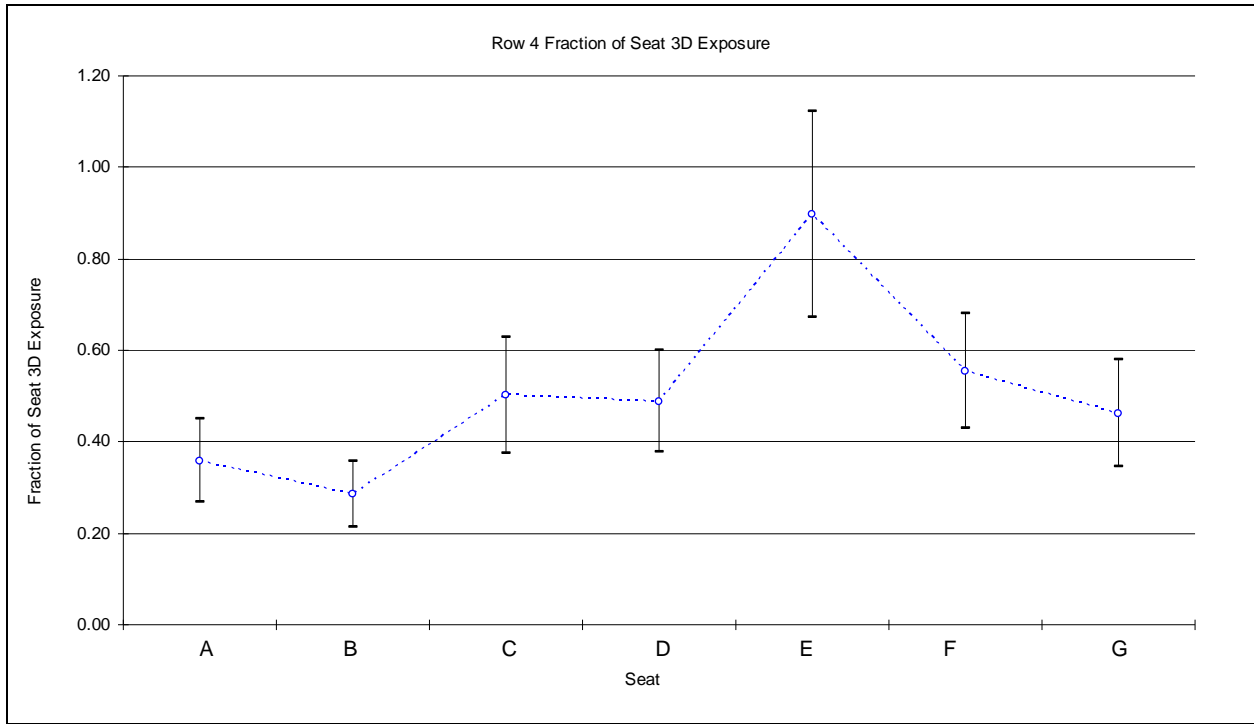


Figure 4.9: Row 4 Fractional Exposure

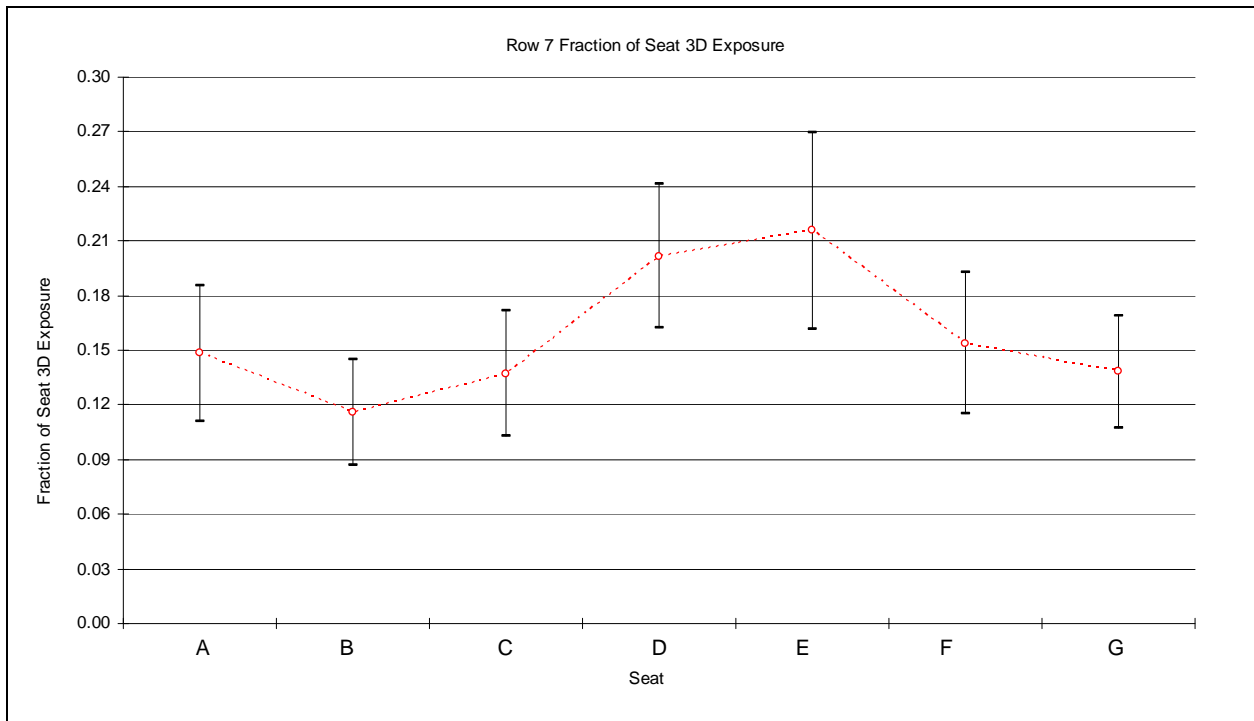


Figure 4.10: Row 7 Fractional Exposure

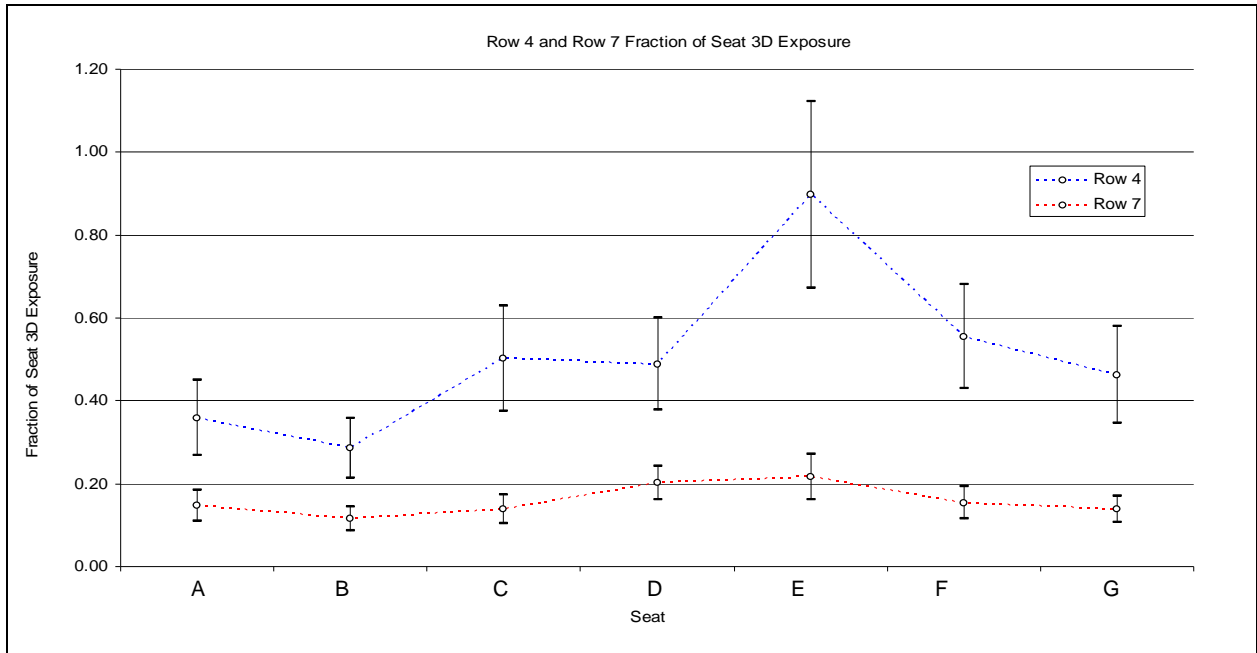


Figure 4.11: Rows 4 and 7 Fractional Exposure

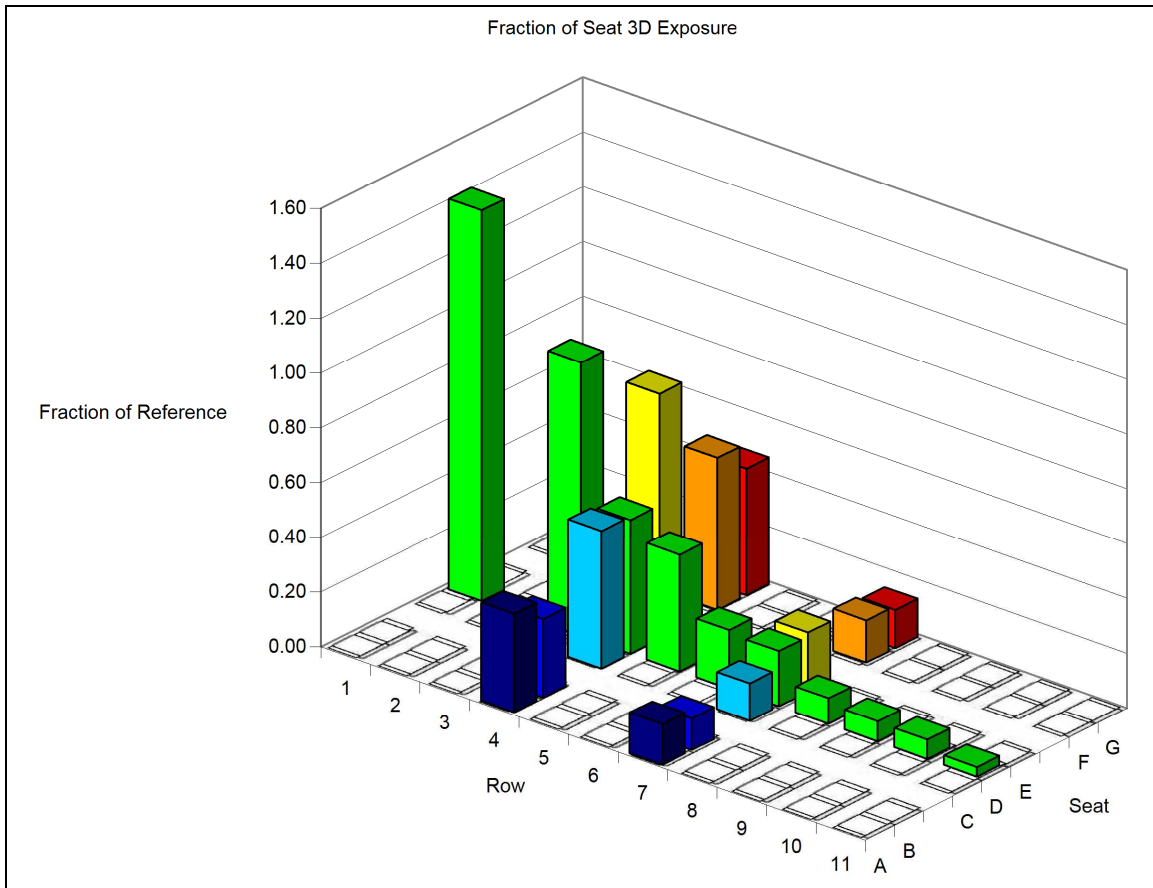


Figure 4.12: Overview of Cabin Fractional Exposure

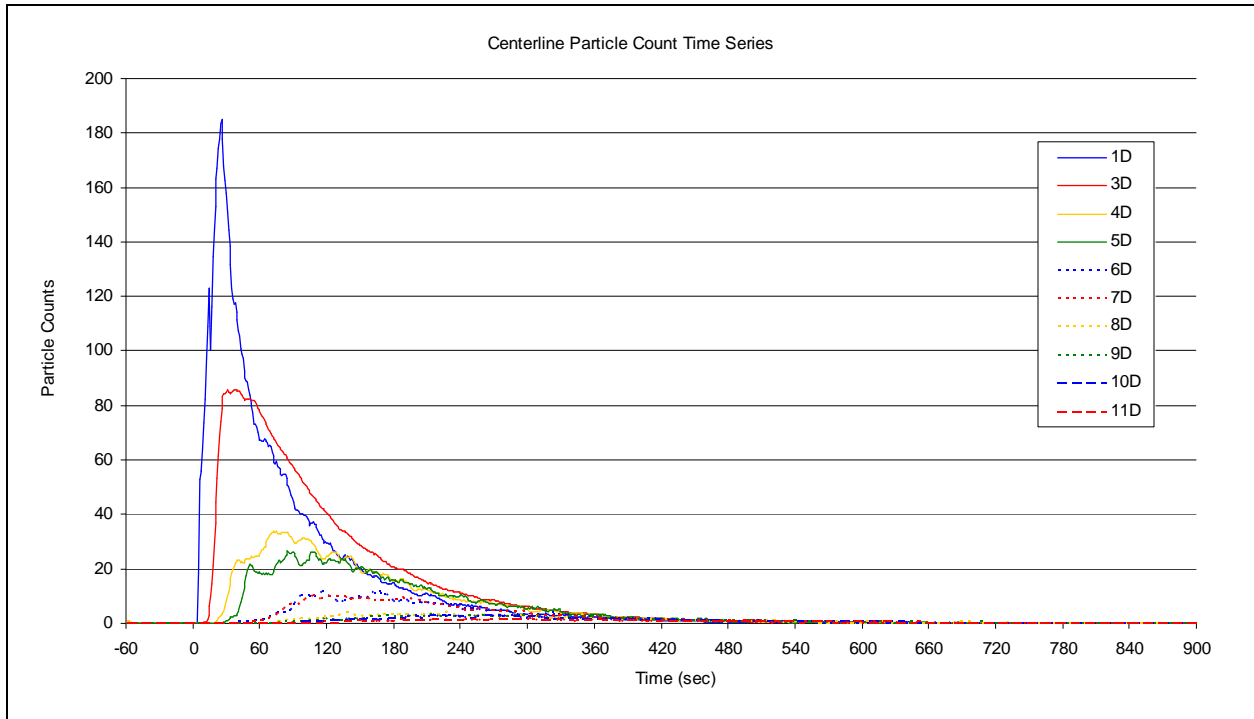


Figure 4.13: Centerline Particle Count Time Series

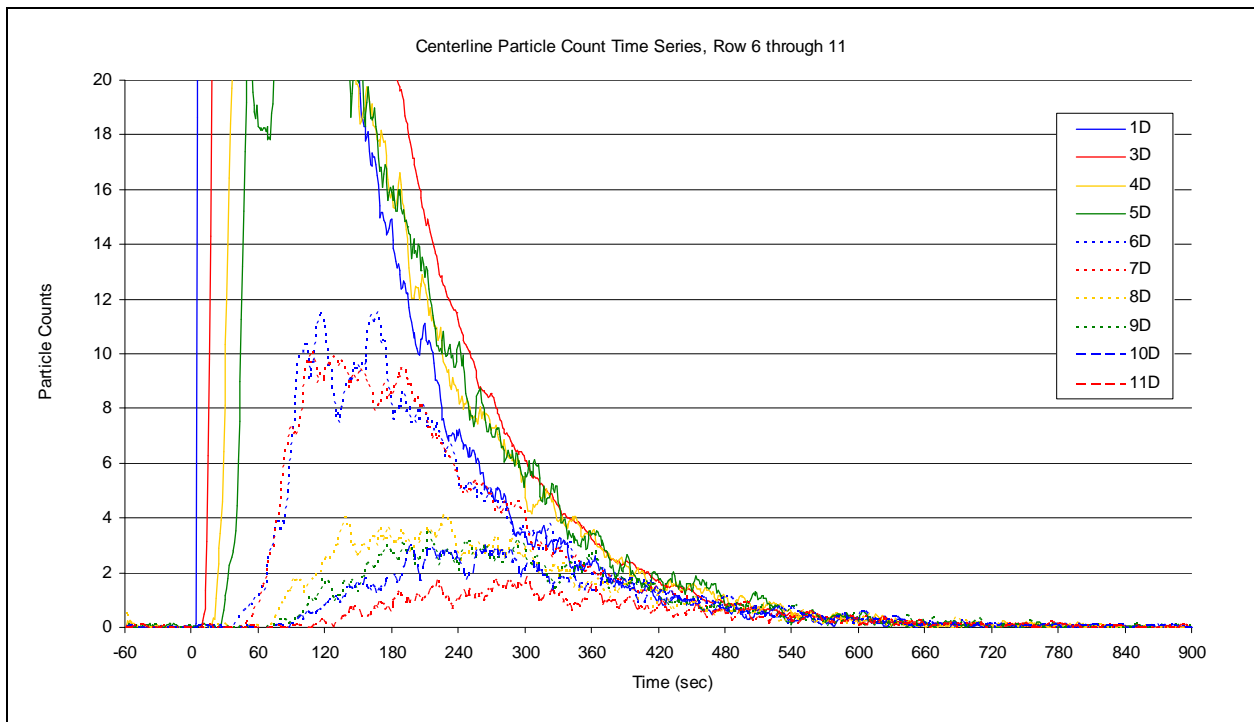


Figure 4.14: Centerline Particle Count Time Series, Reduced Count Scale

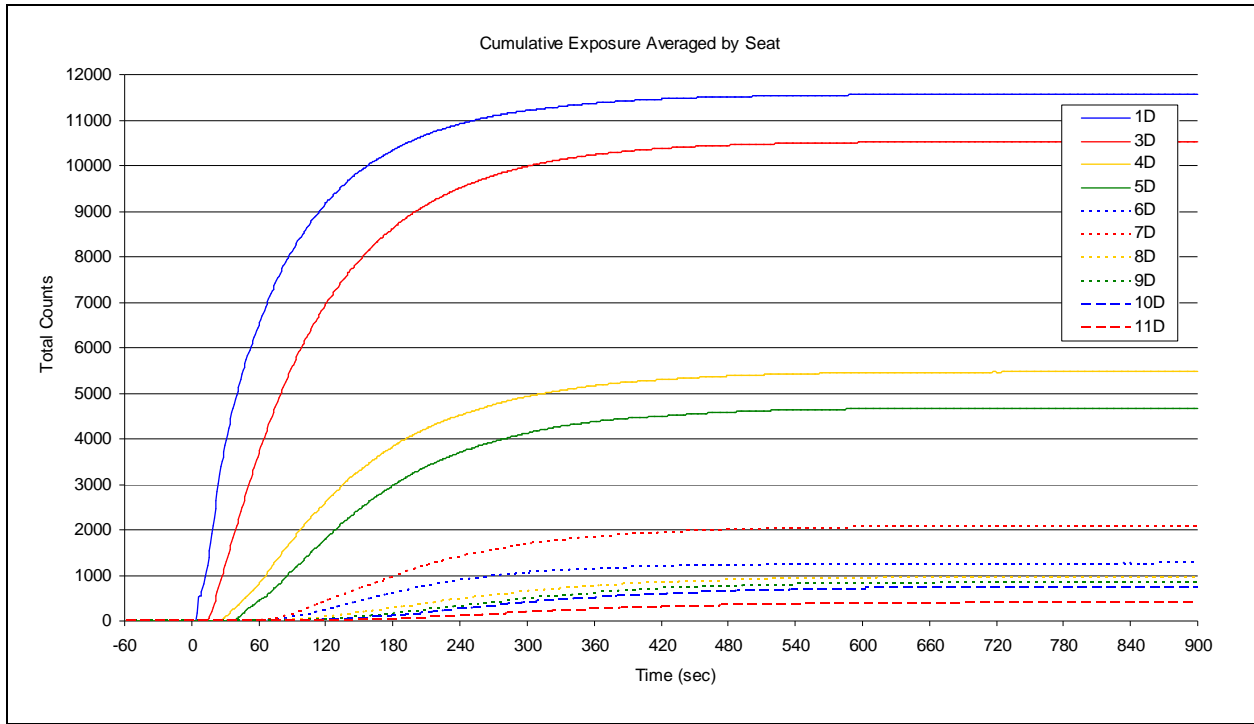


Figure 4.15: Centerline Cumulative Exposure

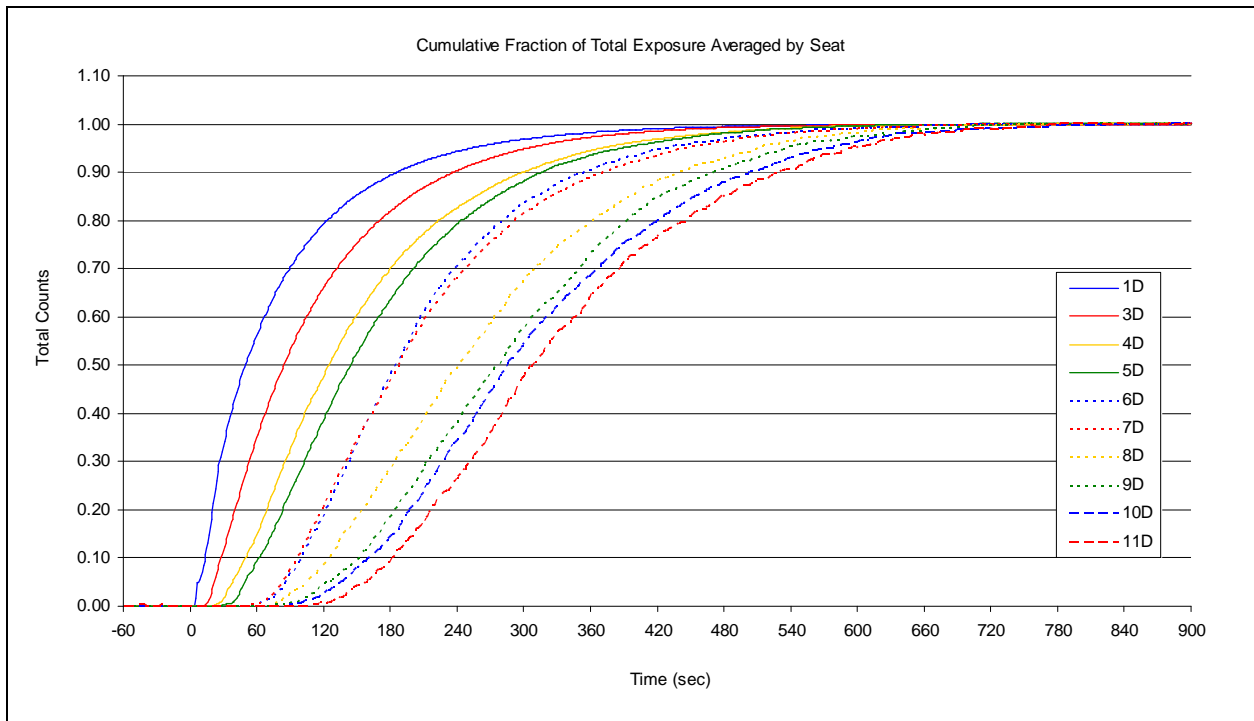


Figure 4.16: Centerline Cumulative Fraction of Total Exposure

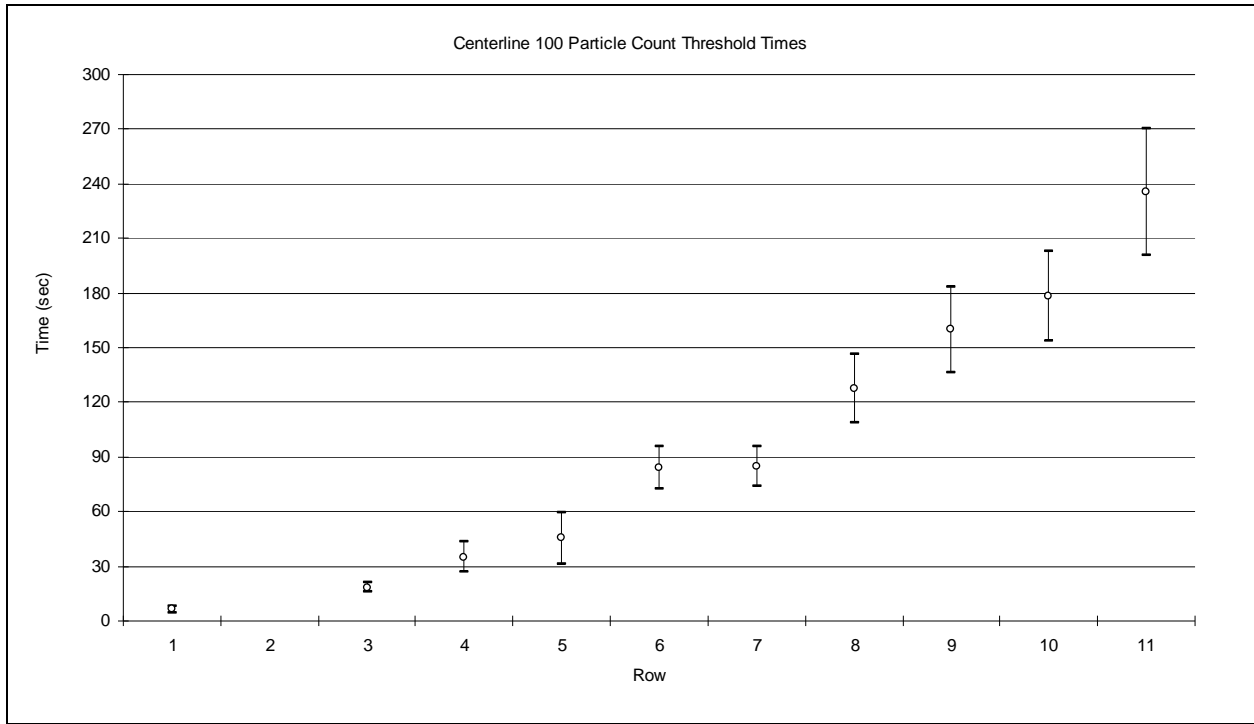


Figure 4.17: Centerline Particle Count Threshold Times

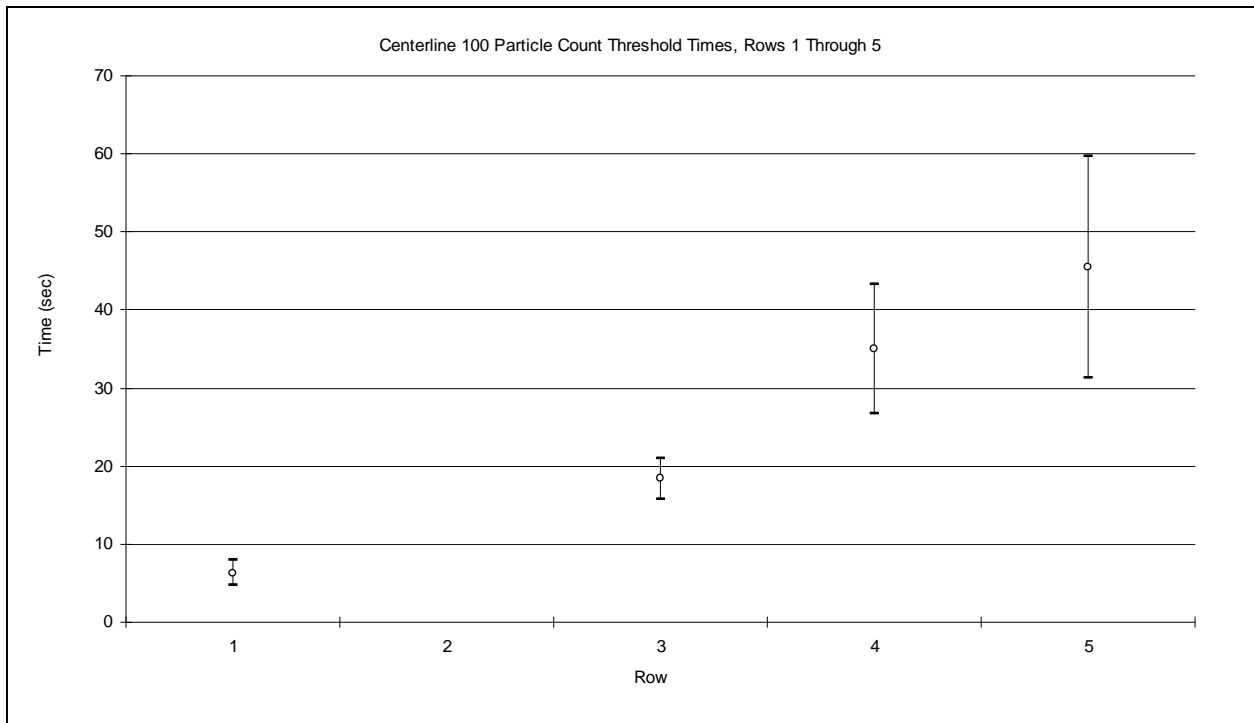


Figure 4.18: Centerline Particle Count Threshold Times, Rows 1 through 5

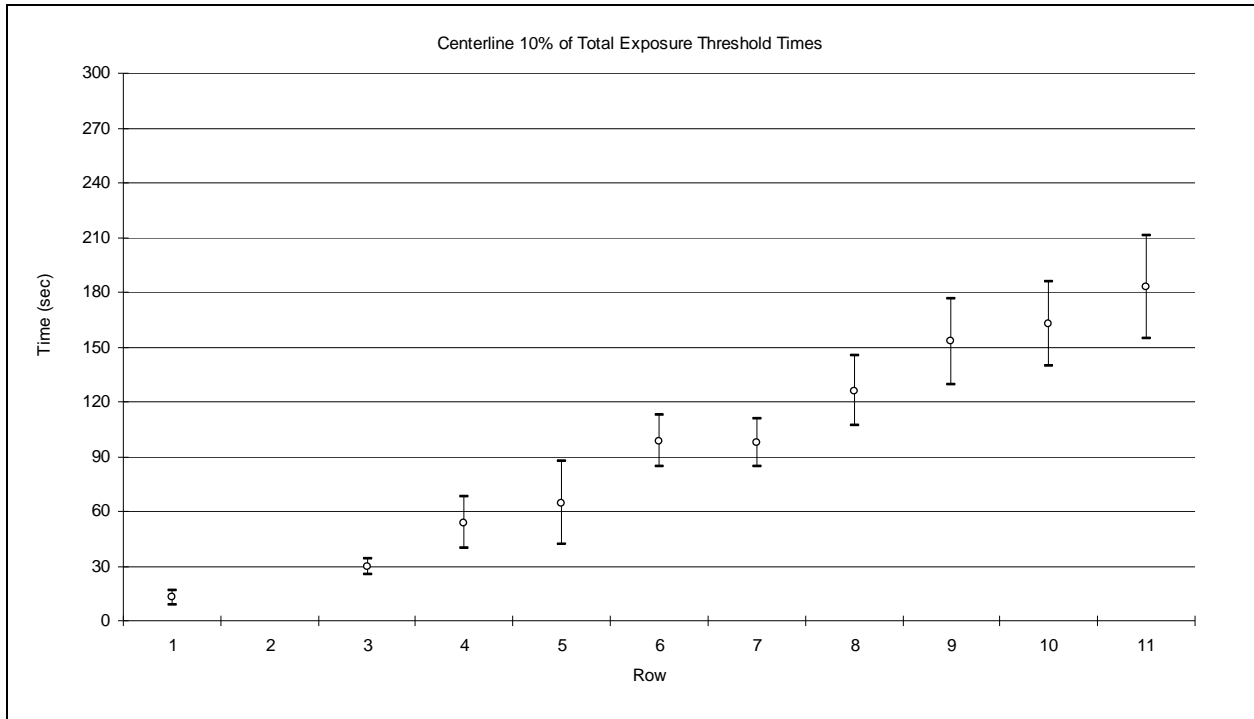


Figure 4.19: Centerline Fraction of Total Exposure Threshold Times

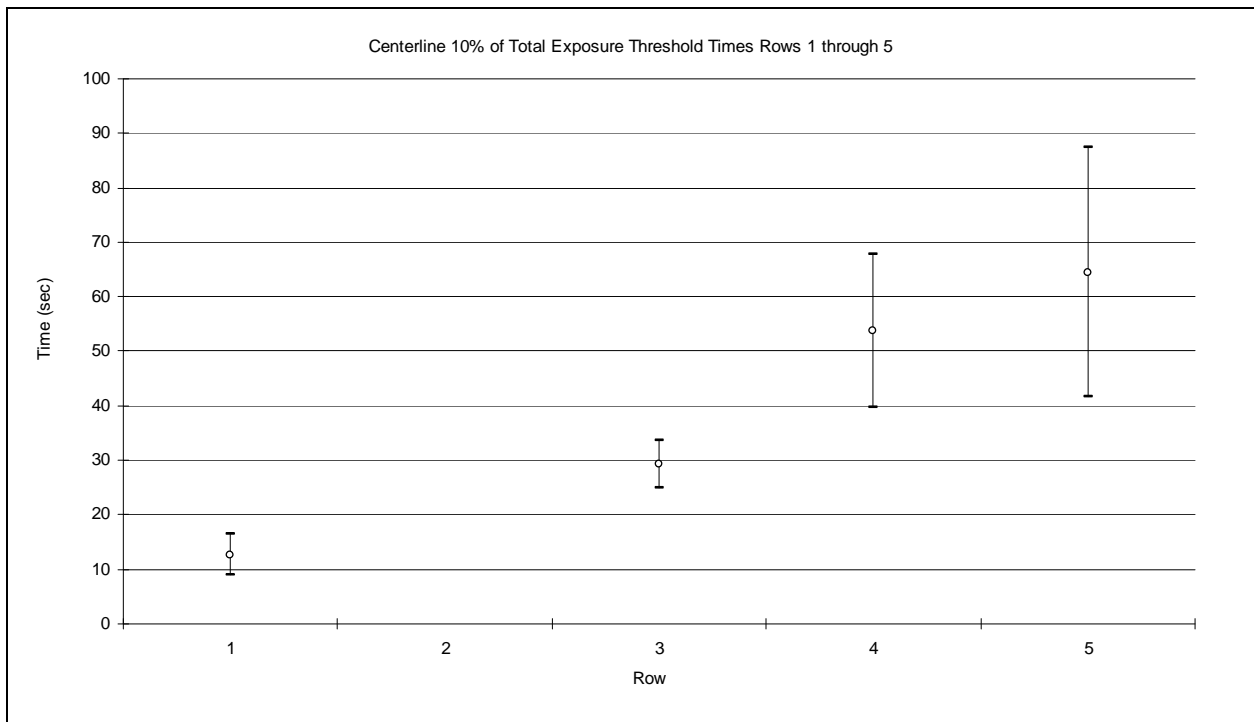


Figure 4.20: Centerline Fraction of Total Exposure Threshold Times, Rows 1 through 5

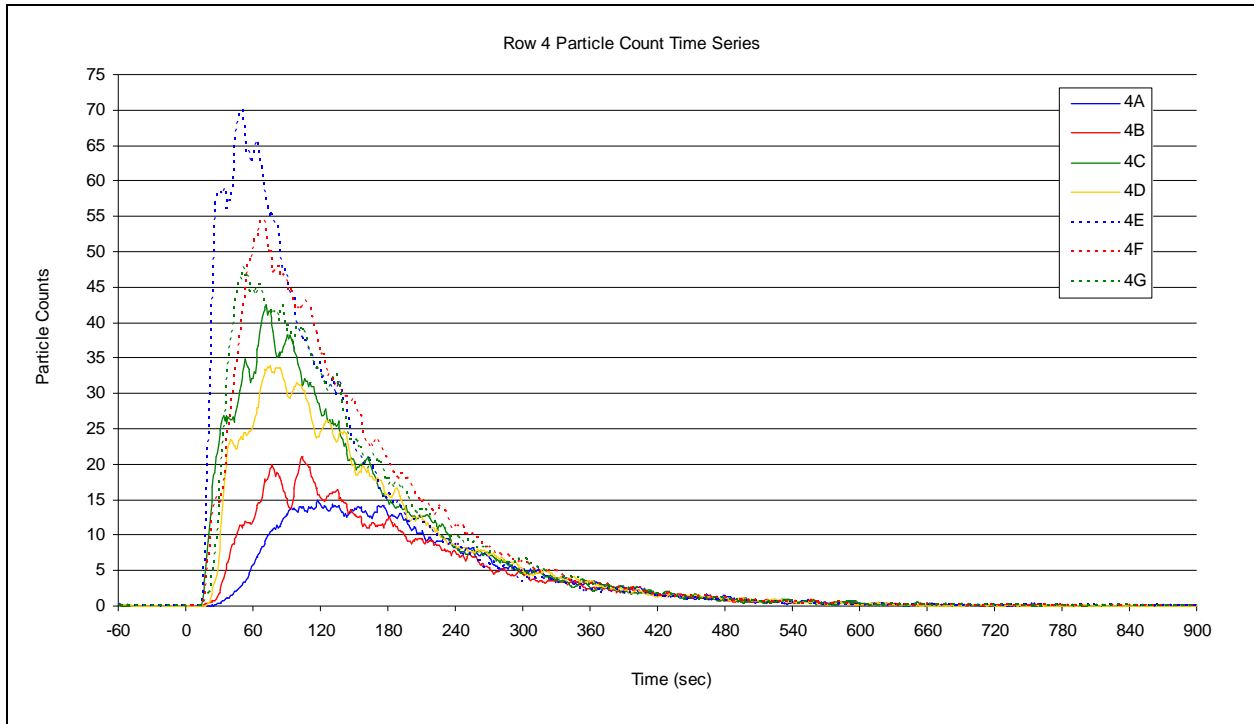


Figure 4.21: Row 4 Particle Count Time Series

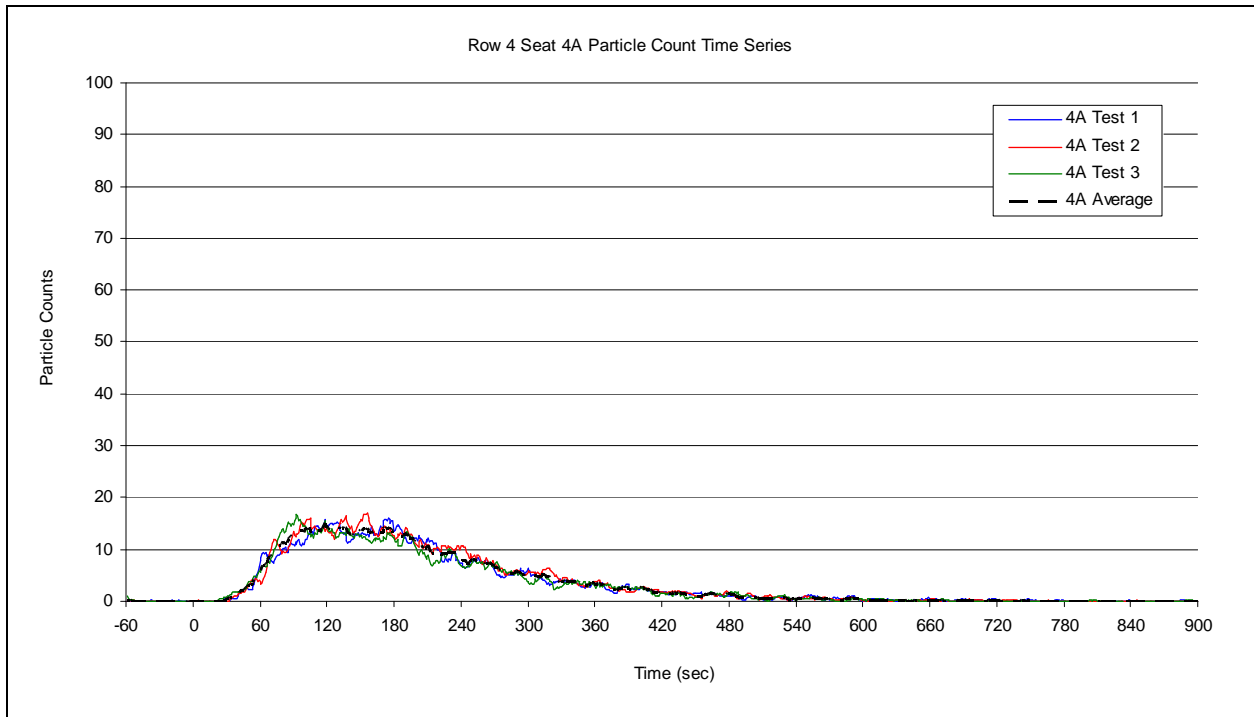


Figure 4.22: Row 4 Seat 4A Particle Count Time Series

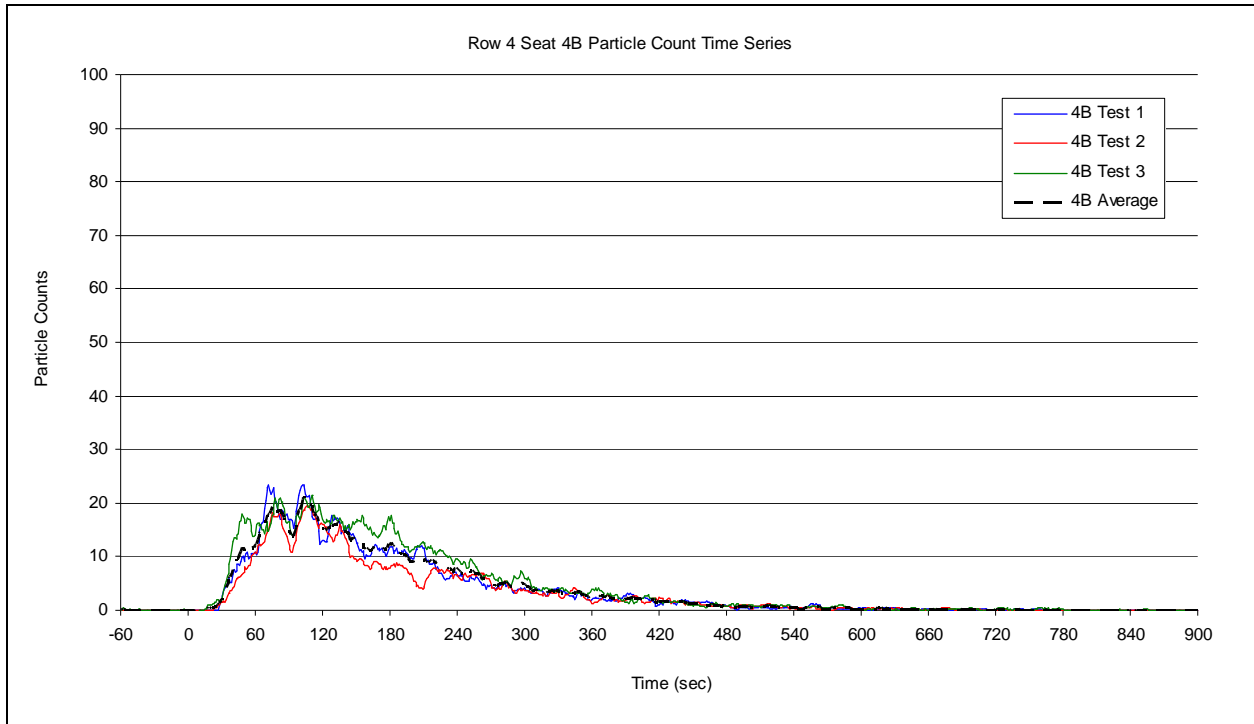


Figure 4.23: Row 4 Seat 4B Particle Count Time Series

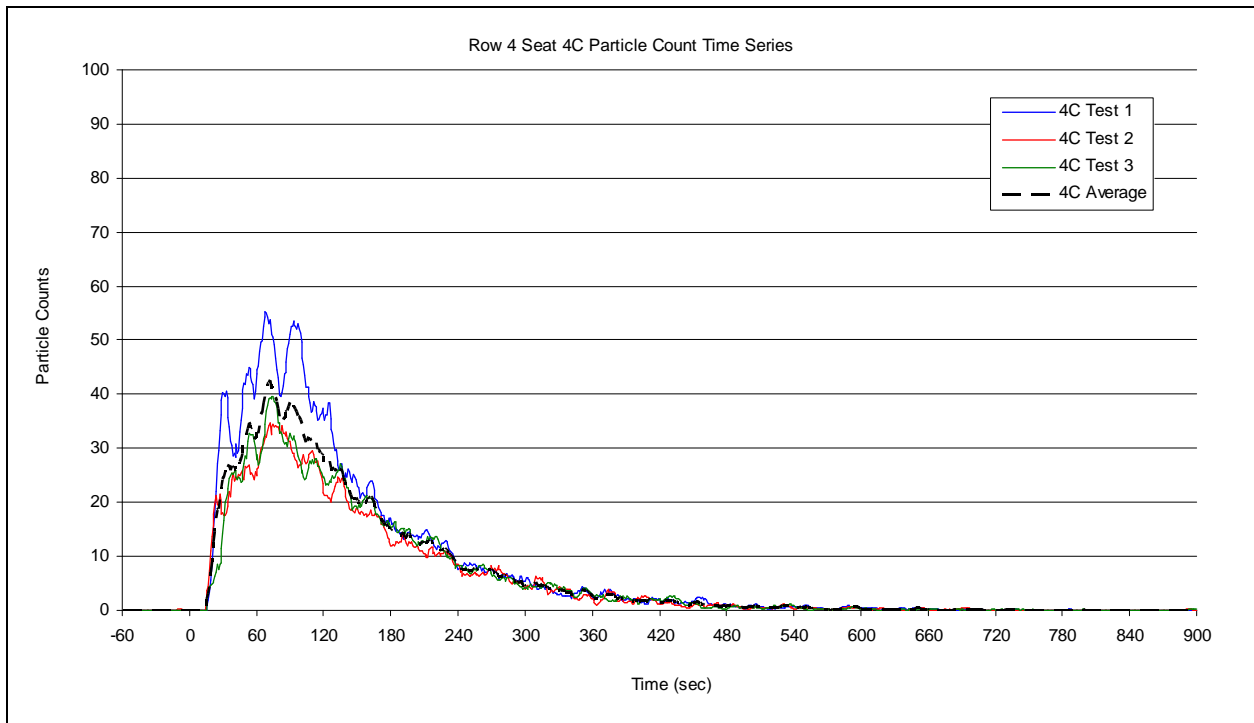


Figure 4.24: Row 4 Seat 4C Particle Count Time Series

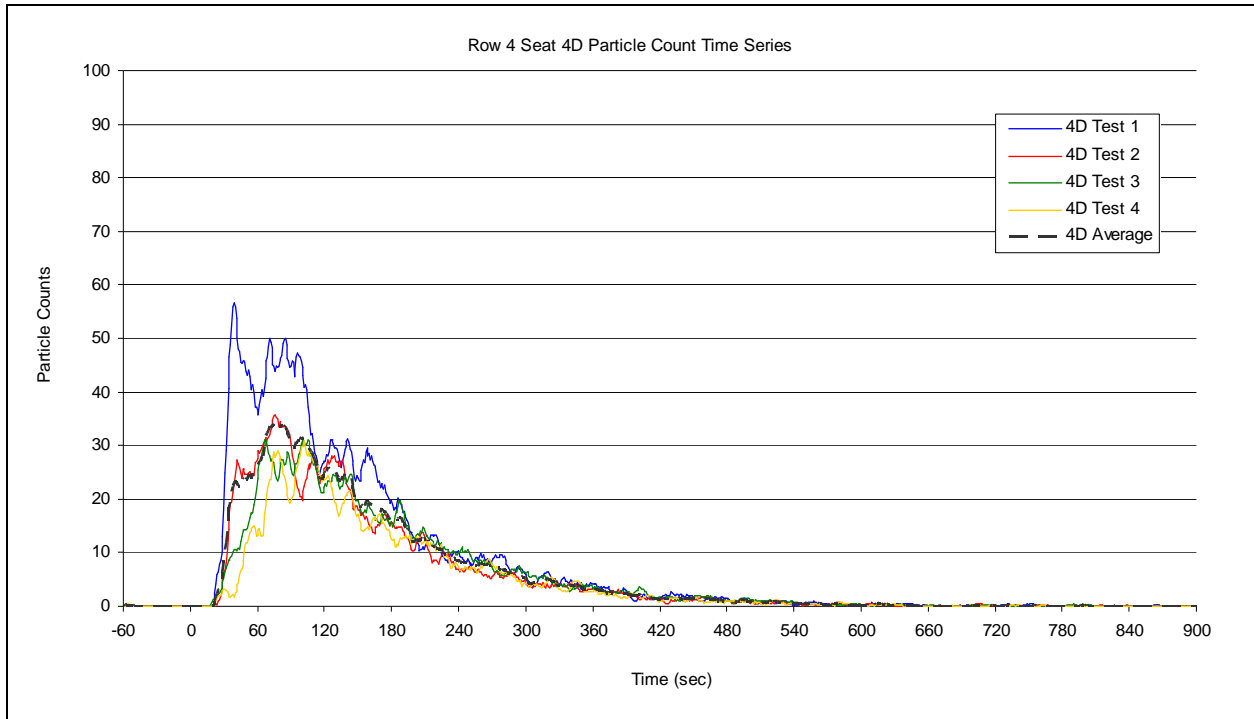


Figure 4.25: Row 4 Seat 4D Particle Count Time Series

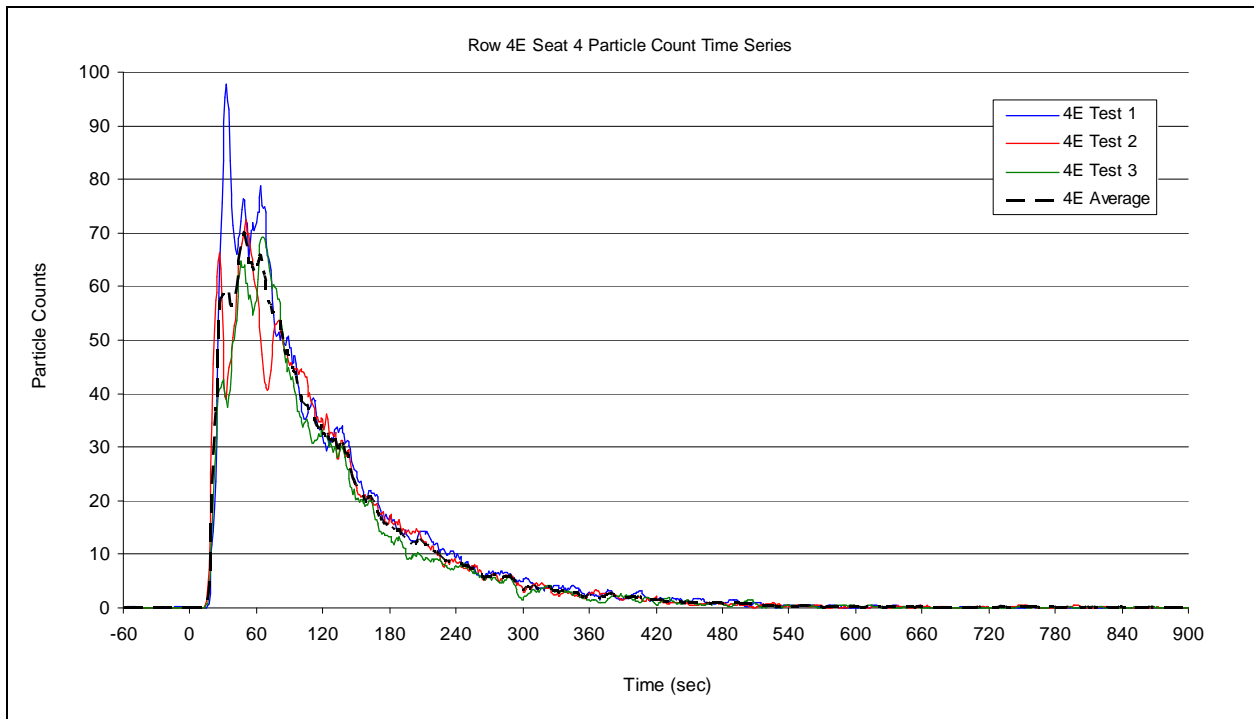


Figure 4.26: Row 4 Seat 4E Particle Count Time Series

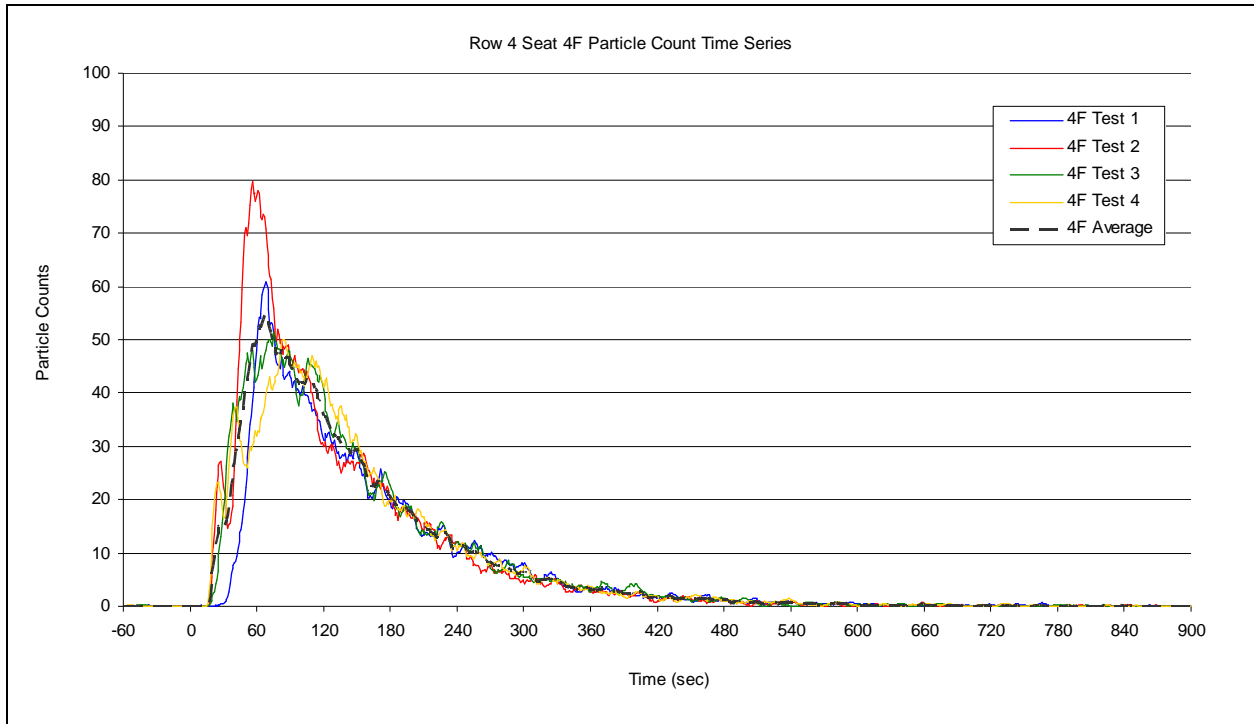


Figure 4.27: Row 4 Seat 4F Particle Count Time Series

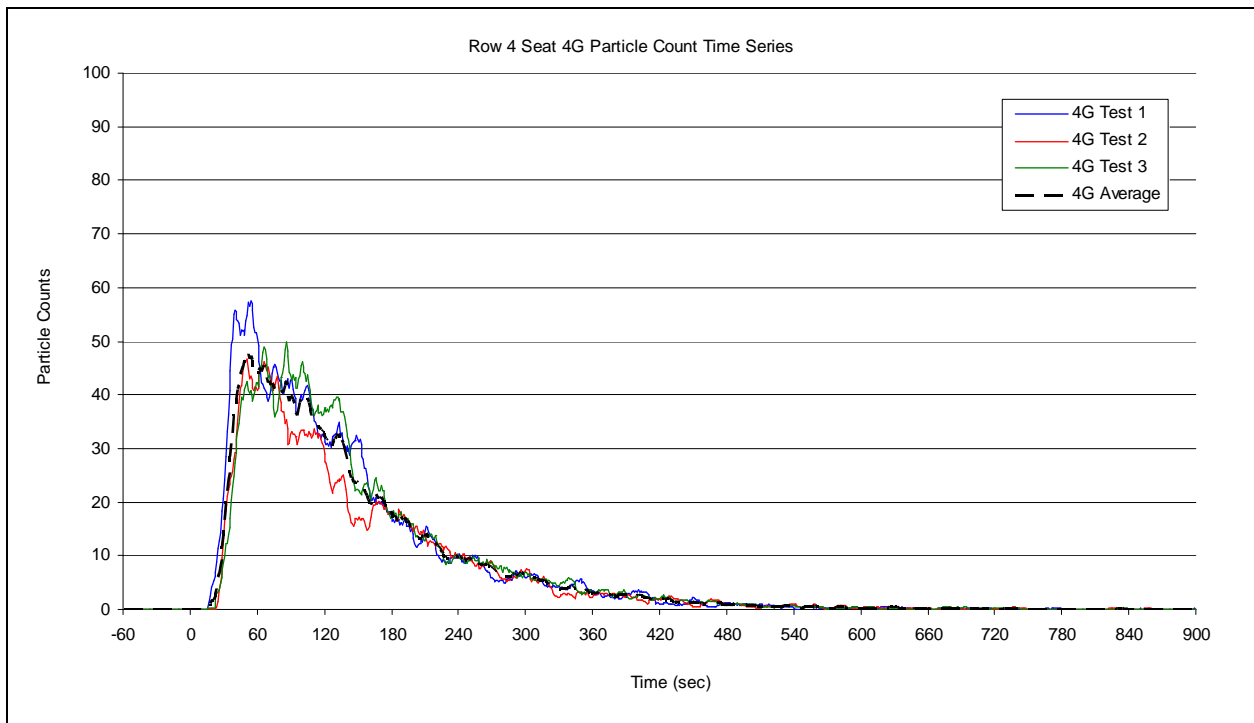


Figure 4.28: Row 4 Seat 4G Particle Count Time Series

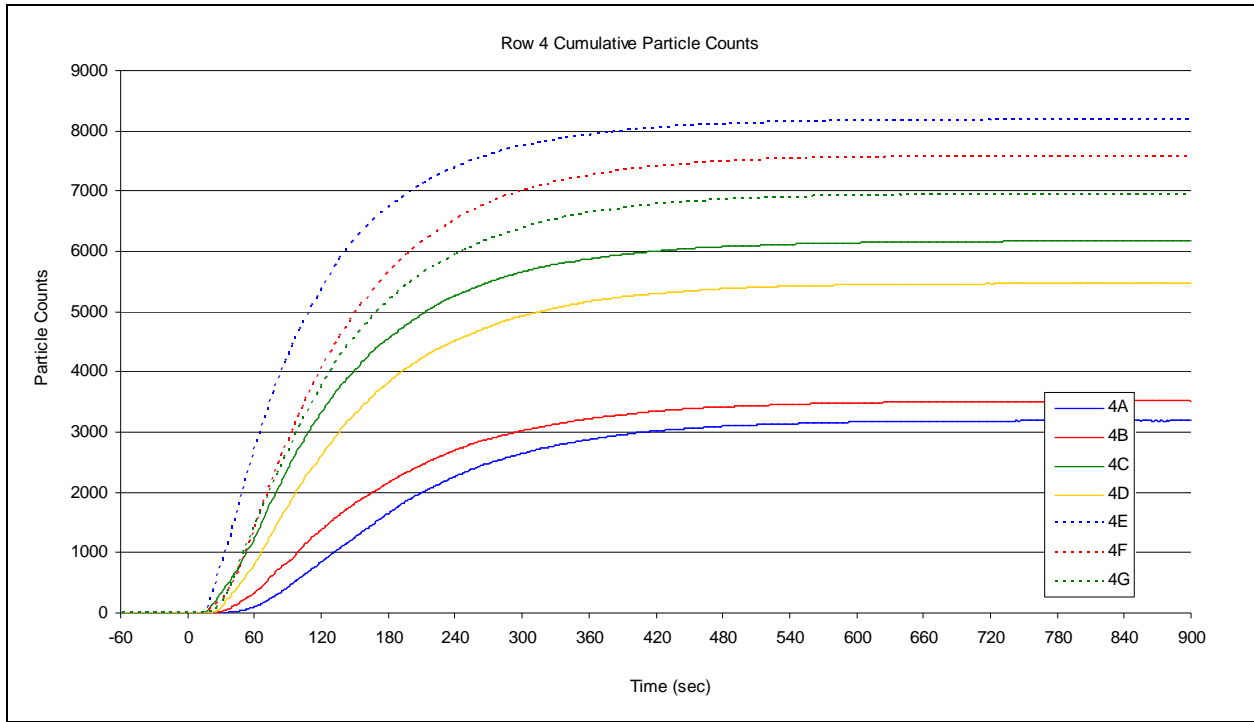


Figure 4.29: Row 4 Cumulative Particle Counts

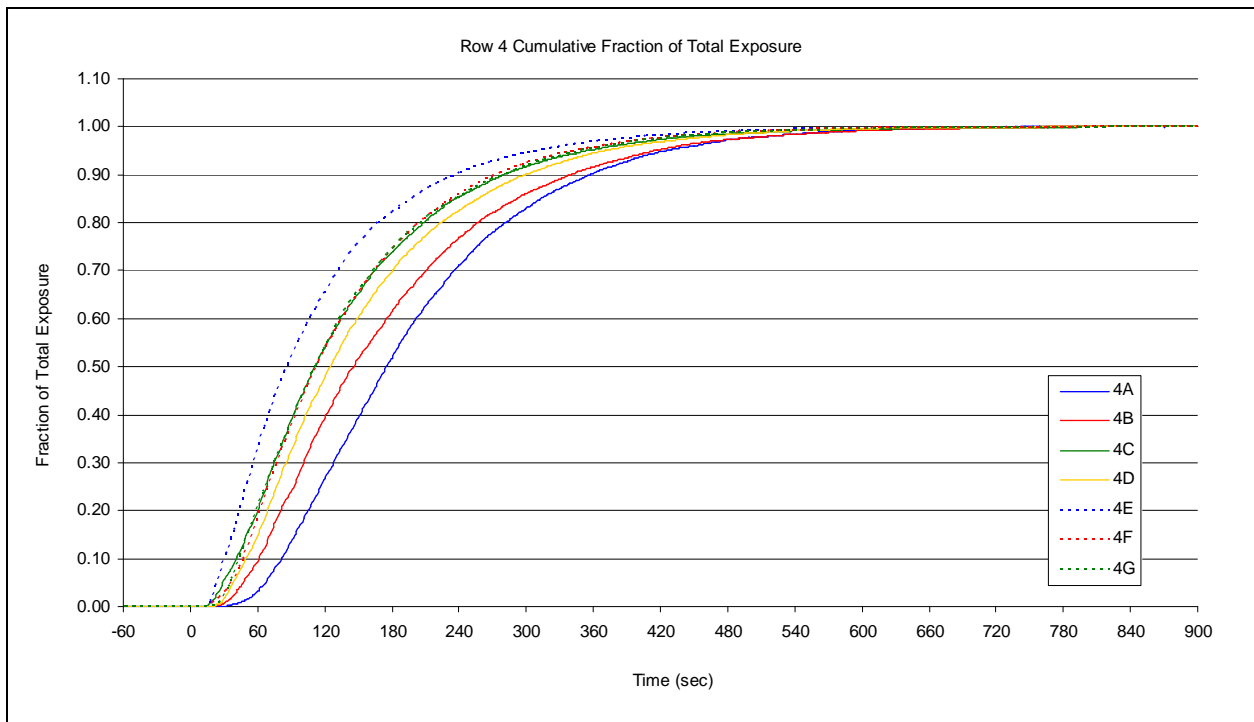


Figure 4.30: Row 4 Cumulative Fraction of Total Exposure

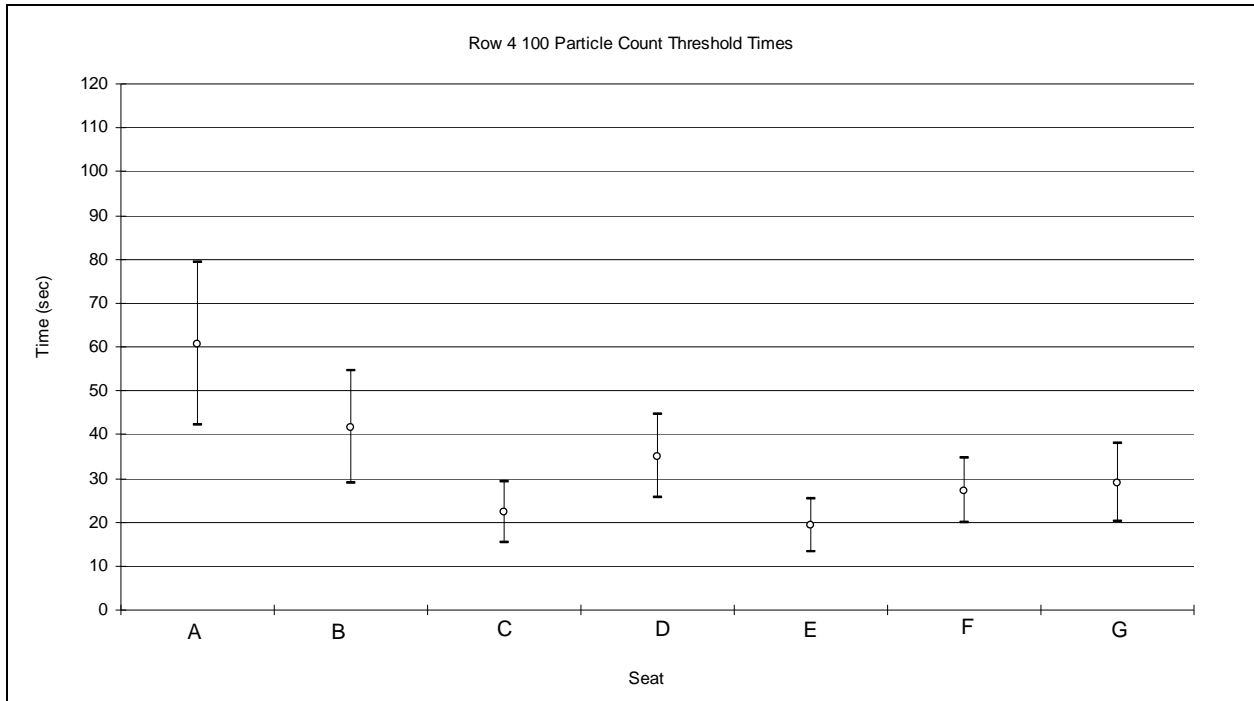


Figure 4.31: Row 4 Particle Count Threshold Times

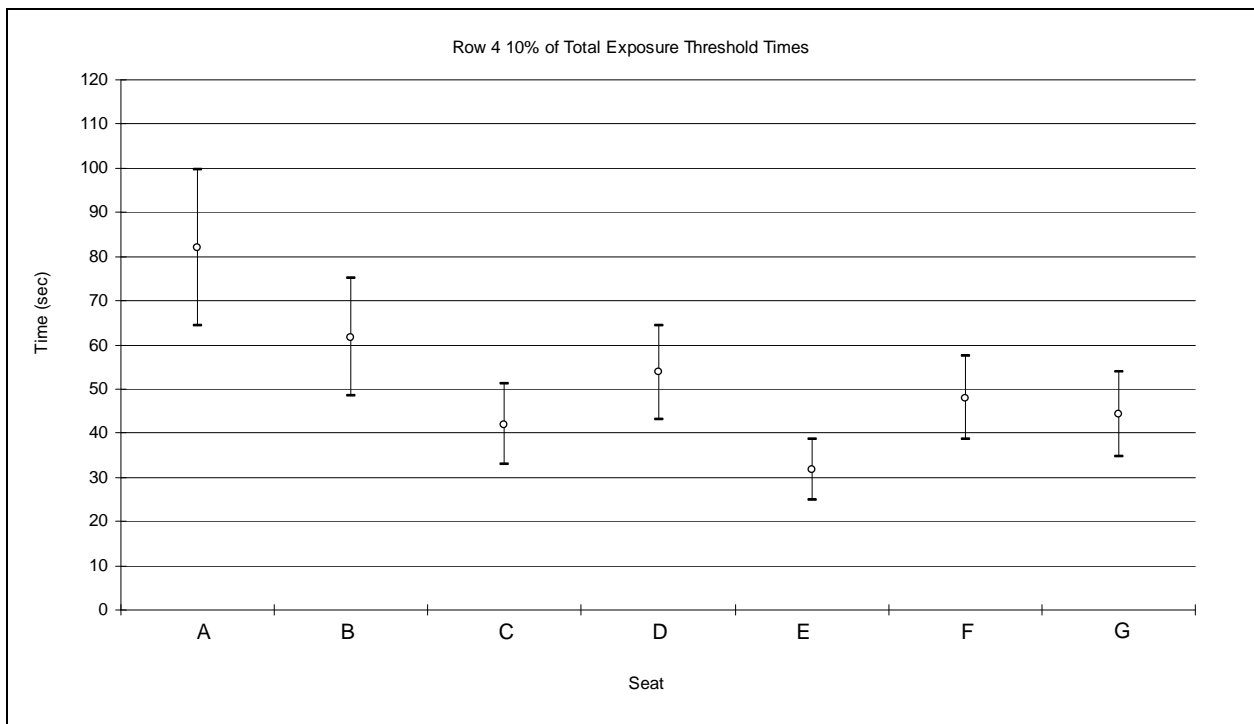


Figure 4.32: Row 4 Fraction of Total Exposure Threshold Times

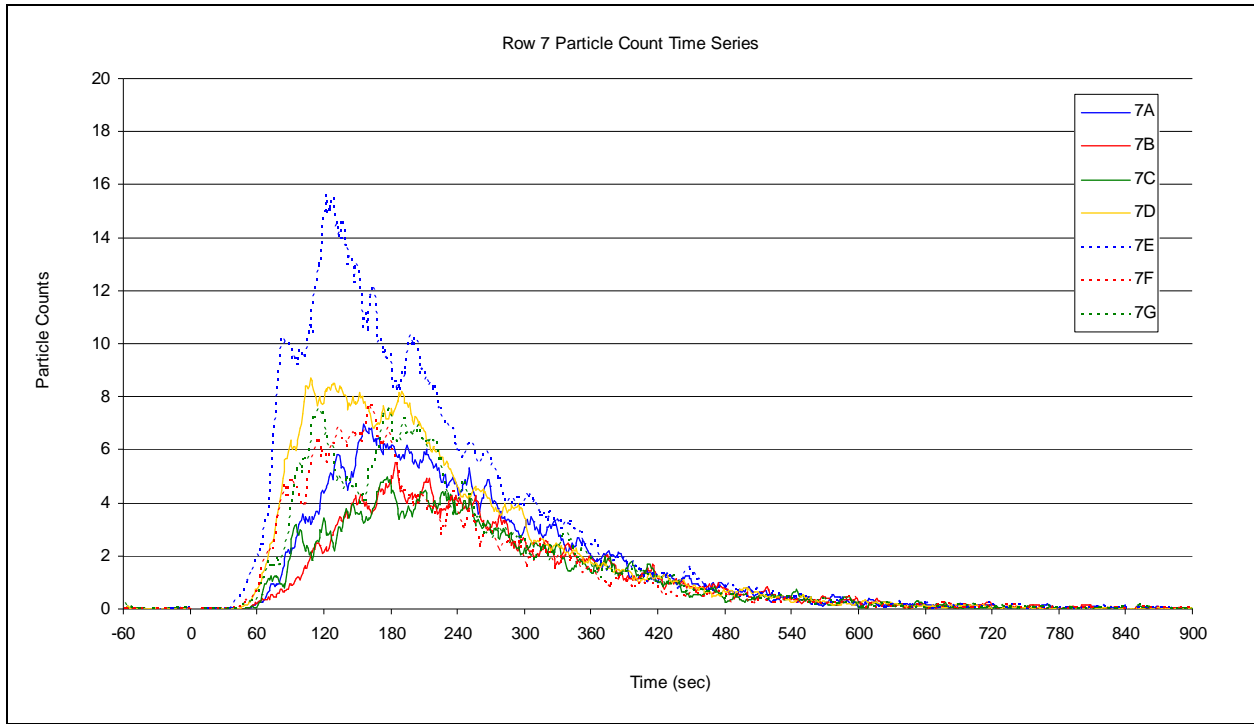


Figure 4.33: Row 7 Particle Count Time Series

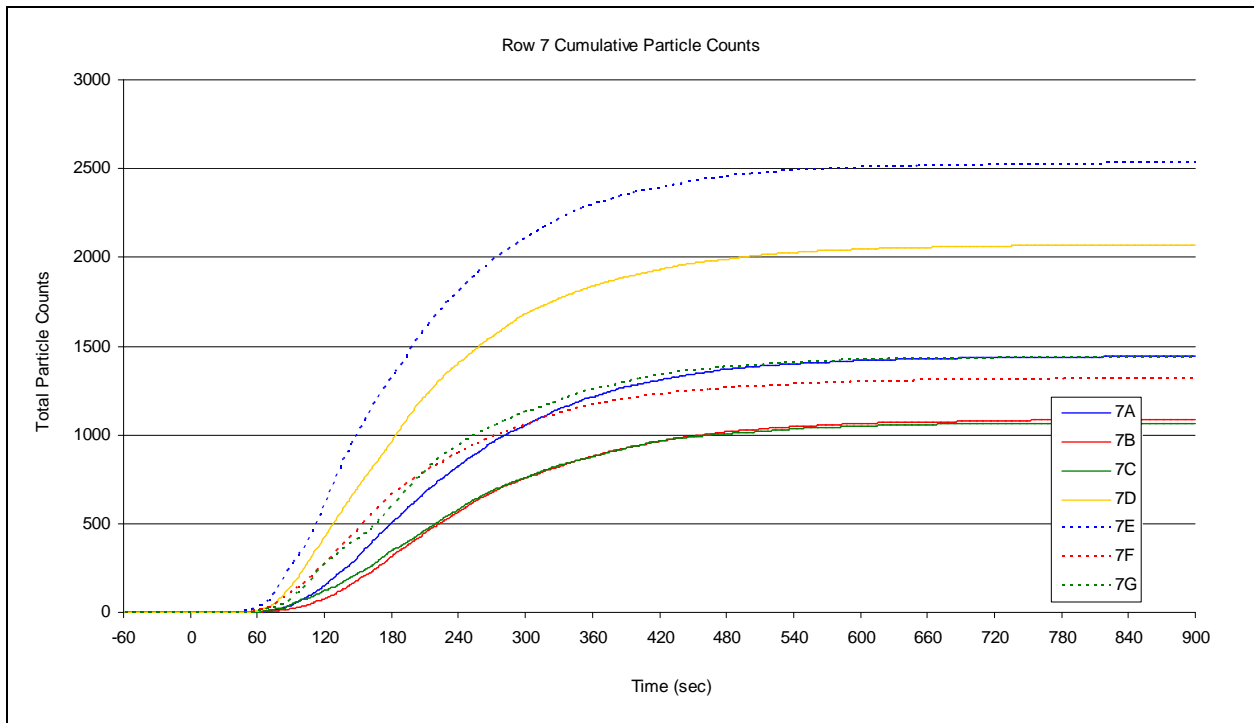


Figure 4.34: Row 7 Cumulative Particle Counts

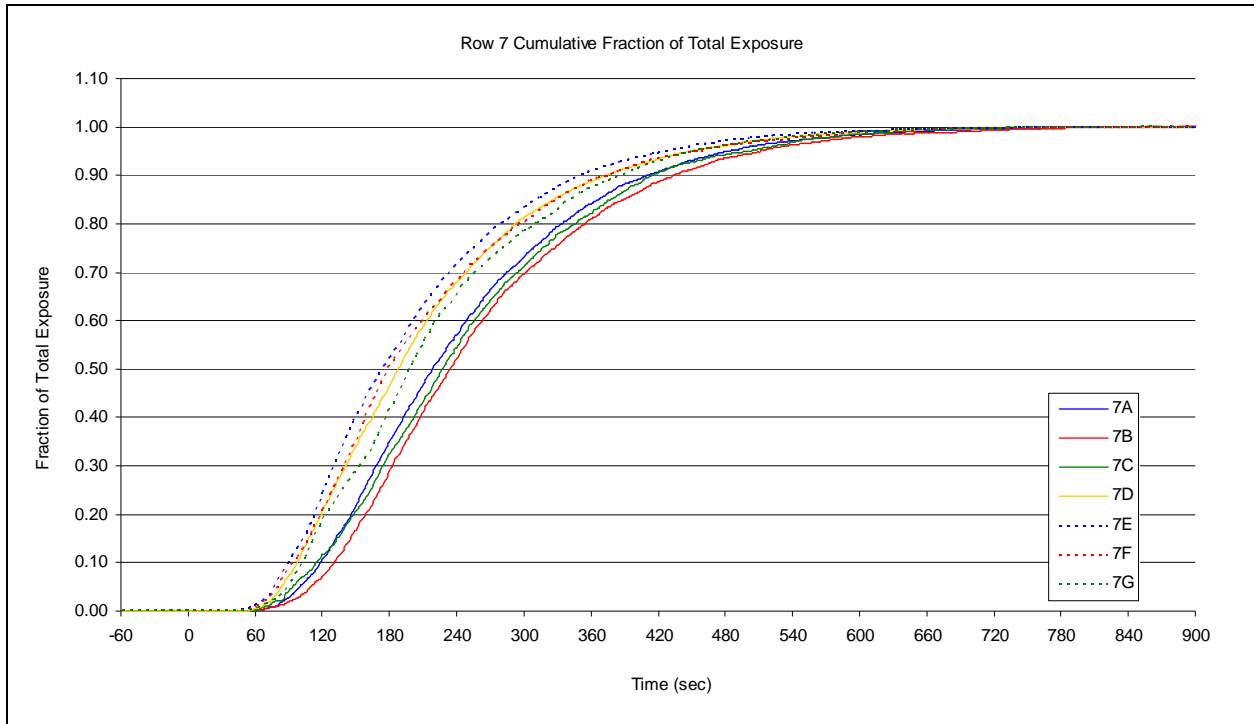


Figure 4.35: Row 7 Cumulative Fraction of Total Exposure

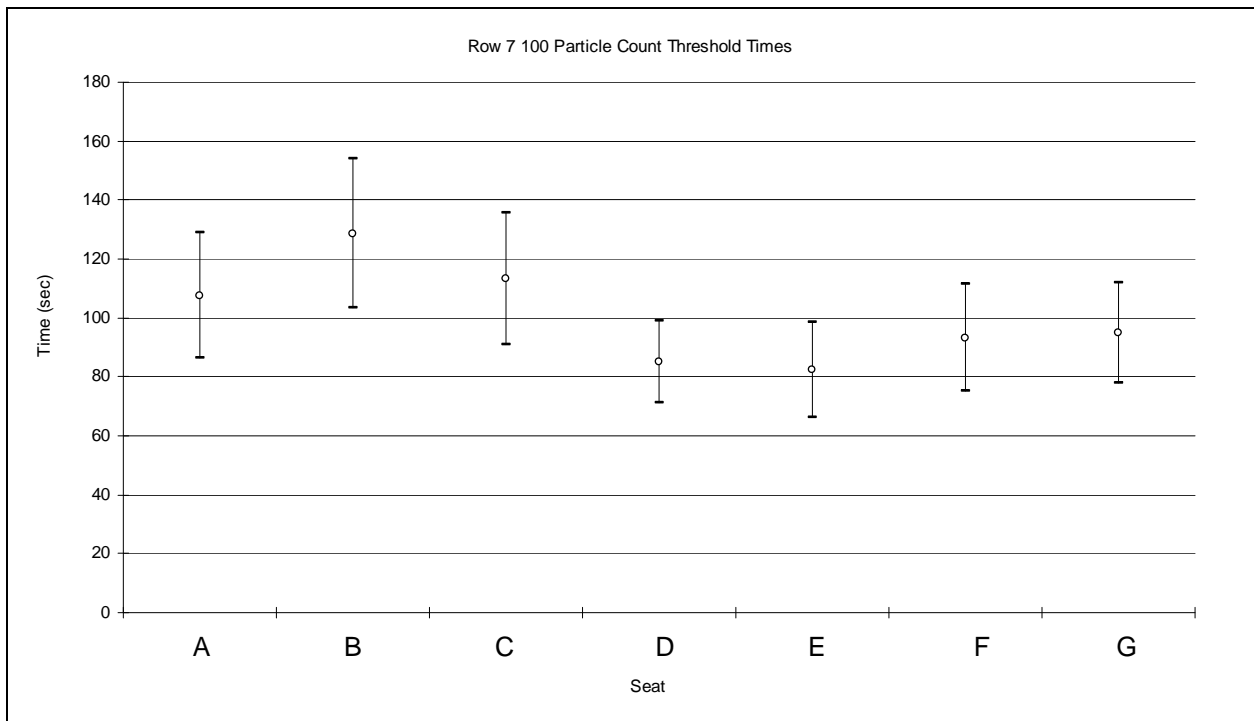


Figure 4.36: Row 7 Particle Count Threshold Times

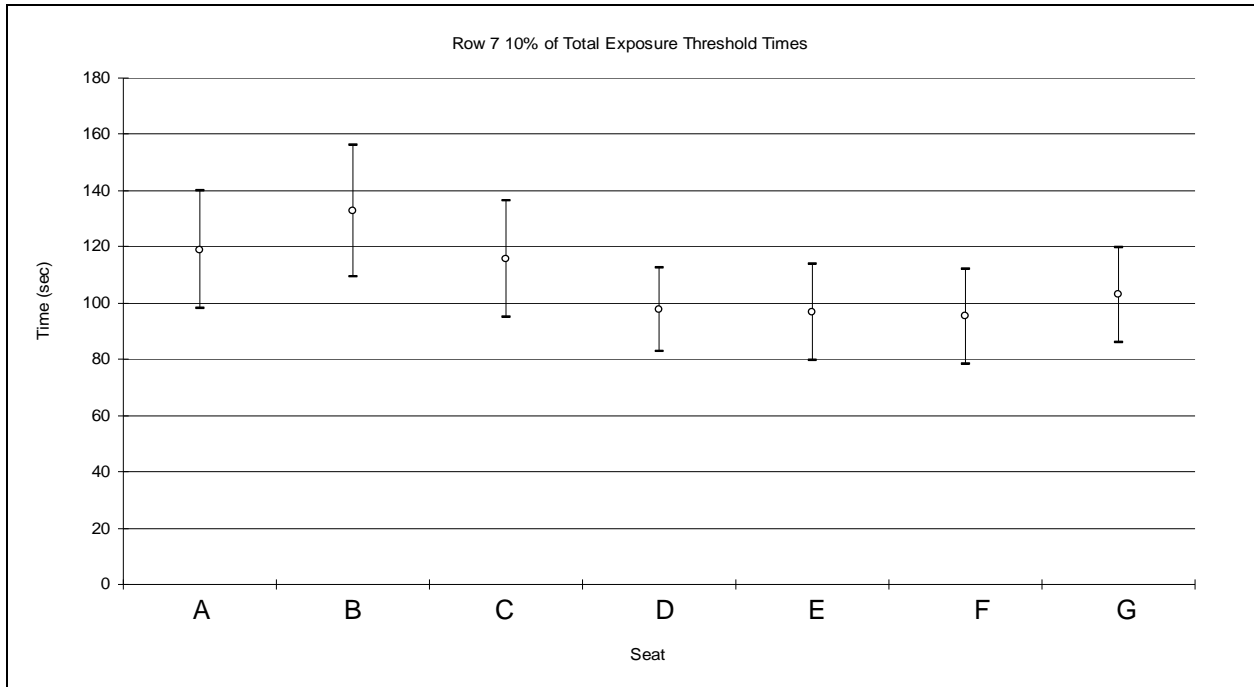


Figure 4.37: Row 7 Fraction of Total Exposure Threshold Times

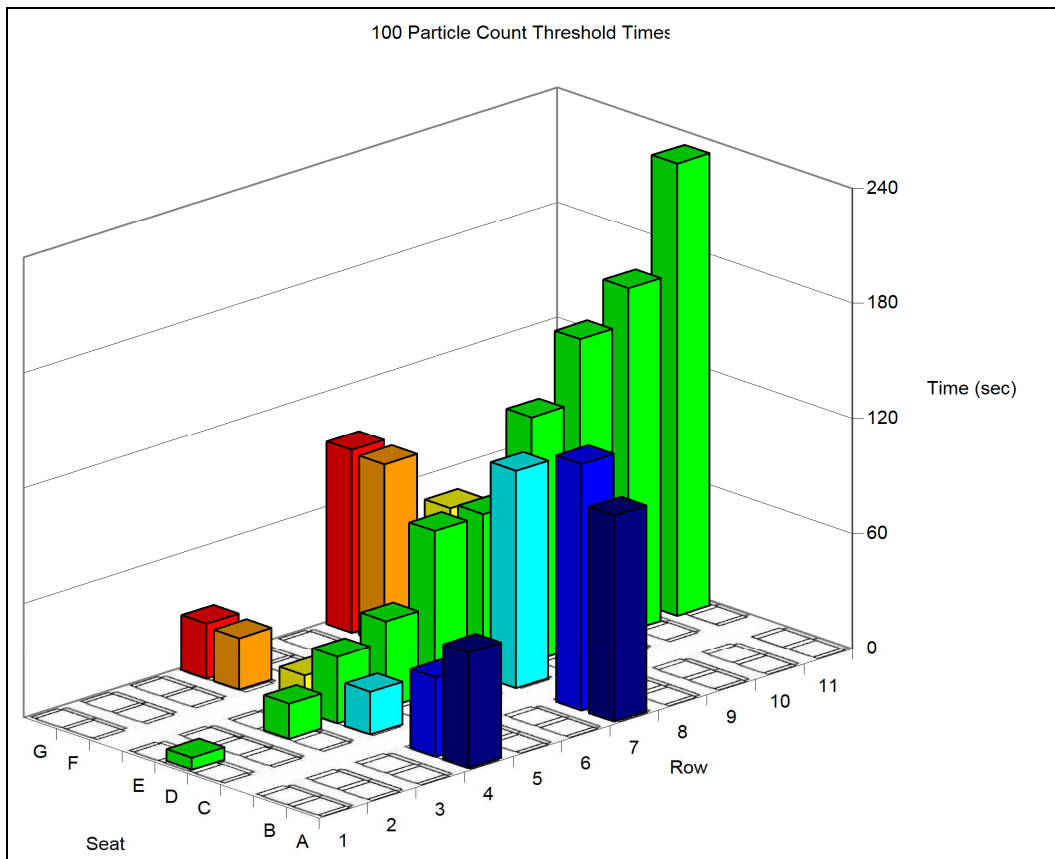


Figure 4.38: Overview of Cabin Particle Count Threshold Times

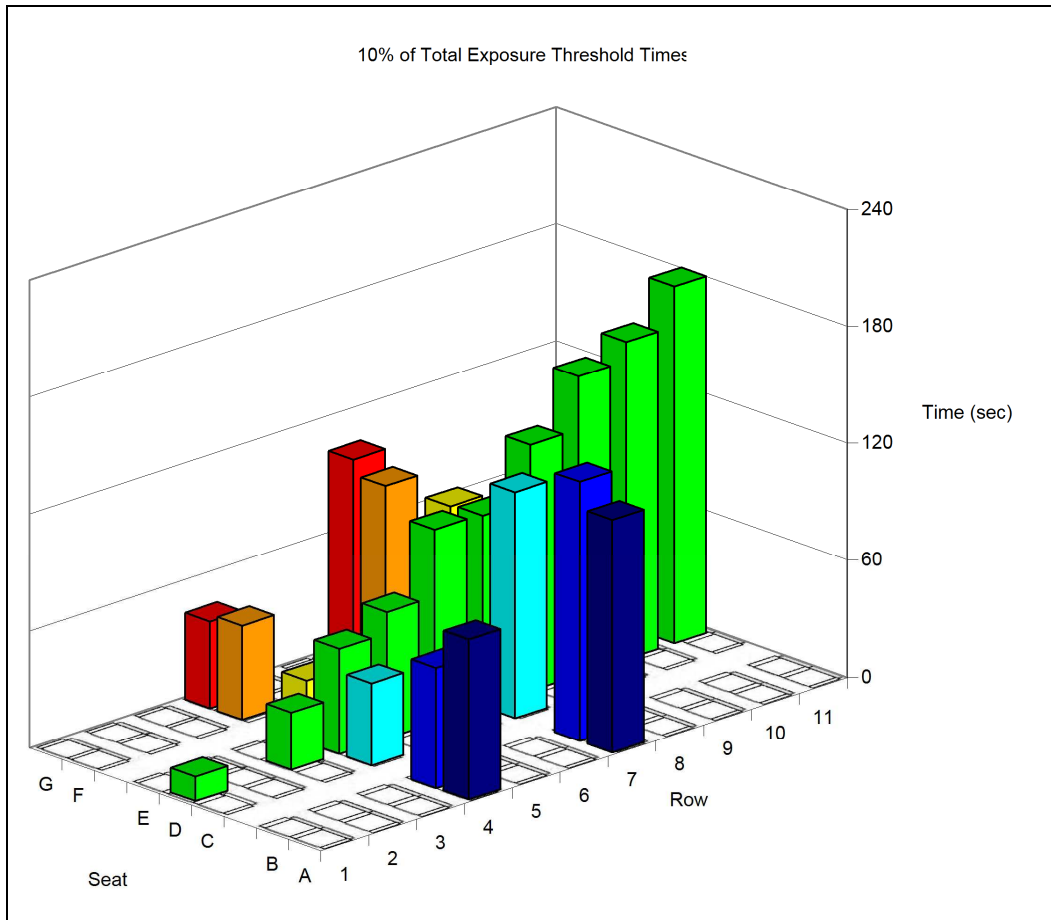


Figure 4.39: Overview of Cabin Fraction of Total Exposure Threshold Times

CHAPTER 5 - Data Analysis

The data presented in the results section received adjustment using the methods outlined in this section. Adjustments to the data include normalization for background counts, various averaging methods, and calculation of uncertainties associated with each result.

5.1. Normalization

For the tests conducted, it was noticed that in lieu of the steps taken to establish a clean environment with an insignificant number of background particles, a zero background count remained unachievable. To account for the background counts, the particle counts in the first and last minute were used and the data was corrected using Equation 5.1.

$$c'_i = c_i - \delta_{ik} \quad (5.1)$$

let,

$$i = -60, -59 \dots 899, 900$$

$$j = \left\lfloor \frac{120}{C_1 + C_{16}} \right\rfloor$$

$$k = j \times \left\lfloor \frac{i}{j} \right\rfloor$$

where,

- i is the time in seconds
- j is interval between background particles
- k is a multiple of the interval
- C_1 is the total particle counts during the first minute
- C_{16} is the total particle counts during the last minute
- c'_i is the normalized number of counts at time i
- c_i is the original number of counts at time i

The calculation of the interval between background particles (j), and the multiples of interval (k), both employ the floor function denoted by the floor brackets, $\lfloor \ \rfloor$ (Graham 1994). The effectiveness of this process is discussed in the verifications section. The majority of the

tests average well over 1000 particle counts of total exposure from the injection and the average estimated background count is only 41 particles. However, the data collected in seats farthest from the source averaged between 397 and 956 particles in which case the background counts represented potentially about 10% of the total counts. So normalization is implemented on all tests regardless of location in the cabin.

5.2. Settling Losses

To estimate the rate at which particles would settle in the cabin without the supply air, the aerodynamic diameter of the particles measured is used in calculating the settling velocity. In order to appropriately estimate the settling velocity in still air, the particles aerodynamic diameter as computed by the APS' must be corrected for particle density.

5.2.1 Aerodynamic Diameter Correction

An APS calculates the diameter based on the time of flight between two lasers in an accelerating air flow. It is mentioned in the literature provided by the manufacturer that the aerodynamic diameter can be estimated incorrectly if the particle has a density below 0.9g/cm³ or more than 1.1g/cm³. The density of talcum particles is between 2.58 and 2.83 g/cm (EPA 1992).

To correct the aerodynamic diameter for a non-unity density the Equations 5.2, 5.3, and 5.4 from (Wang and John 1987) are used as suggested in the APS' software manual (TSI 2006).

$$D_{a2} = D_{a1} \left[\frac{6 + R_2^{2/3}}{6 + R_1^{2/3}} \right]^{1/2} \quad (5.2)$$

$$R_1 = \frac{\rho_a (U - \bar{V}) D_{a1}}{\mu \sqrt{\rho_1}} \quad (5.3)$$

$$R_2 = \frac{\rho_a (U - \bar{V}) D_{a2}}{\mu \sqrt{\rho_2}} \quad (5.4)$$

where,

D_{a2} is the corrected aerodynamic diameter

D_{a1} is the uncorrected aerodynamic diameter

ρ_a is the air density (1.205×10^{-3} g/cm³)

ρ_1 is the calibration particle density (1.05 g/cm³)

- ρ_2 is the actual particle density (2.58 to 2.83 g/cm³)
- U is the air velocity (15000 cm/s)
- V is the average particle velocity (9510 to 12310 cm/s)
- μ is the air viscosity (1.81×10⁻⁴ dyne•s/cm³)

The equations above contain a loop in the fact the R_2 term refers to the corrected diameter so iterations are required to solve the set of equations. Using the outlined process the measured aerodynamic diameters 2.13µm are then corrected. To consider the broadest range the particles may represent, the upper end of the density is used with the smallest measured diameter and the lower density is used with the largest diameter. The smallest particles included in this thesis have a measured aerodynamic diameter of 1.11µm. Using a particle density of 2.83g/cm³, the corrected aerodynamic diameter is found to be 0.87µm after ten iterations. Also, for the included particles with a measured aerodynamic diameter of 2.13µm and a particle density of 2.58 g/cm³, the corrected aerodynamic diameter is 1.70µm.

With the corrected aerodynamic diameter, the calculation of the approximate geometric diameter is done with a ratio of densities. This calculation is shown in Equation 5.5.

$$D_{geometric} = \frac{D_{a2}}{\sqrt{\rho_2}} \quad (5.5)$$

where as in Equation 5.4, D_{a2} is the corrected aerodynamic diameter

ρ_2 is the actual particle density

As with the aerodynamic diameter, the geometric diameter assumes the particles are all near perfect spheres. For the particles counted during the tests outlined in this thesis, the geometric diameter then has a range of 0.52µm to 1.06µm.

5.2.2. *Settling Rate*

Based on Stoke's Law, the terminal settling velocity of the particles is calculated using the corrected aerodynamic diameter and Equation 5.6.

$$V_s = \frac{\rho D^2 g}{18\mu} \quad (5.6)$$

where,

V_s	is the settling velocity
ρ	is the particle density
D	is the particle diameter
g	is gravitational acceleration
μ	is the air viscosity

In this situation the aerodynamic diameter is being used, so the true density of the particle is ignored and a density of unity is used as is the definition of the aerodynamic diameter. The corrected diameters of 0.87 μm and 1.70 μm , representing the upper and lower ends of the interested range, have settling velocities of 2.29×10^{-5} m/s and 8.73×10^{-5} m/s respectively.

With the settling velocities established, particle loss from settling is not considered a significant mechanism by which the particles are removed from the cabin. The magnitudes of the settling velocities are significantly smaller than other documented velocities in the cabin (FAA 2008).

5.3. Averaging Methods

The value reported at each location to represent the average for the criteria being tested was achieved in the following manner. The parameter looked at in each type of test was first calculated for each test run and then the results of all the tests at that location were averaged together. This process applies to the total exposure, fraction of reference exposure, time to exposure threshold, and time to fractional exposure threshold tests.

The time series plots were obtained by first averaging each individual test using a 10 second trailing average given,

$$c_{avg,i} = \frac{1}{10} \sum_{n=0}^9 c_{i-n} \quad (5.7)$$

where,

$c_{avg,i}$	is the average at time i
c_i	is the counts at time i

Once each of the individual tests was averaged using Equation 5.7 values at each time step were averaged together for all the tests at that location. The results of this process are visible in Figures 4.22 through 4.28 representing the row 4 seats.

5.4. Uncertainty Analysis

To derive the 95% confidence intervals of the average for each of the tests a variety of elements that could impact the nature of the flows within the cabin are considered.

5.4.1. Particle System Uncertainties

The uncertainties from the equipment used in the dispersion and counting of particles are explained in this section.

5.4.1.1. Cabin Supply Air

The flow rate of air into the cabin is first examined. The flow rate is set at 1400 cfm and has an observed absolute uncertainty of ± 10 cfm. Using Equation 5.8 this yields a relative uncertainty of 0.7%.

$$u_Q = \pm \frac{U_Q}{Q_{cabin}} = \pm \frac{10}{1400} = \pm 0.7\% \quad (5.8)$$

5.4.1.2. Particle Dispersion System

The particle injection system has uncertainty in both the volume of air used to disperse the particles and the amount of powder loaded into the system. The volume of air released at atmospheric pressure is calculated in Equation 5.9 and the uncertainty is calculated in Equations 5.10 through 5.14.

$$V = \frac{(P_1 - P_2)V_T}{P_{atm}} = \frac{(60 - 45)0.0413}{14.7} = 0.042 \text{ ft}^3 \quad (5.9)$$

where,

P_1 is the pressure in the tank before discharge

P_2 is the pressure in the tank after discharge

P_{atm} is the atmospheric pressure

V_T is the measured volume of the charging tank

V is the volume of air released at atmospheric pressure

The volume of the charging tank was found to be $71.40\text{in}^3 \pm 0.31\text{in}^3$ by measuring the amount of water required to fill tank. The relative uncertainty of the tank volume is calculated in Equation 5.10 and represents the bias error of the tank volume,

$$u_{VT} = \pm \frac{U_{VT}}{V_T} = \pm \frac{0.31}{71.40} = \pm 0.4\% \quad (5.10)$$

The uncertainty of the pressure change in the tank prior to and after the controlled discharge is calculated in Equation 5.11 and 5.12. Only the uncertainty from the resolution of the gage used is applicable since any bias in the gage would affect both P_1 and P_2 in the same manner and therefore is correlated, and will cancel out. The random error from the reading resolution is applied twice since the gauge is read at both ends of the charge-discharge cycle.

$$U_{P_1-P_2} = \pm \sqrt{\frac{2P_{res}}{2}} = \pm \sqrt{\frac{2 \times 2}{2}} = \pm 1.4 \text{ psig} \quad (5.11)$$

$$u_{P_1-P_2} = \pm \frac{U_{P_1-P_2}}{P_1 - P_2} = \pm \frac{1.4}{15} = \pm 9.3\% \quad (5.12)$$

The uncertainty of the atmospheric pressure throughout the duration of all the tests is given in Equation 5.13 and is based on the maximum change in barometric pressure during the months of testing. The data is from (Wunder 2009) and is used as the random uncertainty of the atmospheric pressure.

$$U_{Patm} = \pm 0.3 \text{ psi}$$

$$u_{Patm} = \pm \frac{0.3}{14.7} = \pm 2.0\% \quad (5.13)$$

The combination of the relative uncertainties for the volume of air released by the tank are combined in Equation 5.14 relative uncertainty for the volume of air discharged.

$$u_V = \pm \sqrt{\theta_{P_1-P_2}^2 u_{P_1-P_2}^2 + \theta_{Patm}^2 u_{Patm}^2} \quad (5.14)$$

where,
$$\theta_i = \frac{\partial X_i}{\partial V}$$

The uncertainty of the tank volume is not included since only the random uncertainty of the pressures will cause variation from test to test. The relative uncertainty calculated for the volume of air released is 9.3%. However, the uncertainties associated with the volume of air released likely affected on the outcome of the tests little as long as there is sufficient air to create the initial cloud. During the initial testing phase of the dispersion system, discussed in the Verifications section, it was observed that by varying the volume of air released more than 10% the dispersion was not noticeably affected. The system effectively dispersed all the particles from the caps and remained visually consistent.

The consistency of loading the talcum powder into the dispersion system is estimated to have a random uncertainty of $\pm 5\%$. This level of uncertainty is reasonable based on the results from seats in rows 1 and 3 as shown in the verifications section. In addition, the talcum powder loading is the only element of the particle distribution system whose uncertainty directly reflects in the number of particles released and, in turn, counted.

5.4.1.3 Particle Counting

The accuracy of the APS is given as $\pm 10\%$ from the manufacture data sheet. Since the number of particles counted is a function of both the quantity of particles released and the ability to count them, the total particle counting system uncertainty is estimated at 11.2%.

$$u_{system} = \pm \sqrt{u_{APS}^2 + u_{Disp}^2} = \pm \sqrt{10^2 + 5.0^2} = \pm 11.2\% \quad (5.15)$$

5.4.2. Result Uncertainties

This thesis includes data from 172 tests at 27 locations within the chamber. To calculate uncertainties in the data, a pooled relative standard deviation, s_p , is used throughout this section to estimate the relative population standard deviation. The number of samples at each location is then used to find the relative standard deviation of the average at that location, by dividing the pooled relative standard deviation, by the square root of the number of samples. Equation 5.16 is used whenever a pooled relative standard deviation is referenced.

$$s_p = \sqrt{\frac{\sum_{i=1}^k (n_i - 1)s_i^2}{\sum_{i=1}^k (n_i - 1)}} = \sqrt{\frac{(n_1 - 1)s_1^2 + (n_2 - 1)s_2^2 + \dots + (n_k - 1)s_k^2}{n_1 + n_2 + \dots + n_k - k}} \quad (5.16)$$

where, n_i is the number of tests at a location
 s_i is the location's relative standard deviation of the sample
 k is the number of locations

For all the applications of Equation 5.16 in this thesis, the relative sample standard deviations from different locations are combined with Equation 5.16 to calculate the pooled relative standard deviation. This relative standard deviation is utilized due to the large variations in magnitude throughout the cabin. The pooling of the relative standard deviations is done to account for the low number of tests at each individual location.

5.4.2.1. Exposure Test

The exposure tests consist of two types of tests as explained in the experimental procedure section, the total exposure tests and exposure as a fraction of the reference. For the total exposure tests Table 5.1 shows some of the typical values for the sample standard deviation, relative standard deviation, average value, number of tests at each location, and other results discussed below. For all the total exposure tests the relative deviations were pooled with Equation 5.16 for a relative sample deviation of about 21%. This is used with Equation 5.17 to calculate the relative deviation of the average counts, $s_{c,r}$, at each location in the total exposure tests.

$$s_{c,r} = \frac{s_{p,r}}{\sqrt{n}} \quad (5.17)$$

where, $s_{p,r}$ is the pooled relative sample deviation
 n is the number of tests at the location

Equation 5.18 converts each location's deviation of the average to a relative uncertainty since the pooling function creates populations greater than ten (Coleman and Steele 1999).

$$u'_c = \pm t_{95\%} s_{c,r}^- = \pm 2s_{c,r}^- \quad (5.18)$$

The total relative uncertainty is found by combining the random uncertainty from the test results with the systematic uncertainty of the equipment setup. The only systematic uncertainty present is that from the APS machines.

$$u_c^- = \pm \sqrt{u_c'^2 + u_{APS}^2} \quad (5.19)$$

Multiplication of the relative uncertainty at each location yields the absolute uncertainty of the average with a 95% confidence interval.

$$U_c^- = \pm u_c^- \bar{c} \quad (5.20)$$

Similar to the total exposure uncertainty, the exposure as a fraction of the reference uses a pooled standard deviation for all the data points collected throughout the cabin. Using Equation 5.19 results in 19.5% relative sample standard deviation. The application of Equations 5.20 through 5.23 then yields a 95% confidence interval at each of the locations.

5.4.2.2. Time Series

The time series tests consist of time limits for the data to reach either 10 percent of their total exposure or 100 particle counts. The tests in row 4, row 7 and along the centerline were all addressed separately for the uncertainty calculations. The centerline data was split in a pooled relative uncertainty for rows 1 through 5 and another pooled relative uncertainty for rows 6 through 11. Therefore, the four different groups each have two tests categories and the resulting eight, pooled sample standard deviations from the application of Equation 5.16, are given in Table 5.2. They range from $\pm 7.0\%$ to $\pm 25\%$ and are applied to the corresponding locations within the cabin for each test using Equations 5.17 through 5.20 to again find the 95% confidence intervals for the data.

5.5 Exposure Analysis

The exposure test results as shown in the results section are presented in two forms. The first looks at the sheer number of particles accumulated at each location during a test. The

second relates each location's individual test totals to the reference location's total during the same test.

5.5.1 Total Exposure

The first test results presented as part of the total exposure section look at the seats located along the centerline of the cabin. In Figure 4.1 and Table 4.1 it is observed that the total particle count decreases as the testing location is moved farther from the dispersion row. This type of behavior is expected and is similar in nature to previous steady state work (FAA 2008). Figure 4.2 shows more clearly the data at the rear of the cabin between rows 6 and 11 which are 4 to 9 rows from the particle source. In comparison with the data collected close to the source there is an order of magnitude decrease in the values at locations 6 to 7 rows away.

The row 4 and row 7 data presented in Figures 4.3 and 4.4 show results for tests covering the width of the cabin. When presented graphically, even though the particles were released across all seats in row 2, there is a noticeable variation across rows 4 and 7. The average across all the seats in each row is plotted in Figure 5.1 along with the row 4 and 7 data. While the centerline seat in row 7, seat 7D, overestimates the row average, the average across row 4 is well represented by the centerline seat, 4D. However the variations from this average across the rows, show that even if the centerline seat represents the average, as in row 4, the average may not represent the remaining seats of the row with good accuracy.

A combination of all the locations in which two or more seats in the same row were tested is represented in Figure 4.5. This data illustrates the general trends across the rows with the appropriate 95% confidence interval for each average. To gain a better spatial perspective of the data the three dimensional image in Figure 4.6 shows both the lateral and longitudinal trends. The total exposure tests show the seats to the right of center tend to accumulate more of the dispersed particles than those on the left. Also, in lieu of the fact the locations in row 1 and row 3 were the same distance from the source, row 1 shows a significantly higher particle count at all locations.

5.5.2 Exposure as a Fraction of the Reference Location

As with the total exposure tests, the centerline seat results are presented to illustrate the trend through the length of the cabin. By representing the exposure as a fraction of the reference location, seat 3D, the potential for a trend in the data to have occurred out of coincidence is

reduced. In the centerline distribution, as shown in Figure 4.7, Figure 4.8, and Table 4.2, it is observed overall distribution is very similar to the results for the total exposure tests as expected.

Looking at the data from row 4 and row 7, both individually and then together in the Figures 4.9, 4.10, and 4.11, variation across the rows remains. Figure 5.2 shows both rows 4 and 7 with their respective row averages and as before the centerline seat in row 4 is close to the average in that row there is significant variation from the average across the row.

Combining all the reference test data, Figure 4.12 shows the averages with a value of 1.00 for the fraction representing seat 3D. While in general the seats along the right aisle have greater fractions of the reference exposure than the surrounding seats, both window seats on the left side, seats 4A and 7A, have higher average fractions than their aisle seats.

5.6 Time Series Analysis

While the goal of this thesis is to provide experimental data for the trends of a time based release of particle, the nature of how those particles spread over time is also important. The time series data help to illustrate the spread of particles through the cabin and focus on series of tests along the centerline, across row 4, and across row 7.

5.6.1. Dynamic Particle Counts

The introduction of particles into the cabin causes varying responses through out the cabin as can be seen in Figures 4.13 and 4.14, which show the centerline time series data. While the behavior for seats 1D and 3D is similar to a step change, the data from row 4 and back show a more gradual growth. Although in Figure 4.21, which shows all the seats across row 4, the data for seat 4E has a very quick rise to the peak value also resembling to a step change. Row 7 data in Figure 4.33 shows a much more gradual rise in most of the seats across row 7. However, seat 7E which is directly behind seat 4E is also the quickest rising and highest peaking in its row. The rise of the particle counts within the cabin in the various locations is anticipated because as the distance from the source increases so does volume of clean air through which the particles must travel.

Regardless to the manner in which the peak values were reached or the location within the cabin, all the data in Figures 4.13, 4.14, 4.21, and 4.33 exhibit an exponential decline in particle counts over time. Again, this behavior is expected since clean air is continually introduced into the cabin.

The manner in which each location is exposed to and removes particles is just a portion of the transient behavior. In Figures 4.13, 4.14, 4.21, and 4.33 even though the lines on the charts represent the average behavior of multiple tests averaged over 10 seconds there is a noticeable unevenness. To better illustrate where this variation comes from, Figures 4.22 through 4.28 show the individual test results and their average for the row 4 seats. The individual test results show a cyclic behavior for at least one test at most of the seats. The individual test results also show the magnitude of the fluctuations varies by seat and in some cases, the timing is such that they nearly negate each other in the averaging process. This situation is shown with Figure 4.28 and seat 4G where the oscillations of the different tests are far greater than those reflected in the average.

5.6.2. Cumulative Exposure

The cumulative exposure data as well as the cumulative fraction of total exposure data both present the opportunity to look at the rate particles are introduced and then removed at each location. The first figures with cumulative data, Figures 4.15 and 4.16 show the centerline seat data. The data from locations closer to the source are not only exposed to more particles, but the particle accumulation occurs more quickly. Seats 6D and 7D grow to differing values in Figure 4.15 with the total in seat 7D only about two-thirds of the total reached in 6D. In spite of the fact they reach different totals, when the values are normalized and expressed as a fraction of their own total, the two series are very similar as shown in Figure 4.16.

The cumulative data for row 4, Figures 4.29 and 4.30, seats 4C, 4F, and 4G show growth to different total particle counts but are nearly indistinguishable when normalized. The shape of the curve for seat 4D has a shape very close to that of 4C, 4F, and 4G although it is slightly shifted behind the other curves.

Row 7 data show a variety of curves from the cumulative particle counts in Figure 4.34 which are then separated into two main groups in Figure 4.35. When the particle counts are given as a fraction of their total, seats 7A through 7C seem to trend together. This is also true for seats 7D through 7G which do not appear similar until presented as a fraction of their total. Also while seats 7E and 7F are the closest to one another over much of their path in Figure 4.35 they separate almost immediately with seat 7E doubling the values reached by 7F in Figure 4.34.

5.6.3. Exposure Threshold Times

The threshold tests analyze the data attempting to quantify the rate in which the particles disperse within the cabin. As with the previous time series data the time to reach established limits or thresholds is separated into two types to give more perspective to the data. For the centerline tests, the times to reach 100 particles in Figures 4.17 and 4.18 show a linear trend from row 3 and increasing toward the rear of the cabin. Figure 5.3 shows data from Figure 4.17 from row 3 through 11 and a linear fit to the data. The zero intercept of the line is set at one second since it is assumed the accumulated particle counts in row 2 will be greater than 100 particles in the first second. The fact row 2 is the location of the initial particle dispersion at time zero is the justification for this assumption, based on data available in rows 1 and 3.

Another approach from which to look at the spread of particles is with the data in Figures 4.19 and 4.20, which show the time to reach 10 percent of their total exposure. Again, a linear trend appears and as with the 100 particle count data and a linear approximation is applied. Figure 5.4 illustrates the rework of Figure 4.19 with the addition of the linear trend for which the intercept is set at 10 seconds. The value of 10 seconds is chosen since it is assumed row 2 will reach its peak just after time zero and the particle counts will decrease with a similar exponential trend as the other locations. In addition, a 10 second intercept sets row 2 below the values in rows 1 and 3 and still allows for the fact it will not be as instantaneous as the 100 particle limit. As shown on their respective charts, the centerline seat trend lines for both the 100 particle and 10 percent tests have similar slopes around 20 seconds per row.

The results for row 4, Figures 4.31 and 4.32, and row 7, Figures 4.36 and 4.37, illustrate the 100 particle count threshold and 10 percent of total exposure threshold times again have similar trends. While the 10 percent times are about 20 second slower than the 100 particle count times the shapes are very similar with the exception of seat 4G which is only 15 seconds slower for the 10 percent time. The row 7 data also shows very similar trends between the 10 percent exposure times and the 100 particle times with a variation of between 2 and 14 seconds between the tests. The combination of all the tests for exposure threshold times shown in Figures 4.38 and 4.39 and reiterate the similarities between the 10 percent and 100 particle count threshold tests.

5.7 Verifications

This section looks at the verification of several different components responsible for the final results and their presentation in this thesis. The verifications include the particle measurement and dispersion systems, as well as the normalization method applied to the measured data.

5.7.1 Particle Measurement

To verify that the two APS' used for particle sizing and counting in this thesis the two units were placed next to one another in the lab near the testing chamber. Data was collected for a three-hour period at a counting rate of one hertz. The total counts for APS2 were 7% more than the total counts for APS1 for particles in the range of 1.114 to 2.129 μm in uncorrected aerodynamic diameter as measured by the APS'. This variation is within the manufactures listed 10% uncertainty for counting. A comparison of the particle counts separated by size is given in Figure 5.5 with the APS' confidence interval of $\pm 10\%$. To illustrate the agreement of the two instruments over time, Figures 5.6 and 5.7 show the time series data with 60 second and 10 minute averaging respectively. The averages are trailing averages and use Equation 5.7 with 60 and 600 seconds as opposed to 10.

5.7.2 Dispersion System

The first method of verification for the dispersion system is visual and included recording video of the dispersion process. The video was captured in front of a dark surface marked with lines at six inch increments, the first six inches above the mounting surface. All ventilation systems for the room were temporarily shut off so the dispersion system itself would be the main source of particle movement. Figure 5.9 shows a 15 frame progression of a typical dispersion process.

Data from the exchange tests in rows 1 and 3 also provide a certain level of verification for the dispersion system. As previously explained data was collected in the same seat column, B, D, or F in both row 1 and 3 simultaneously. The total particle counts for these tests are listed in Table 5.5. The summation of the counts on both sides of the dispersion row is done to help reduce the effect of the ventilation system and measure the repeatability of the particle

dispersion. The averages for column sums and the related statistics are in Table 5.4. Of the tests in seat column B one of the tests resulted in a 50% larger particle exposure than any of the other tests at that location. Since it is unlikely 50% more particles were used, this fluctuation is attributed to the cabin airflows and considered an outlier in the data for verification purposes.

As indicated in Table 5.4 the 95% confidence interval of the relative uncertainty is 5, 7, and 4.5% for columns B, D, and F. These results are within the uncertainty of the APS' and indicate the 5% loading uncertainty is reasonable.

5.7.3 Normalization

To verify the normalization process described at the beginning of this chapter the correction was applied to a 16 minute test. The effectiveness of this normalization method is shown in Figure 5.8. While the method is not perfect and slightly over corrects both 16 minute test in this case, it does reduce the deviation from zero.

For all the centerline tests the total particles counted in the first and last 60 seconds of each test were averaged before and after normalization was applied. The values in Table 5.3 show significant reduction in the background particles counted with the normalization versus without. Also, the standard deviations show that there is less variation for the normalized data than in the data without any correction for the background counts. Both the smaller average and the reduced deviation from the average support the results seen in Figure 5.8.

Table 5.1: Example Data for Total Exposure Tests

Seat	1D	4D	4E	4G	7C	7D	7E	10D
Average Particle Counts	13538	5469	8192	6951	1067	2068	2529	736
Sample Standard Deviation	2207.6	1283.1	734.9	577.4	156.9	209.9	562.9	83.1
Relative Sample Standard Deviation	0.163	0.235	0.090	0.083	0.147	0.101	0.223	0.113
Pooled Relative Sample Standard Deviation	0.211	0.211	0.211	0.211	0.211	0.211	0.211	0.211
Relative Standard Deviation of the Average	0.086	0.106	0.122	0.122	0.122	0.086	0.122	0.122
Number of Tests	6	4	3	3	3	6	3	3

Table 5.2: Pooled Deviations for Threshold Tests

Pooled Relative Sample Standard Deviations for Threshold Tests	
100 Particle Limit Tests	
Centerline Rows 1-5	0.205
Centerline Rows 6-11	0.063
Row 4	0.245
Row 7	0.137
10% of Total Exposure Limit Tests	
Centerline Rows 1-5	0.236
Centerline Rows 6-11	0.070
Row 4	0.157
Row 7	0.115

Table 5.3: Normalization Effects on Centerline Tests

	Average Particles Counted in First and Last 60 Seconds	Standard Deviation of Counts
With background	2.815	2.403
Normalized	-0.056	0.564

Note: the counts in the first and last minute for each test were added together then averaged

Table 5.4: Dispersion System Consistency Summary with Outlier Effects

	Column			
	Seat B	Seat D	Seat F	Seat B with outlier
Average	19175	21189	28649	20984
Sample Standard Deviation	1062	1819	1455	4531
Relative Standard Deviation	0.055	0.086	0.051	0.216
Relative Deviation of the Average	0.025	0.035	0.023	0.088
95% Confidence Interval	0.050	0.070	0.045	0.176

Note: the confidence interval doesn't include system uncertainties

Table 5.5: Dispersion System Consistency Data from Row 1 and 3 Exchange Tests

Test Number	Seat	Total Counts		Test Total	Column Averages (combined by B, D, &F)	
		Row 1	Row 3			
1832	1B	13359		18941	19175	
	3B		5582			
2008	1B	13870		19474		
	3B		5604			
2157	1B	12260		17502		
	3B		5242			
1637	1B	23890		*30027		
	3B		6137			
1710	1B	15926		20348		
	3B		4422			
1744	1B	14814		19609		
	3B		4795			
1634	1D	11610		21318		21189
	3D		9708			
1713	1D	10939		18876		
	3D		7937			
1749	1D	12171		19300		
	3D		7129			
1705	1D	16017		23394		
	3D		7377			
1738	1D	15395		22832		
	3D		7437			
1812	1D	15098		21411		
	3D		6313			
2302	1F	15890		28118	27871	
	3F		12228			
2341	1F	15292		31004		
	3F		15712			
0944	1F	16779		27186		
	3F		10407			
1044	1F	19348		28933		
	3F		9585			
1137	1F	17360		23976		
	3F		6616			
1630	1F	19728		28006		
	3F		8278			

* this value varies from the other at the same location by about 50% and is not included in the column average presented above

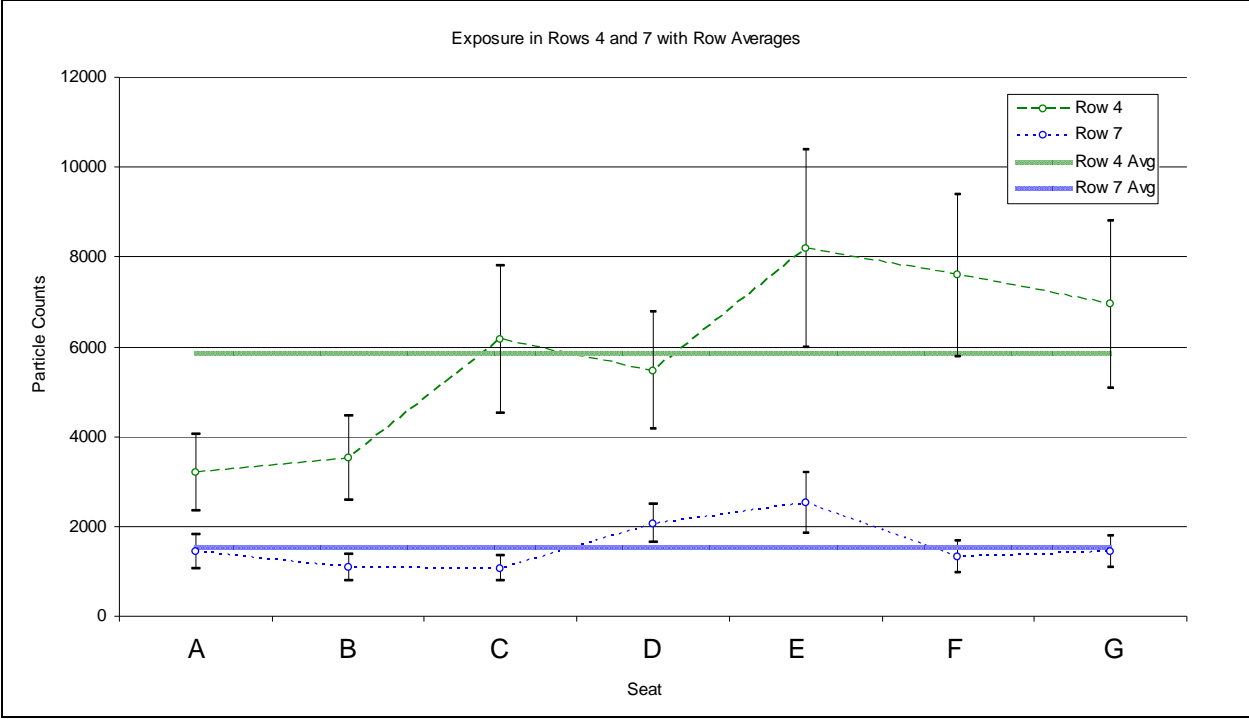


Figure 5.1: Rows 4 and 7 Total Exposure with Row Averages

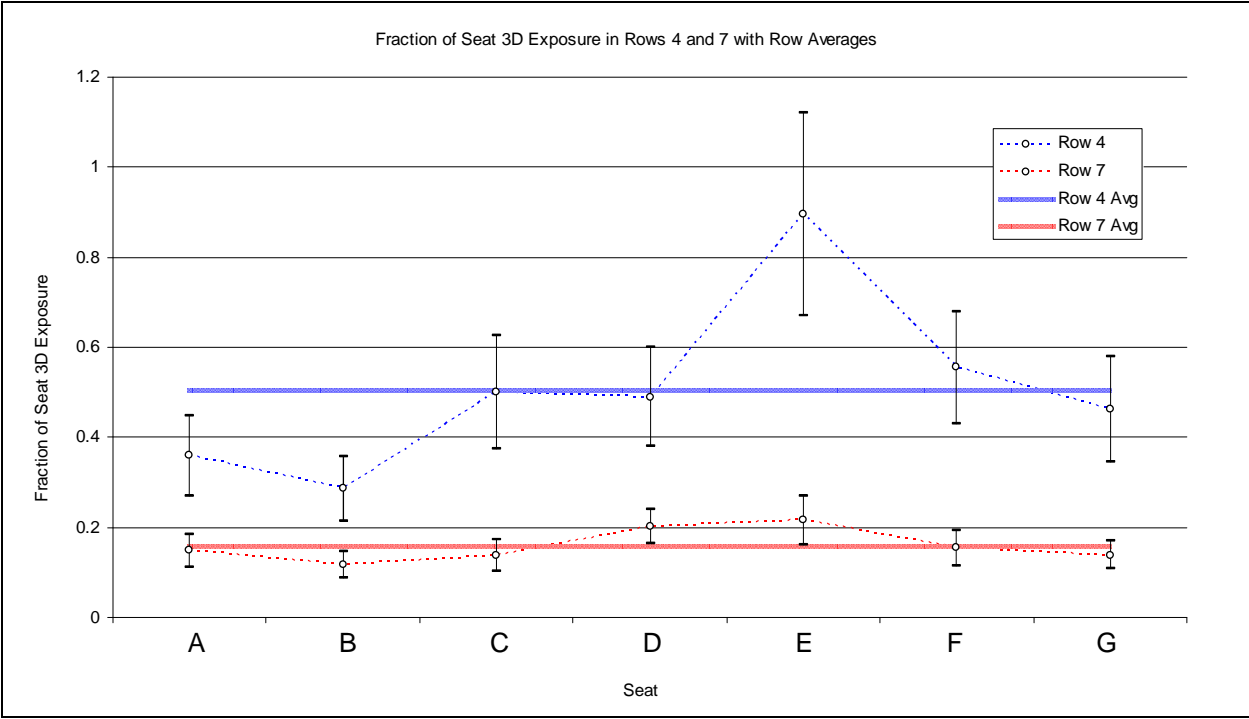


Figure 5.2: Rows 4 and 7 Fraction of Reference Exposure with Row Averages

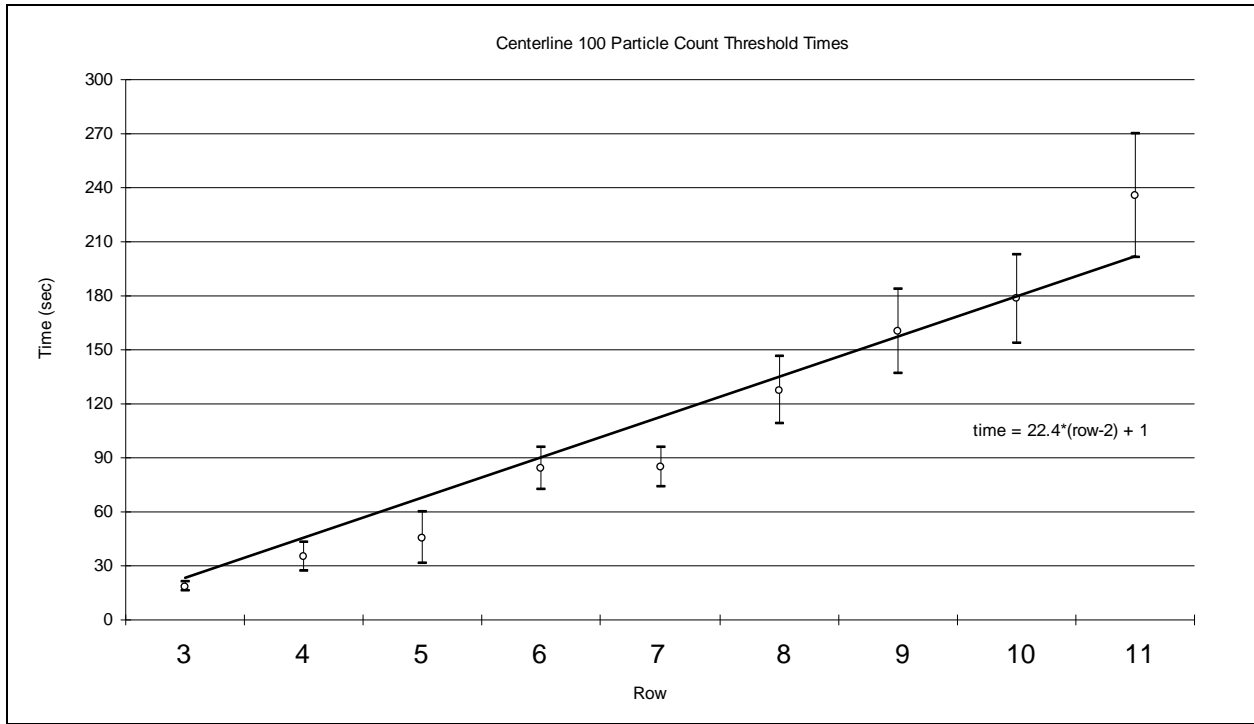


Figure 5.3: Centerline Particle Count Threshold Times with Linear Trend

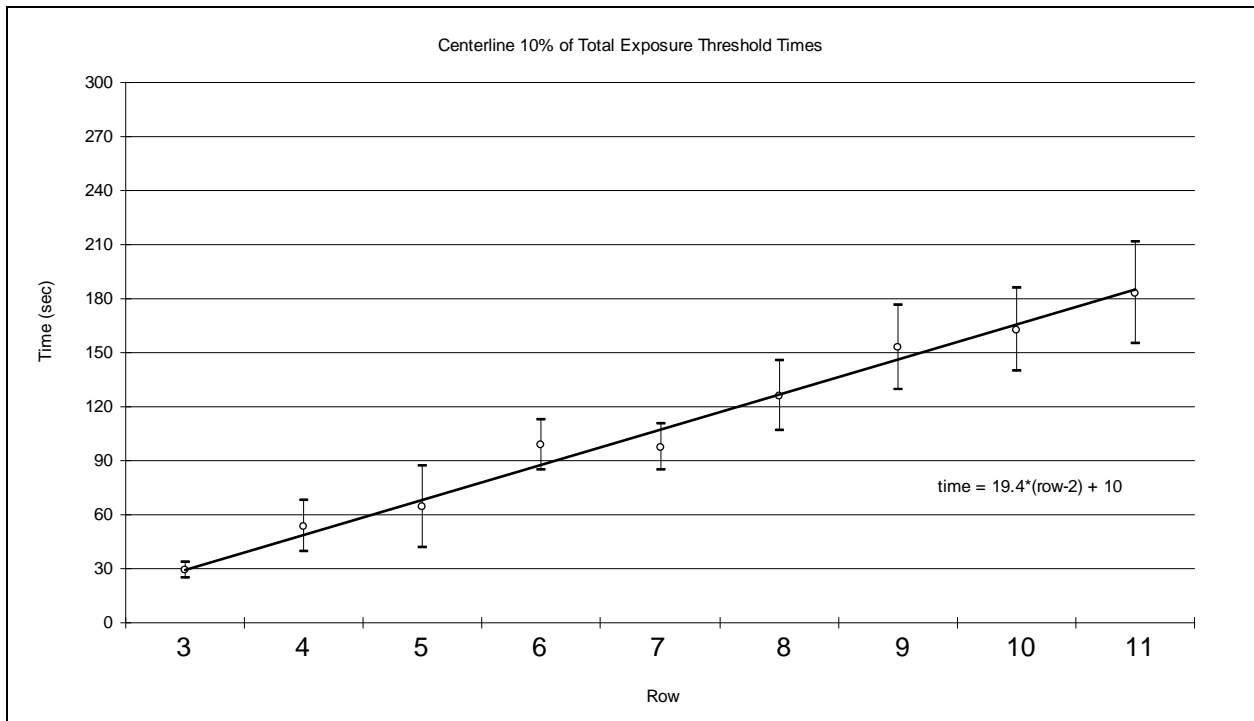


Figure 5.4: Centerline Fraction of Total Exposure Threshold Times with Linear Trend

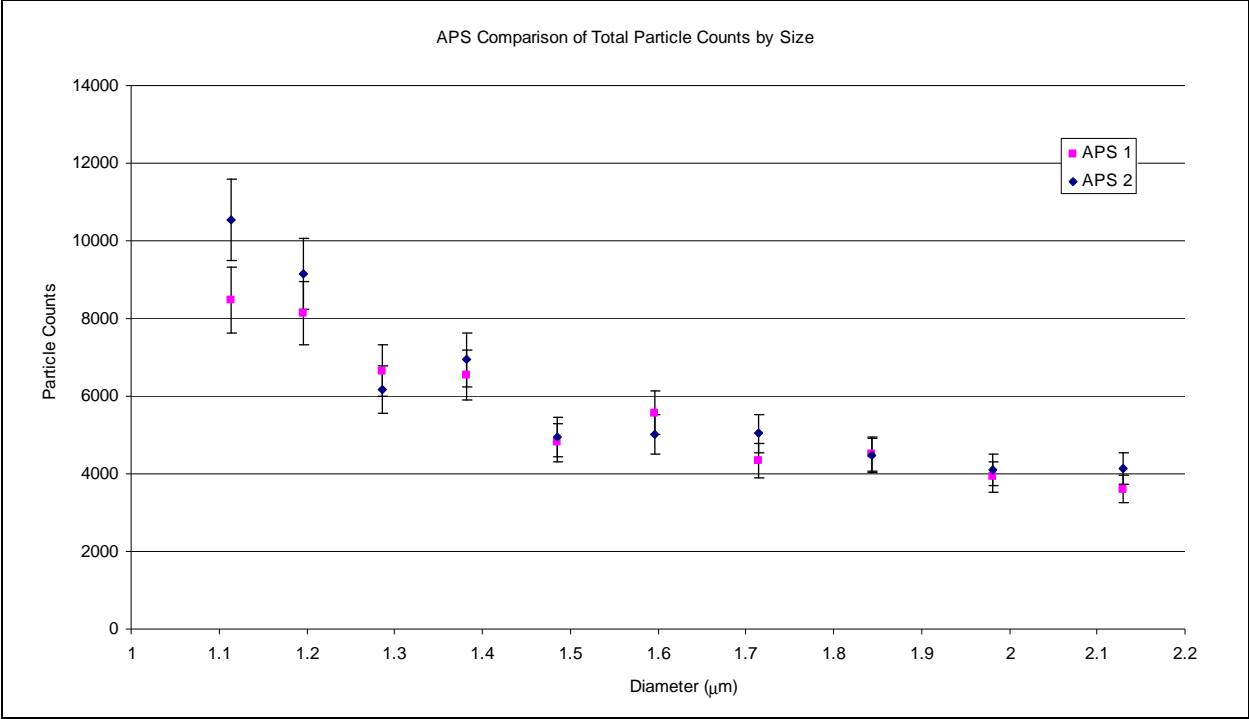


Figure 5.5: APS Comparison of Total Counts by Particle Size

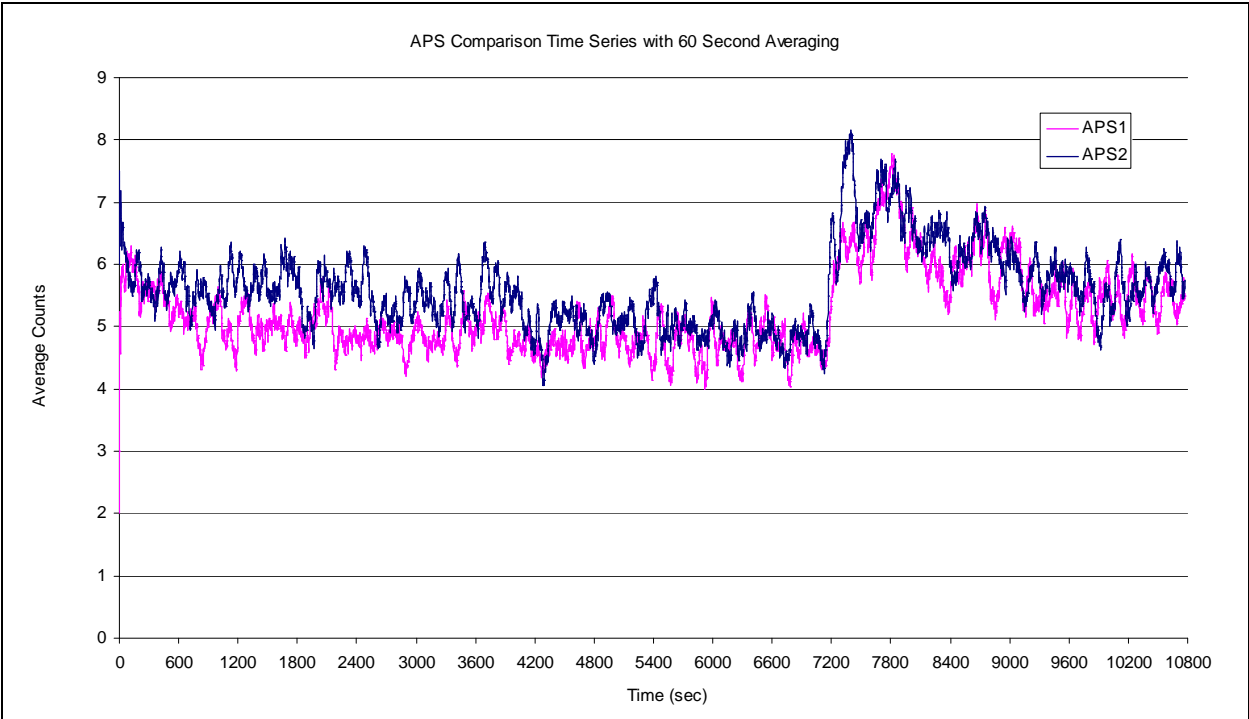


Figure 5.6: APS Comparison Time Series, 60 Second Averaging

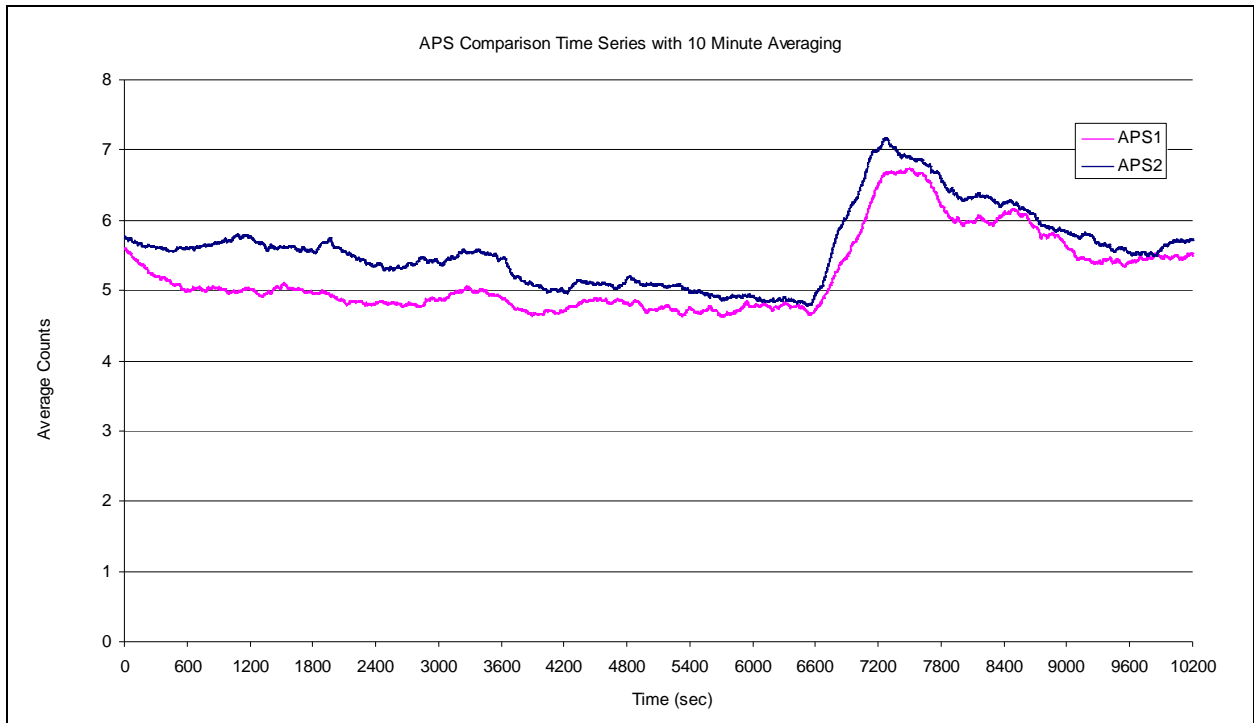


Figure 5.7: APS Comparison Time Series, 10 Minute Averaging

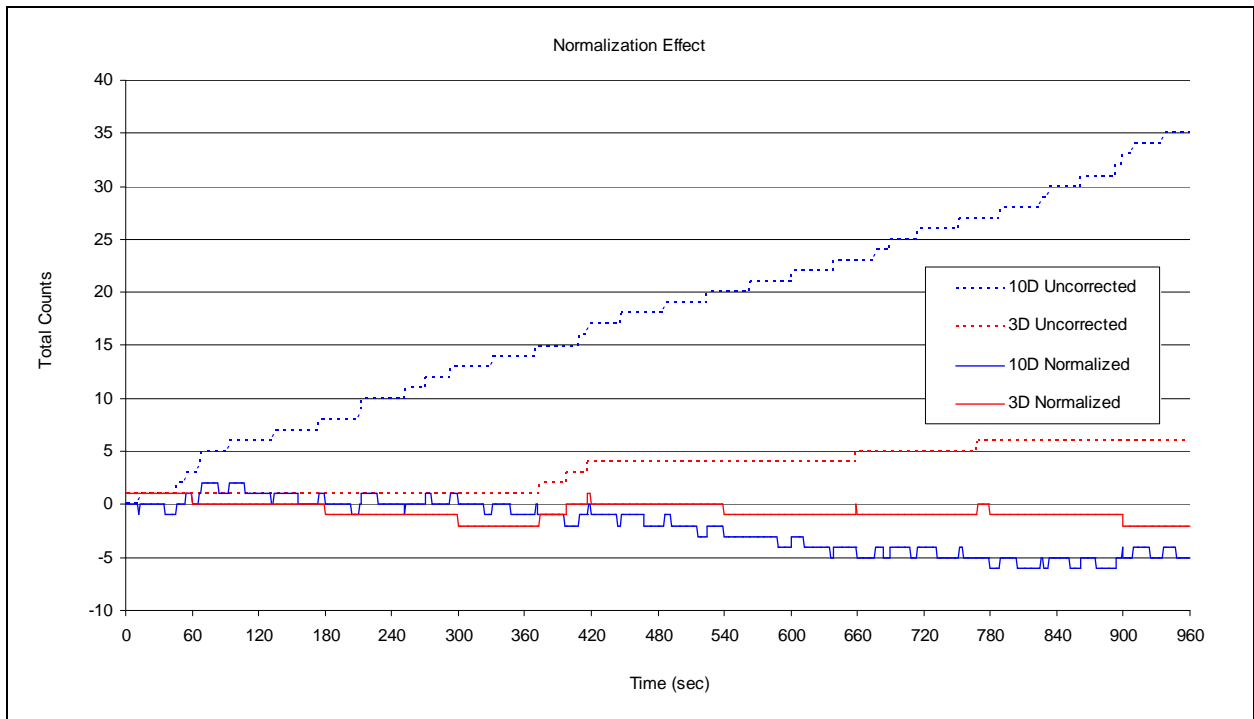


Figure 5.8: Normalization Effect Time Series

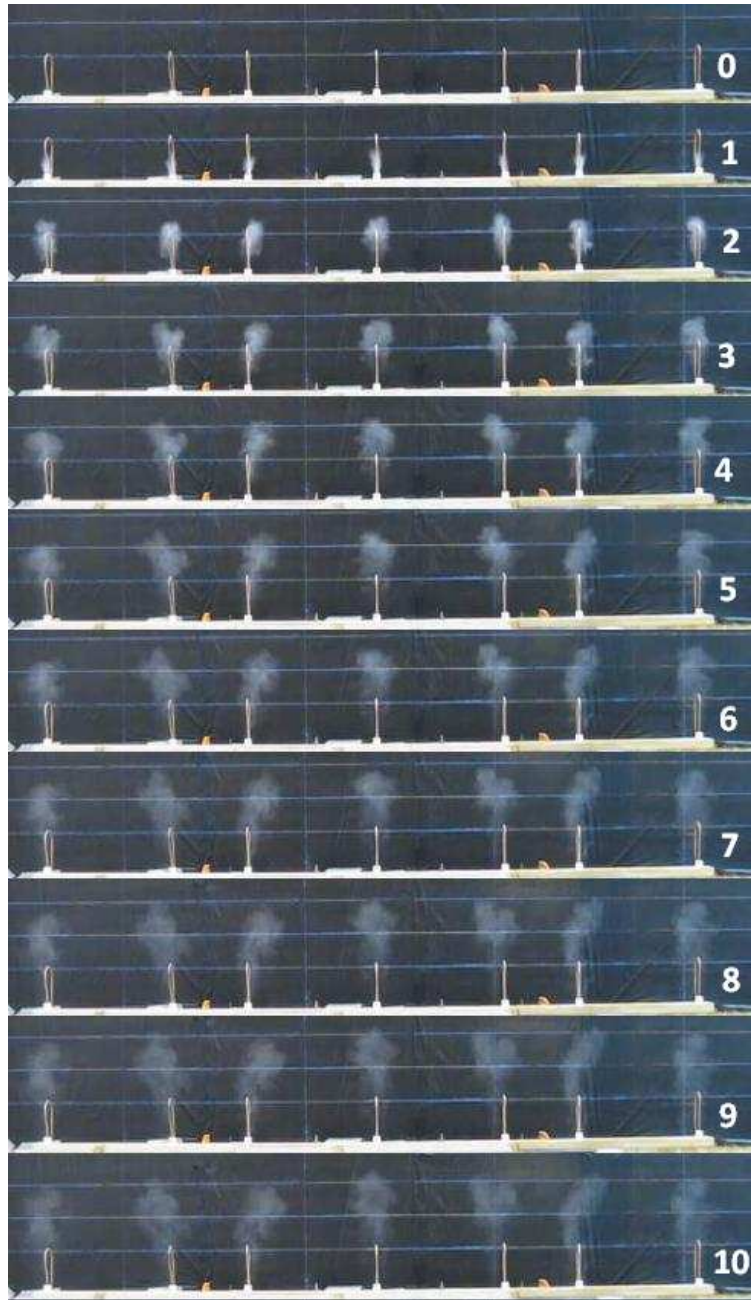


Figure 5.9: Particle Dispersion Visual Verification at 0.1 Second Intervals

CHAPTER 6 - Conclusions and Recommendations

This thesis focused on collecting experimental data from the release of particles across the second row of a Boeing 767-300 mockup involving 11 rows total. The release of the particles required the development and implementation of a dispersion system. A total of 172 data sets were collected from 27 different locations within the cabin in which the particles having a corrected aerodynamic diameter of 0.87 to 1.70 μm were counted once a second. These collected data were normalized and then analyzed using various criteria. While variations close to the source remained large through the various tests and methods of analysis, the locations farther from the source showed results that are more consistent. This indicates the dispersion system behaved with the estimated uncertainty. In addition, this means the regions in the cabin that experienced high levels of variation did so largely due to the unstable airflows in the cabin.

6.1. Exposure

The first approach focused on the total number of particles counted during a 16 minute test. The results of these tests show the rows closest to the source row received the highest exposure while those farther away showed less, as expected. Recalling the particle dispersion took place in row 2, the highest counts occurred in seat 1F averaging 17400 particle counts. The lowest average total particle count, of 397 particles, took place in seat 11D that was the test location farthest from the source. The particle counts along and just to the right of center in the cabin two to five rows behind the source did not behave as predictably however. The variations in this region were higher than the surrounding seats and are an indicator of the complex nature of the flows within the cabin.

The second analysis of the data focused on tests in which a reference location was used to normalize the data. For these tests, 136 data sets from 22 locations were used and developed a distribution pattern. Again the highest numbers occurred in row 1, this time in seat 1D collecting 1.43 times the counts of seat 3D for the same tests. As with the total exposure data the lowest numbers were collected in seat 11D counting only 3.4 percent of the exposure seen in seat 3D. The normalization with the reference seat removed the relative variations in the distribution across row 7 while increasing the relative variations across row 4. Seat 4E actually shows 90 percent of the exposure seen relative to seat 3D despite being another row removed from the

source. This correlation to the reference location indicates a possible path of dispersion within the cabin.

6.2. Transient Behavior

After normalization of the data the resulting time series plots illustrate the way in which each of the 22 locations tested is exposed to the particles released. The locations closer to the source experience a dramatic rise to a peak number of counts and then dissipate in a decaying nature that is expected in this environment with fresh air introduced continually. Locations farther from the source show a gradual increase to a peak and then share the same curve of dissipation as the rows with higher exposures. The time series data however does show some cyclic nature in the results. Figures 4.23 and 4.24 showing seats 4B and 4C indicate the cyclic behavior is not a random process because the data from the three tests in seat 4B align between 60 and 120 seconds after the release. Even if the timing of the release was coincidental and allowed the peaks to align, the period of the cycles is very similar for the three separate tests.

The second portion of the time series tests focused on the time required for the various locations within the chamber to reach two different thresholds. The first limit was established at 100 particle counts of total exposure. This varies between less than 1 percent of the average total exposure at some locations to more than 25 percent at another. Seat 1D reached the limit the quickest on average at 6.3 seconds while seat 11D was the slowest at 183.0 seconds on average. While the variation in the time to the exposure limit varied across the cabin for the tests in rows 4 and 7 the behavior along the centerline was fairly linear.

The second threshold established as part of the time series tests focused on the time required to accumulate 10 percent of the total particles counted during each individual test. While the nature of this test is similar to the 100 particle limit, the criteria is very different as it changes relative to the location and test. In lieu of the different limit, the centerline tests showed similar results with a linear nature from the source rearward. In comparison to the lateral results from the 100 particle count limit in rows 4 and 7, the data for the 10 percent exposure limit exhibit less relative variation across the cabin.

6.3. Recommendations

The dispersion of particles in row 2 allowed for particle collection at greater distances from the source but introduced the possibility of the end wall affecting the distribution near the source. Further testing with the source close to the center of the cabin would allow for a better understanding of the direction the particles move because of the airflows within the cabin. Additionally, the location chosen as a reference location early in the testing process proved to have a high level of variation from one test to the next. Based on the data available, it appears that utilizing a location farther from the source would provide more stable data from which to normalize the test results. Lastly, further tests are recommend that focus on the cyclic behavior, seen most clearly in the seat 4B time series.

References

- ACER-COE. (2009) RITE/ACER Center of Excellence. United States. *Airliner Cabin Environment Research*.
- ASHRAE. (2005a) "Chapter 9 – Indoor Environmental Health." *2005 ASHRAE Handbook of Fundamentals*. 9.4. Airborne Contaminants.
- ASHRAE. (2005b) "Chapter 12 – Air Contaminants." *2005 ASHRAE Handbook of Fundamentals*. 12.2-3. Particulate Contaminants.
- ASHRAE. (2005c) "Chapter 30 – Nonresidential Cooling and Heating Load Calculations." *2005 ASHRAE Handbook of Fundamentals*. 30.3-30.4. Internal Heat Gains.
- ASHRAE. (2007) "Aircraft." *2007ASHRAE Handbook – Heating, Ventilation, and Air-Conditioning Applications*. 10.5. Air Quality.
- Baron, Paul, Deye, Gregory J., Martinez, Anthony B., Jones, Erica N. and Bennett, James S. (2008, Mar. 1) "Size Shifts in Measurements of Droplets with the Aerodynamic Particle Sizer and the Aerosizer", *Aerosol Science and Technology*, Vol. 42: 201-09.
- Bowen, John T., Jr., and Christian Laroe. (2006, June) "Airline Networks and the International Diffusion of Severe Accute Respiratory Syndrome(SARS)." *The Geographical Journal*. London. Vol. 172:Part 2:130+.
- BTS., Bureau of Transportation Statistics, United States. (2010). "Air Carrier Traffic Statistics."
- Coleman, Hugh W. and W. Glenn Steele. (1999) "Experimentation and Uncertainty Analysis for Engineers." 2nd Ed. New York, NY: John Wiley and Sons.
- EPA., Environmental Protection Agency, United States. (1992). "Health Assessment Document for Talc." EPA-600/8-91/217. Environmental Protection Agency Office of Research and Development. Washington, D.C.
- EPA., Environmental Protection Agency, United States. (2008) "Particulate Matter."
- FAA. (2008, December). "Draft Final Technical Report, Contaminant Transport in Airliner Cabins Project", FAA Cooperative Agreement 04-C-ACE-KSU, Institute for Environmental Research, Kansas State University.
- Graham, R. L.; Knuth, D. E.; and Patashnik, O. (1994) "Integer Functions." *Concrete Mathematics: A Foundation for Computer Science, 2nd ed.* pp. 67-101. Reading, MA: Addison-Wesley.

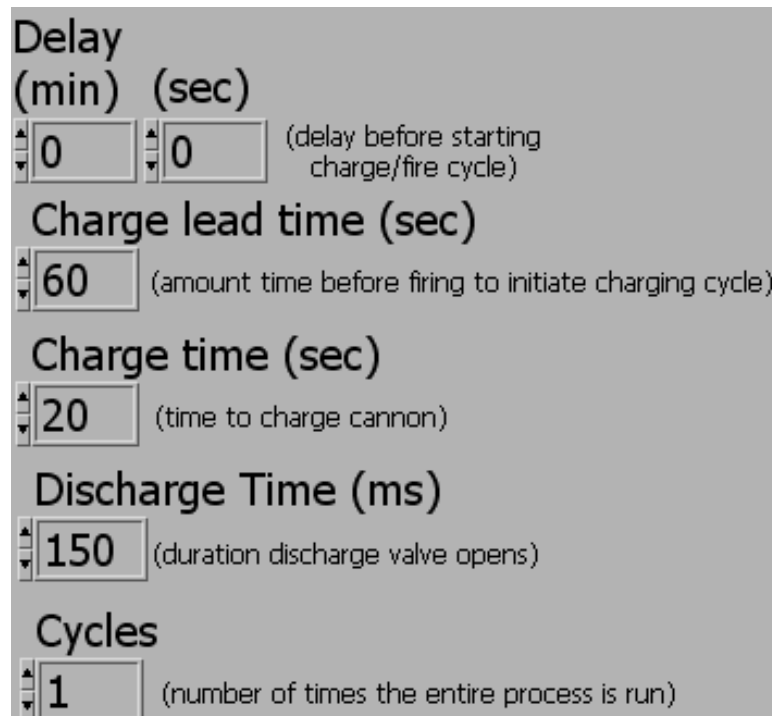
- Hatch, Theodore F. (1961, Sept.) "Distribution and Deposition of Inhaled Particles in Respiratory Tract." *Microbiology and Molecular Biology Reviews*. Vol. 25:Iss. 3:237-40.
- Hunt, Elwood H., Reid, Don H.,Dr., Space, David R. and Tilton, Fred E.,Dr. (1995) "Commercial Airliner Environmental Control System: Engineering Aspects of Cabin Air Quality." The Boeing Company.
- Jones, B.W. (2009, Sept. 17-18) "Advanced Models for Predicting Contaminants and Infectious Disease Virus Transport in the Airliner Cabin Environment: Experimental Dispersion Data," *National Academies Transportation Research Board, Symposium on Transmission of Disease in Airports and Aircraft.*, Washington, D.C.
- Lebbin, Paul.(2006) "Experimental and Numerical Analysis of Air, Tracer Gas, and Particulate Movement in a Large Eddy Simulation Chamber." Diss. Kansas State University, Manhattan, KS.
- Lin, C. H., Horstman, R. H., Ahlers, M. F., Sedgwick,L. M., Dunn,K. H., Topmiller,J. L., Bennett,J. S., Wirogo,S. (2005a) "Numerical Simulation of Airflow and Airborne Pathogen Transport in Aircraft Cabins-Part I:Numerical Simulation of the Flow Field" *ASHRAE Transactions*, Vol. 111.
- Lin, C. H., Horstman, R. H., Ahlers, M. F., Sedgwick,L. M., Dunn,K. H., Topmiller,J. L., Bennett,J. S., Wirogo,S. (2005b) "Numerical Simulation of Airflow and Airborne Pathogen Transport in Aircraft Cabins-Part II:Numerical Simulation of Airborne Pathogen Transport" *ASHRAE Transactions*, Vol. 111.
- McNaught, A.D., and A. Wilkinson. (1997). "IUPAC Compendium of Chemical Terminology, The Gold Book". 2nd Ed., Blackwell Science.
- NAAQS. Environmental Protection Agency, United States. (2010 Feb). "PM_{2.5} NAAQS Implementation." *National Ambient Air Quality Standards*.
- Padilla, Angeline M. (2008) "Experimental Analysis of Particulate Movement in a Large Eddy Simulation Chamber." MS Thesis. Kansas State University, Manhattan KS.
- Space, David R. and Elwood H. Hunt. "The Airplane Cabin Environment: Issues Pertaining to Flight Attendant Comfort." The Boeing Company.
- TSI. (2006, Apr.) "Aerosol Instrument Manager Software for Aerodynamic Particle Sizer Spectrometers, User's Manual." Revision E. TSI Incorporated.
- Wang, Hwa-Chi and Walter John. (1987, Jan 01) "Particle Density Correction for the Aerodynamic Particle Sizer", *Aerosol Science and Technology*, Volume 6:191-98.
- Wunder. (2009, March 1) "History for Manhattan, KS." <http://www.wunderground.com/history/airport/KMHK/>.

Appendix A - LabView Programs

This appendix contains images and descriptions of the program written in LabView6.1 to control the air charging and discharging cycles of the dispersion system. The program itself is titled “Cannon Control” and the only subroutine not available in the standard LabView library is “DAQ_Analog_OUT”. This program is listed in the section following “Cannon Control”.

A.1. Cannon Control Program

The following program is used to control the charging tank fill and discharge. It is designed to control two solenoid operated valves via two solid state relays and the DAQ board.



The screenshot displays the front panel of the Cannon Control program with the following settings:

- Delay (min) (sec)**: 0 (min), 0 (sec) (delay before starting charge/fire cycle)
- Charge lead time (sec)**: 60 (amount time before firing to initiate charging cycle)
- Charge time (sec)**: 20 (time to charge cannon)
- Discharge Time (ms)**: 150 (duration discharge valve opens)
- Cycles**: 1 (number of times the entire process is run)

Figure A.1: Cannon Control Program Front Panel

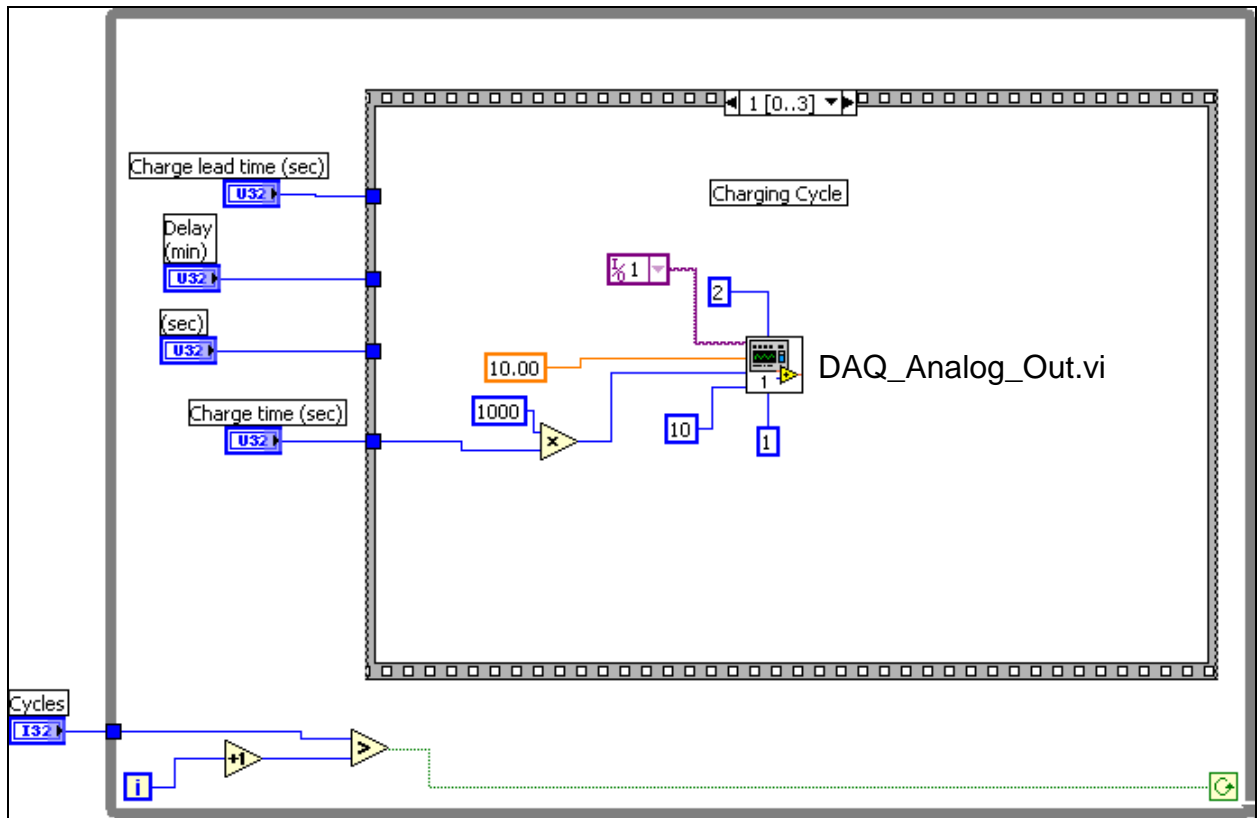


Figure A.2: First Level of the Wiring Diagram with Frame 1 in the Sequence

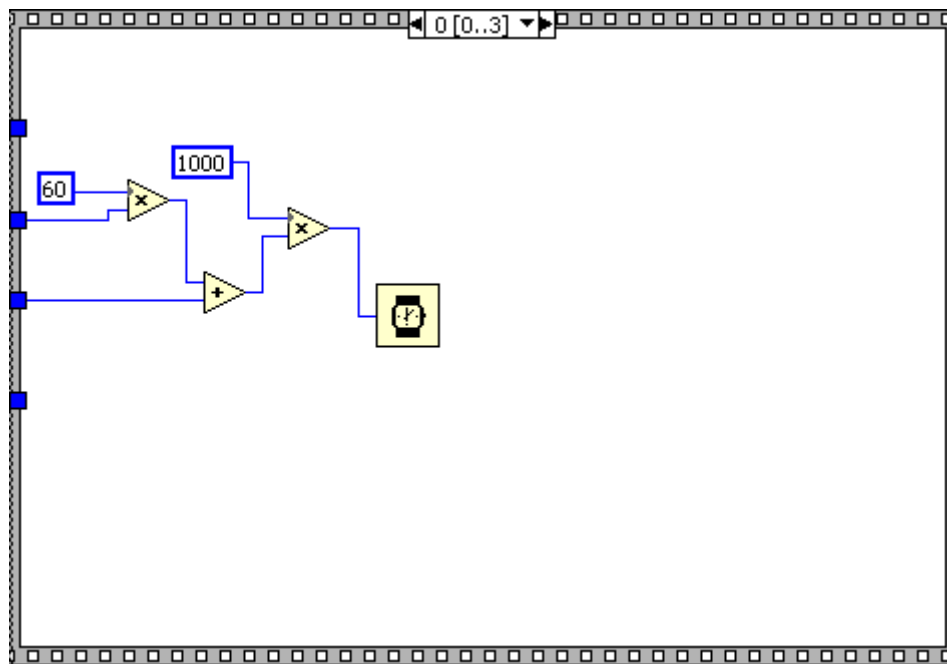


Figure A.3: Wiring Diagram, Frame 0 in the Sequence

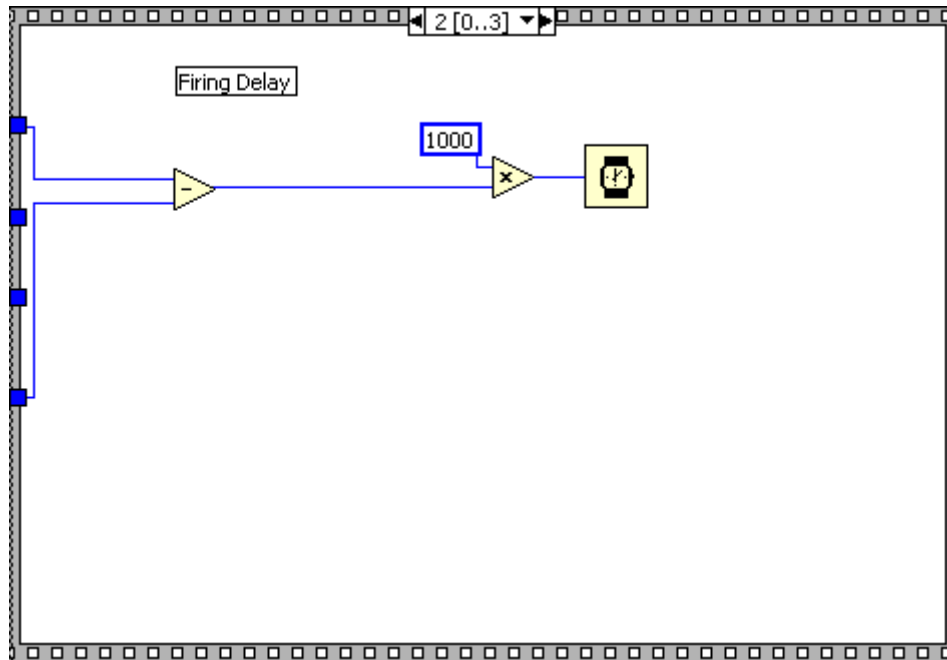


Figure A.4: Wiring Diagram, Frame 2 in the Sequence

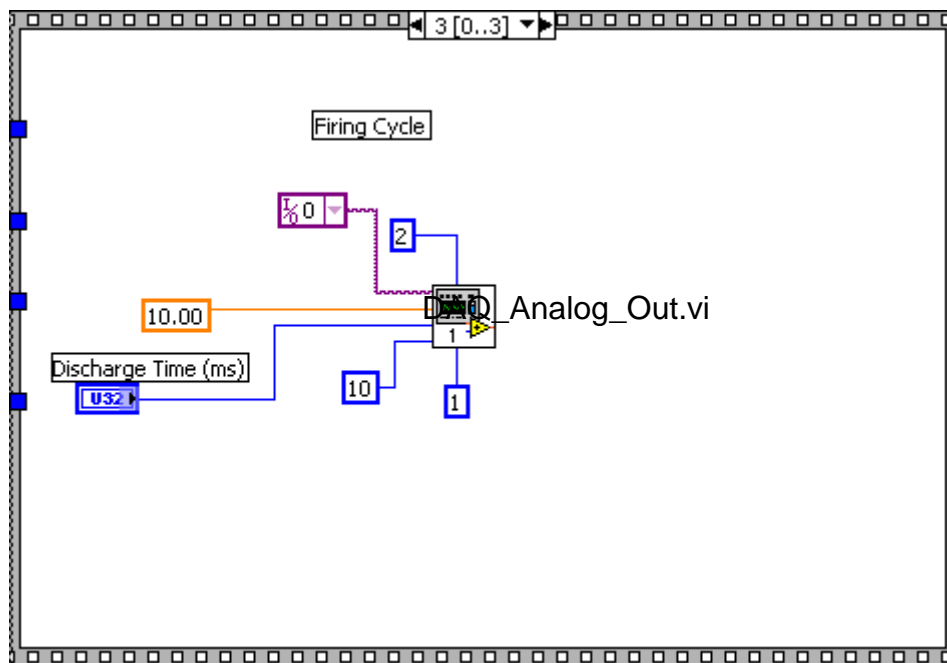


Figure A.5: Wiring Diagram, Frame 3 in the Sequence

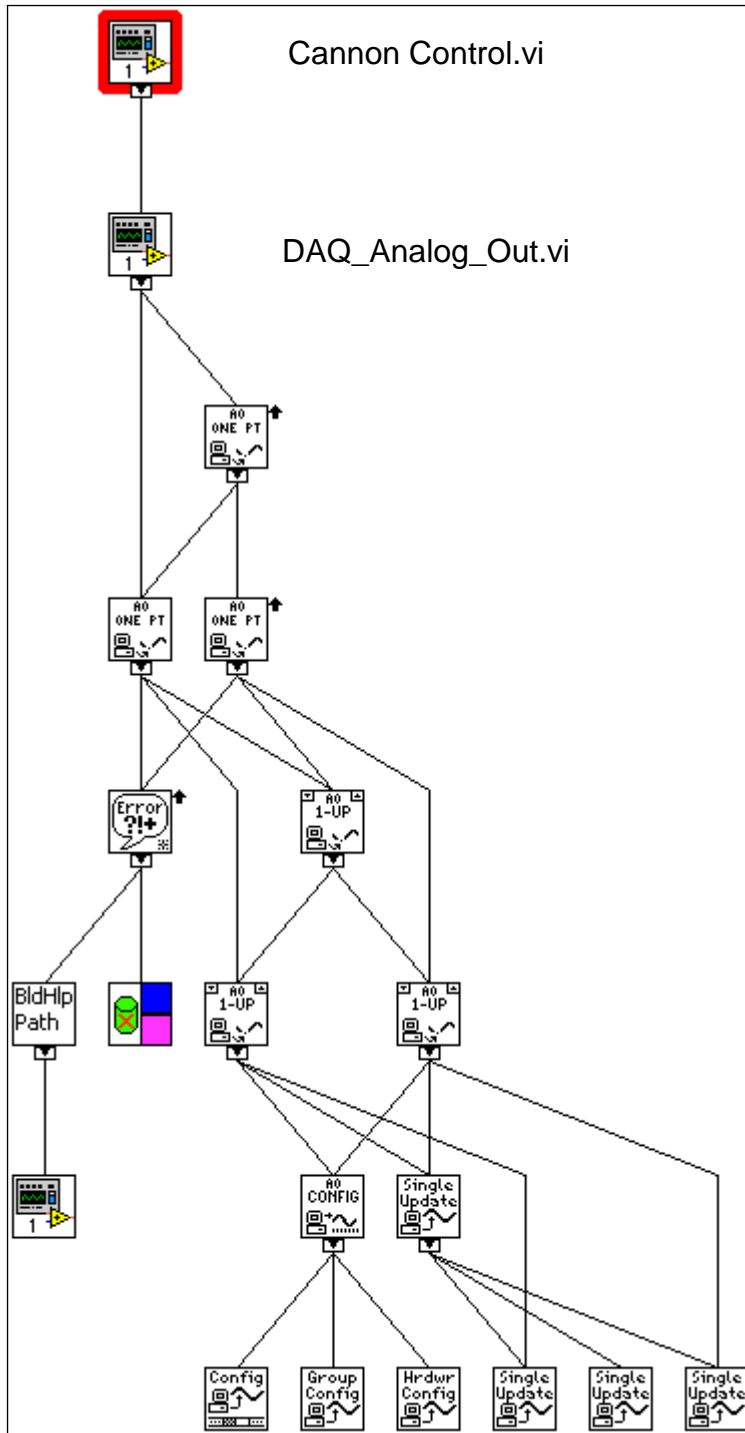


Figure A.6: Full Cannon Control Program Hierarchy

A.2. DAQ Analog Out Program

This section gives the LabView program for the DAQ Analog Out program list second in the Cannon Control Hierarchy.

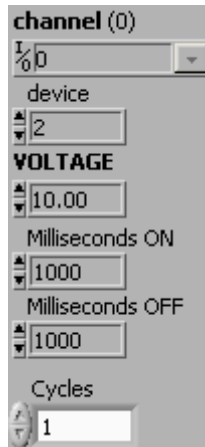


Figure A.7: Front Panel of the DAQ Analog Out Program

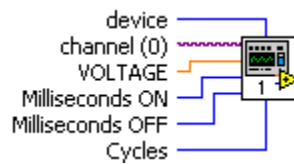


Figure A.8: DAQ Analog Out Terminals

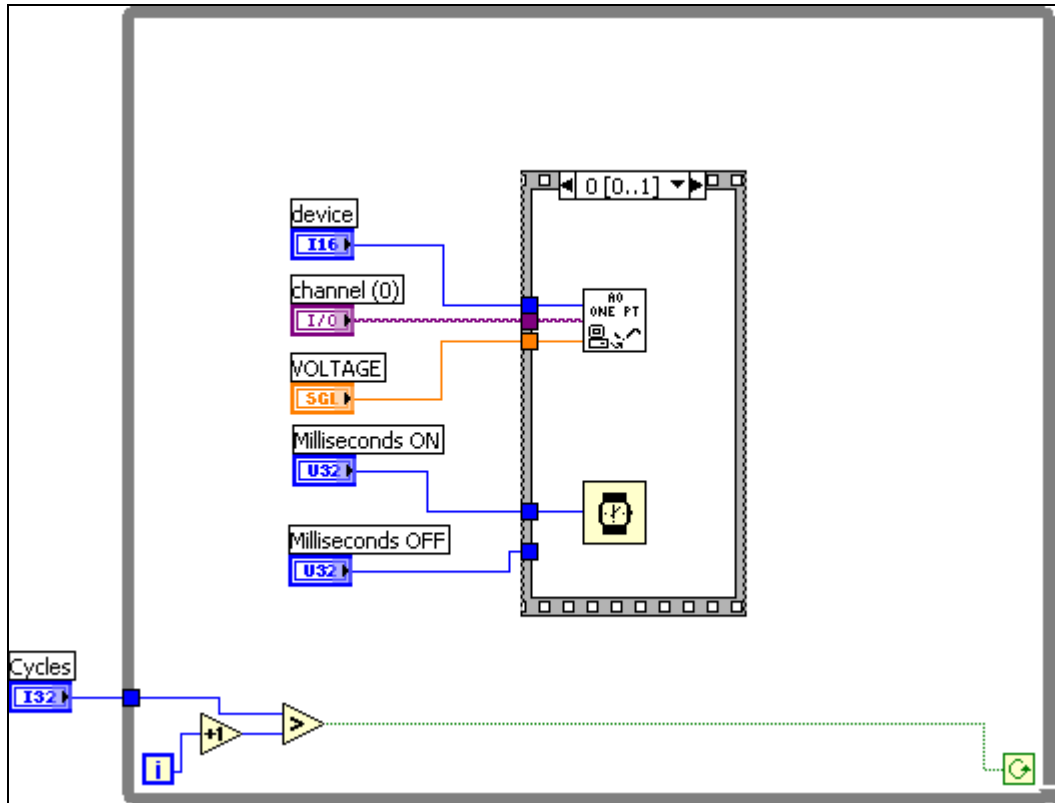


Figure A.9: DAQ Analog Out Wiring Diagram with sequence 0

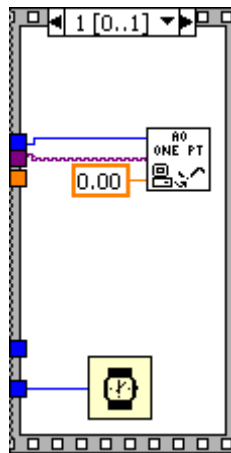


Figure A.10: DAQ Analog Out sequence 1